

BOUNDARY LAYER TRANSPORT OF SMALL PARTICLES

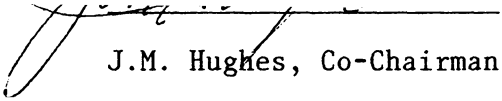
by

DAVID MCCREADY

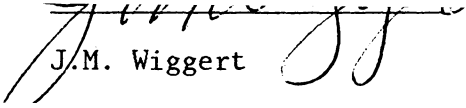
Dissertation submitted to the Graduate Faculty of the  
Virginia Polytechnic Institute and State University  
in partial fulfillment of the requirements for the degree of  
DOCTOR OF PHILOSOPHY  
in  
Civil Engineering

APPROVED:

\_\_\_\_\_  
B.B. Hicks, Co-Chairman

  
\_\_\_\_\_  
J.M. Hughes, Co-Chairman

\_\_\_\_\_  
R.P. Hosker

  
\_\_\_\_\_  
J.M. Wiggert

\_\_\_\_\_  
G.D. Boardman

  
\_\_\_\_\_  
C.W. Randall

June, 1984

Blacksburg, Virginia

## ACKNOWLEDGEMENTS

I would like to extend my gratitude to the Department of Energy, the Atmospheric Turbulence and Diffusion Division of the National Oceanic and Atmospheric Administration, and the Oak Ridge Associated Universities for the use of their facilities as well as their financial assistance to perform this research.

Thanks are due to my advisory committee at Virginia Tech; Dr. J.M. Hughes, Dr. C.W. Randall, and Dr. J.M. Wiggert and my committee at the ATDD; B.B. Hicks and Dr. R.P. Hosker.

Special thanks are due to :

- Bruce Hicks for his advice on the selection of a research topic and the acquisition of equipment.
- Ray Hosker for direction, many helpful suggestions, and the review of my dissertation.
- for advice on fluid modeling and instrumentation, assistance with data collection, and the review of my dissertation.
- for the discussions on micrometeorology and the review of my dissertation.

-

and for helping build the experimental  
equipment.

-

for instruction in use of the word  
processor.

## TABLE OF CONTENTS

		<u>Page</u>
	ACKNOWLEDGEMENTS .....	ii
	LIST OF FIGURES .....	vii
	LIST OF TABLES .....	xi
I.	INTRODUCTION .....	1
II.	AERODYNAMIC BOUNDARY LAYERS .....	11
	Laminar Flow .....	15
	Flow Separation .....	23
	Turbulent Flow .....	23
III.	DRY DEPOSITION MECHANISMS .....	25
	Gravitational Settling .....	25
	Inertial Impaction .....	29
	Brownian Diffusion .....	30
	Eddy Diffusion .....	31
	Electrostatic Attraction .....	33
IV.	PARTICLE DEPOSITION THEORY .....	38
	Stagnant Film Theory .....	38
	Deposition Across a Laminar Boundary Layer .....	40
	Deposition Across a Turbulent Boundary Layer .....	41
	Intermittent Turbulence Theory .....	47
V.	PARTICLE RESUSPENSION .....	49
	Particle Adhesion .....	49
	London-van der Waals Forces .....	50
	Electrostatic Forces .....	50
	Relative Humidity and Temperature .....	51
	Contact Area .....	52
	Resuspension .....	52
	Bounce-off .....	53
	Re-entrainment .....	54
	Agglomerates .....	55
VI.	PREVIOUS EXPERIMENTAL DEPOSITION STUDIES .....	57

TABLE OF CONTENTS (cont.)

	<u>Page</u>
VII. MATERIALS AND METHODS .....	64
Wind Tunnel Modeling .....	64
Wind Tunnel .....	65
Aerosol Generation System .....	67
Electrostatic Charge Neutralizer .....	71
Aerosol Analyzer System .....	72
Air Velocity Measurement .....	77
Electrostatic Charge Measurement System .....	78
Experimental Deposition Plate .....	80
Quantification of Particle Deposition .....	82
Aerosol Generation and Deposition System .....	83
VIII. CALIBRATION RESULTS .....	85
Wind Tunnel Calibration .....	85
Surface Flow Visualization .....	93
Aerosol Generation .....	98
Aerosol Dispersion .....	100
Background Aerosol Concentrations .....	105
Electrostatic Charge Measurement .....	107
Velocity Boundary Layer .....	111
Particle Concentration Over Experimental Plate ...	128
IX. EXPERIMENTAL DEPOSITION RESULTS .....	134
Ideal Surfaces .....	136
Ideal Surface - 0.8 Micron Diameter .....	138
Ideal Surface - 1.1 Micron Diameter .....	141
Non-ideal Surface - 1.1 Micron Diameter .....	141
Gravitational Settling Effect .....	143
Electrostatic Charging Effect .....	147
Effect of Protuberances .....	149
Resuspension - 42 Micron Diameter .....	149
X. DEPOSITION MODEL PREDICTIONS .....	151
Friction Velocity .....	151
Dimensionless Particle Relaxation Time .....	153
Theoretically Predicted Deposition Velocities ....	154
XI. CONCLUSIONS AND RECOMMENDATIONS .....	164
REFERENCES .....	170
APPENDIX A .....	177

TABLE OF CONTENTS (cont.)

	<u>Page</u>
APPENDIX B .....	180
APPENDIX C .....	184
APPENDIX D .....	204
VITA .....	210
ABSTRACT	

## LIST OF FIGURES

<u>Figure</u>		<u>Page</u>
I-1	A Common Aerosol Bimodal Size Distribution . . . .	3
I-2	Laboratory and Field Measurements of Deposition Velocities of Particles to Grass . . . . .	5
I-3	Electrical Analog Model of Particle Transfer to a Forest . . . . .	6
II-1	Velocity Boundary Layers on a Flat Plate in Laminar Airflow . . . . .	13
II-2	Momentum and Concentration Boundary Layers over a Flat Plate in Laminar Airflow . . . . .	16
II-3	The Diffusion Layer Thickness . . . . .	18
II-4	The Rate of Change of Particle Concentration Along the Boundary . . . . .	19
II-5	The Relationship of the Velocity and Diffusion Boundary Layers . . . . .	20
IV-1	Particle Stopping Distance and Surface Roughness Elements . . . . .	45
VII-1	Low-Speed Wind Tunnel for the Particle Deposition Studies . . . . .	66
VII-2	Microsphere Nebulizer Design . . . . .	68
VII-3	Monodisperse Aerosol Generation System . . . . .	69
VII-4	A Schematic of the Electrostatic Charge Neutralizer . . . . .	73
VII-5	Climet Model CI-226 Optical System . . . . .	74
VII-6	The Faraday Cup . . . . .	79
VII-7	A Schematic of the Charge Measurement System . . .	81
VII-8	Particle Generation and Deposition System . . . . .	84
VIII-1	Locations of the Vertical and Horizontal Velocity Profiles . . . . .	87

LIST OF FIGURES (cont.)

<u>Figure</u>		<u>Page</u>
VIII-2	Vertical Velocity Profile .....	88
VIII-3	Horizontal Velocity Profile .....	90
VIII-4	Oil/Pigment Flow at 5 M/S .....	94
VIII-5	Oil/Pigment Flow at 2 M/S .....	96
VIII-6	Oil/Pigment Flow on a Plate at a Seven Degree Angle of Incidence with the 2 M/S Airflow ....	97
VIII-7	Nebulizer Particle Output Versus Time .....	99
VIII-8	Locations of the Horizontal and Vertical Particle Concentration Profiles .....	101
VIII-9	Vertical Particle Concentration Profile .....	102
VIII-10	Horizontal Particle Concentration Profile ....	104
VIII-11	Wind Tunnel and Laboratory Background Particle Concentrations .....	106
VIII-12	Current Amplifier Voltage without Charge Neutralizer .....	109
VIII-13	Current Amplifier Voltage with Charge Neutralizer .....	110
VIII-14	Velocity Profiles With and Without Aerosol Generator Operating .....	112
VIII-15	Velocity Profiles at X = 1, 4, 8, and 12 cm ..	114
VIII-16	Velocity Profiles at X = 16, 20, 24, and 26.5 cm	115
VIII-17	Mean Velocity Profiles and Locations on the Experimental Plate .....	117
VIII-18	Turbulence Intensity Profiles at X = 1, 4, 8 and 12 cm .....	119
VIII-19	Turbulence Intensity Profiles at X = 16, 20, 24, and 26.5 cm .....	120
VIII-20	Velocity Profiles at X = 1, 4, and 8 cm .....	123



LIST OF FIGURES (cont.)

<u>Figure</u>		<u>Page</u>
VIII-21	Velocity Profiles at X = 12, 16, 20, and 24 cm .	124
VIII-22	Turbulence Intensity Profiles at X = 1, 4, 8 cm	126
VIII-23	Turbulence Profiles at X = 12, 16, 20, and 24 cm	127
VIII-24	Typical Particle Concentration Profiles .....	129
VIII-25	Particle Concentration Traverse at Z = 2 mm ....	131
VIII-26	Normalized Particle Concentrations at Z = 2 mm .	132
IX-1	Deposition Velocities for Experiments 7, 4, 11, and 5 for an Ideal Surface .....	137
IX-2	Deposition Velocities for Experiments 6, 7, and 9 for an Ideal Surface .....	139
IX-3	Deposition Velocities with Probable Error Bars for Experiments 7 and 9 .....	140
IX-4	Deposition Velocities for Experiments 10 and 11 for an Ideal Surface .....	142
IX-5	Deposition Velocities for Experiments 12, 13, and 14 for a Non-ideal Surface .....	144
IX-6	Deposition Velocities for Experiments 11, 15, 19 and 20 for an Ideal Surface .....	146
IX-7	Deposition Velocities for Experiments 11 and 17 for an Ideal Surface .....	148
X-1	Predicted Deposition Velocities for the 0.8 Micron Diameter Microspheres .....	155
X-2	Predicted Deposition Velocities for the 0.9 Micron Diameter Microspheres .....	156
X-3	Predicted Deposition Velocities for the 1.1 Micron Diameter Microspheres to an Ideal Surface .....	158
X-4	Predicted Deposition Velocities for the 1.1 Micron Diameter Microspheres to a Non-ideal Surface .....	159

LIST OF FIGURES (cont.)

<u>Figure</u>		<u>Page</u>
X-5	Predicted Deposition Velocities for 1.1 Micron Diameter Microspheres to the Plate Underside ...	161
X-6	Correlation of the Experimental Results to the the Intermittent Turbulence Theory .....	162

## LIST OF TABLES

<u>Table</u>		<u>Page</u>
I-1	Minimum Resistance to Transfer of Airborne Materials to Receptors .....	8
II-1	Thicknesses of the Laminar Velocity and Diffusion Boundary Layers over a Smooth Flat Plate .....	22
III-1	Some Factors Affecting Dry Deposition Removal Rates .....	26
III-2	Dynamic Characteristics of Particles .....	28
III-3	Distribution of Charges on Aerosols According to Boltzmann's Law .....	35
VI-1	Dry Deposition Studies Relevant to this Research	58
VII-1	Climet Model CI-226 Analog Pulse Height Versus Particle Diameter .....	76
VIII-1	Wind Tunnel Test Section Calibration .....	89
VIII-2	Mainstream Turbulence Intensities at Various Wind Tunnel Velocities .....	91
VIII-3	Theoretical and Experimental Velocity Boundary Layer Thicknesses .....	118
IX-1	A Summary of the Experiments .....	135
X-1	Theoretical Friction Velocities and Dimensionless Particle Relaxation Times along the Experimental Plate .....	152
C-1	Wind Tunnel Velocity Calibration - Horizontal .	185
C-2	Wind Tunnel Velocity Calibration - Vertical ...	186
C-3	Laminar Mainstream Velocity Profile at X = 1 CM	187
C-4	Laminar Mainstream Velocity Profile at X = 4 CM	188
C-5	Laminar Mainstream Velocity Profile at X = 8 CM	189
C-6	Laminar Mainstream Velocity Profile at X = 12 CM	190
C-7	Laminar Mainstream Velocity Profile at X = 16 CM	191

TABLE OF CONTENTS (cont.)

<u>Table</u>		<u>Page</u>
C-8	Laminar Mainstream Velocity Profile at X = 20 CM	192
C-9	Laminar Mainstream Velocity Profile at X = 24 CM	193
C-10	Laminar Mainstream Velocity Profile at X = 26.5 CM	194
C-11	Velocity Profile With Aerosol Generator Operating	195
C-12	Turbulent Mainstream Velocity Profile at X = 1 CM	196
C-13	Turbulent Mainstream Velocity Profile at X = 4 CM	197
C-14	Turbulent Mainstream Velocity Profile at X = 8 CM	198
C-15	Turbulent Mainstream Velocity Profile at X = 12 CM	199
C-16	Turbulent Mainstream Velocity Profile at X = 16 CM	200
C-17	Turbulent Mainstream Velocity Profile at X = 20 CM	201
C-18	Turbulent Mainstream Velocity Profile at X = 24 CM	202
C-19	Particle Concentrations Along Experimental Plate at Z = 2 MM .....	203
D-1	Deposition Velocity Results For Experiments 4, 5, and 6 .....	205
D-2	Deposition Velocity Results For Experiments 7, 9, and 10 .....	206
D-3	Deposition Velocity Results For Experiments 11, 12, and 13 .....	207
D-4	Deposition Velocity Results For Experiments 14, 15, and 17 .....	208
D-5	Deposition Velocity Results For Experiments 19 and 20 .....	209

# CHAPTER I

## INTRODUCTION

There is much international concern over the environmental impact of acidic deposition. In particular, plant canopies are an effective sink for acidic deposition due to the large surface areas they present and thus the potential for biological damage is significant (Hosker and Lindberg, 1982).

The dry deposition flux near a source may exceed the wet deposition flux (Hicks, 1983). Although rainout and washout are more efficient removal mechanisms, they occur intermittently. Dry deposition is a less efficient removal mechanism, but it occurs on a more continual basis.

Much of the current "acid rain" research is directed toward quantification of the flux of acidic material into specific watersheds. The determination of this flux is important for several reasons:

1. Environmental damage assessment
2. Emission policy evaluation
3. Comparison of scenarios
4. Regulatory decision making

The methodology for quantification of wet acidic deposition

is fairly advanced; automated equipment capable of collecting and storing numerous samples during a precipitation event are the state of the art. However, dry deposition is more difficult to measure, primarily because the acidic aerosols extend over a wide size range and exhibit a range of properties which affect their deposition rate (Hicks, Wesely, and Durham, 1980). Surrogate surfaces are often used to routinely monitor dry deposition (Lindberg, Harriss, Turner, and Shriner, 1979). Unfortunately, the current methodology for measuring dry deposition is considered inadequate, since surrogate surfaces do not accurately reflect dry deposition on to natural surfaces (which is desired). Natural surfaces have different aerodynamic and surface characteristics, such as sticky surfaces and protuberances (Hicks, Wesely, and Durham, 1980).

Particle origin is an important clue to aerosol properties, as shown in Figure I-1. The mass concentration for small particles (less than two micrometers) is often as large as that for larger particles due to the much greater number concentration of small particles (Thermal Systems Inc., 1979). Aerosols less than approximately one micron in diameter are usually of anthropogenic origin and may be composed of nitrates, sulfates, ammonia, or organic species. Aerosols larger than about one micron are usually of natural origin, produced by grinding or resuspension mechanisms, and may be composed of silicon, iron, or aluminum. Aerosols less than approximately two microns in diameter may penetrate deep into the human respiratory system and are considered a potential

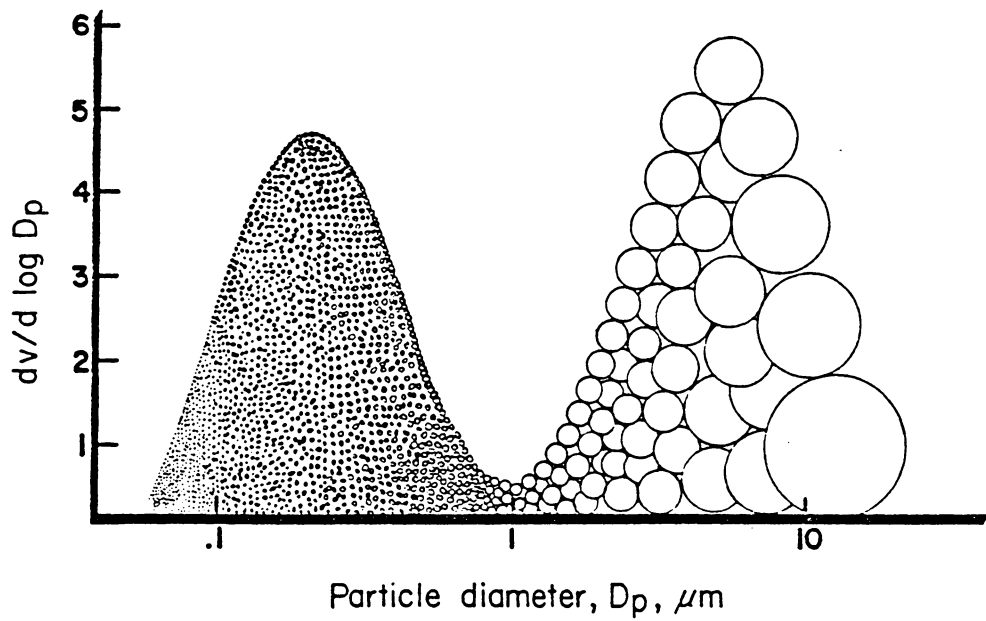


Figure I-1. Particle Mass Concentration ( $dv/d \log D_p$ ) Versus Particle Diameter for a Common Atmospheric Aerosol with a Bimodal Size Distribution, After Thermal Systems, Inc. (1979).

health hazard, especially if they are chemically reactive.

Dry deposition rates are generally compared through the use of the ratio of the dry deposition flux to the atmospheric concentration measured at a specified height within the boundary layer above the surface. This ratio has velocity units, hence it is called deposition velocity (Chamberlain, 1960). The deposition velocity should not be confused with the gravitational settling velocity. The primary advantage of the deposition velocity is that it allows one to compare particle deposition fluxes for situations with different atmospheric concentrations.

Figure I-2 shows a typical dependence of deposition velocity on particle diameter. Large particles are deposited due to gravitational settling. Small particles have Brownian motion (i.e., diffusional) properties similar to those of a gas and do not settle appreciably due to gravity. Aerosols with diameters in the range of 0.5 to 2.0 microns are in a transition range between the two previously mentioned groups and exhibit the minimum deposition velocities. There is a lack of information on deposition for this size range of particles.

A resistance-analog model is frequently used to illustrate the dry deposition process, as shown in Figure I-3 (McMahon and Denison, 1979). In this model the resistance to deposition,  $r_d$ , is the reciprocal of the deposition velocity,  $v_d$ . This resistance



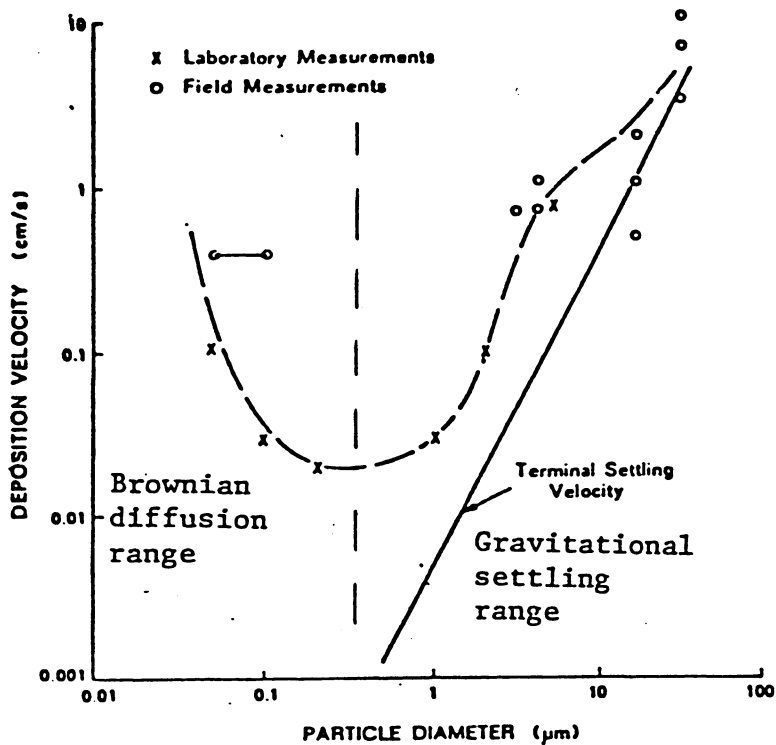
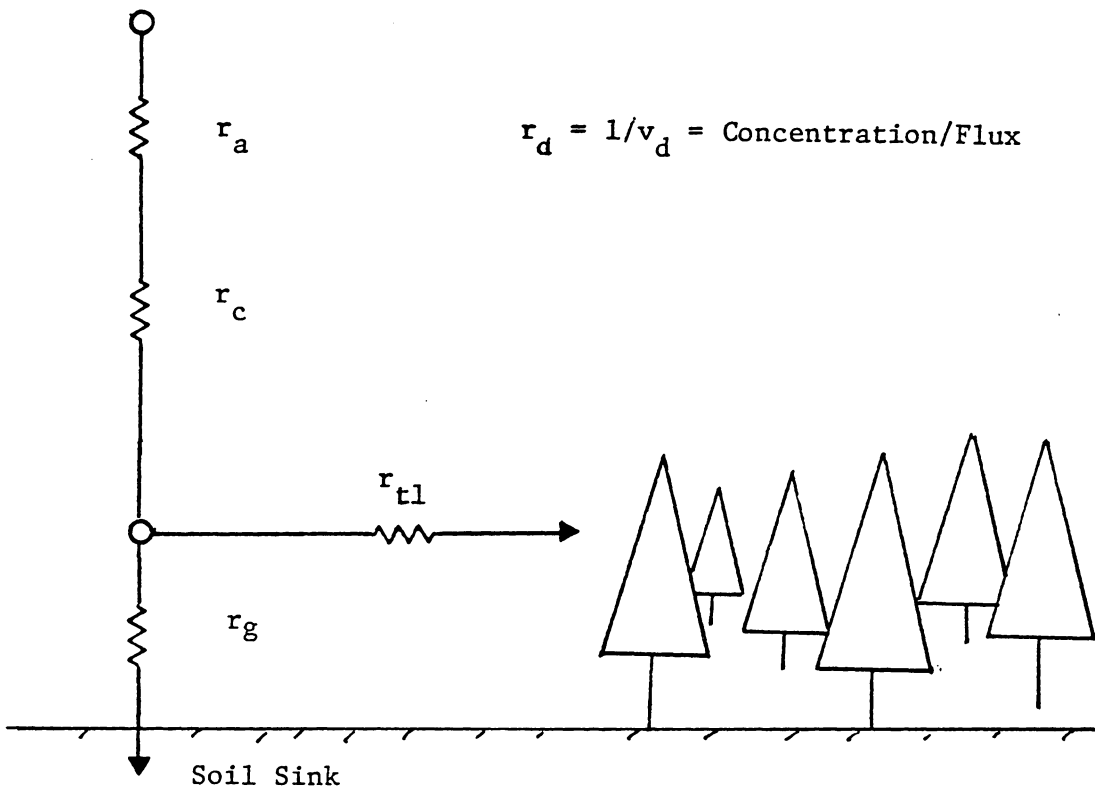
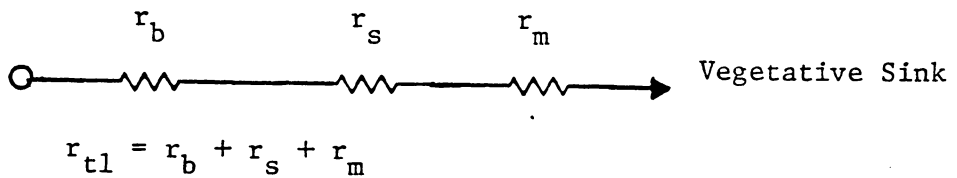


Figure I-2. Laboratory and Field Measurements of Deposition Velocities to Grass after McMahon and Denison (1979).



- a) The Resistances  $r_a$ ,  $r_c$ ,  $r_{tl}$ , and  $r_g$  are the Aerodynamic, Canopy, Transfer-to-leaf, and Ground Resistances to Particle Transport.



- b) The Transfer-to-leaf Resistance,  $r_{tl}$ , is Composed of the Leaf Boundary Layer Resistance,  $r_b$ , the Stomatal Resistance,  $r_s$ , and the Assimilation Resistance,  $r_m$ .

Figure I-3. An Illustration of the Resistance Model for Particle Transfer to a Forest after McMahon and Denison (1979).

can be separated into several discrete resistances; atmospheric (above canopy), plant surface aerodynamic boundary layer, plant uptake, soil surface aerodynamic boundary layer, and soil uptake. The value of the deposition velocity sought is the reciprocal of the sum of the individual resistances. Some researchers, such as W.G.N. Slinn, fail to recognize any usefulness in the resistance model concept; they claim that particles are significantly affected by gravity and are not transported like gases in the lower atmosphere (Hicks, 1984). Others, such as C.I. Davidson, have modified the resistance model concept to include a parallel resistance equal to  $1/V_g$ . Hicks (1984) believes that these represent extreme viewpoints and that this resistance model concept is applicable to particles in the size range of concern, 0.5 to 2.0 microns diameter.

Much of the current dry deposition research seeks to more accurately quantify these resistances, as well as the total resistance to deposition. The largest resistance is the transfer-limiting step and dominates the overall deposition process. Some typical resistance values are shown in Table I-1. Generally, the resistance associated with the transfer across the leaf boundary layer greatly exceeds that of the turbulent air above it (Hosker and Lindberg, 1982), except under very stable atmospheric conditions.

Theoretically-predicted dry deposition rates are frequently a factor of ten less than experimentally-determined dry deposition

TABLE I-1. MINIMUM RESISTANCES TO TRANSFER  
OF AIRBORNE MATERIALS TO RECEPTORS

Type of Resistance	Range of Minimum value, (s/cm)
A. Aerodynamic Resistance:	0.1-1
B. Leaf Resistance:	
1. Leaf Boundary Layer	0.1-2.5
2. Stomatal Resistance:	
2.1 Herbaceous Crops	0.5-2.5
2.2 Trees	0.9-15
2.3 Xerophytes	5-16
3. Assimilation Resistance:	
3.1 Soluble Gases	0.1-1
3.2 poorly Soluble Gases	1-10
C. Ground resistance:	0.2-2

After Hosker and Lindberg (1982).

rates (Slinn, 1982). It is therefore possible that a mechanism which increases the particle deposition rate is presently unaccounted for in the theory. This mechanism may be the electrostatic attraction of particles to a charged surface (Langer, 1965), or it might be particle impaction/attraction onto previously deposited particles (Belot and Gauthier, 1975).

This research program will investigate the dry deposition mechanisms which are important for transfer of particles 0.8 to 2.0 microns diameter across the surface aerodynamic boundary layer on a flat plate, in order to explain the present discrepancies between theoretical and experimental dry deposition rates.

The specific objectives of this study are to determine the following:

1. Can the turbulent flow deposition theory be used to successfully predict particle deposition onto flat plates?
2. Are experimental deposition rates greater than theoretical deposition rates because of a deposition mechanism which is unaccounted for?
3. Does particle resuspension significantly affect deposition? This will be addressed by comparing

deposition onto ideal (oil-coated) and non-ideal surfaces.

This research will result in a better understanding of aerosol transfer across the surface boundary layer and a more accurate quantification of the boundary layer deposition velocity.

CHAPTER II  
AERODYNAMIC BOUNDARY LAYERS

Much theoretical research in fluid mechanics is based on the perfect or ideal fluid (i.e., frictionless and incompressible). However, real fluids will transmit tangential forces (friction) as well as normal forces (pressure), and can be compressed.

Frictional forces are related to the viscosity properties of a fluid. Frictional forces retard the motion of the fluid in a thin "boundary" layer near solid boundaries. If one assumes the condition of no slip at the boundary (i.e., the velocity is zero at the boundary), then the velocity of the fluid increases from zero to the full value corresponding to frictionless flow in the mainstream fluid flow. The condition of no slip near a solid boundary is important, as it requires the modification of the equations of motion for the perfect fluid.

The tangential shearing stress,  $\tau_0$ , in a laminar boundary layer is defined as :

$$\tau_0 = \mu(dU/dz) \quad \text{(laminar)} \quad \text{(II-1)}$$

where  $\mu$ , the coefficient of absolute (or dynamic) viscosity, is a coefficient of proportionality, and  $dU/dz$  is the velocity gradient above the boundary. Air has a small coefficient of absolute viscosity ( $\mu = 2.09 \times 10^{-4}$  g/cm s at 20 C).

Shear stress build up in the boundary layer causes a turbulent

outburst which relieves the stress. The transfer of momentum is a result of turbulent outburst and is given as:

$$\tau_0 = - \rho \overline{u' w'} \quad (\text{turbulent}) \quad (\text{II-2})$$

where  $u'$  and  $w'$  are the instantaneous velocity components parallel and normal to the boundary (Davies, 1966). For flow over a surface the tangential stress is greatest at the boundary and decreases linearly from the boundary. Outside the viscous sublayer the tangential stress is equal to the Reynolds stress ( $\rho \overline{u' w'}$ ).

Figure II-1 is an illustration of the boundary layer development on a sharp-edged flat plate at zero incidence to a laminar airflow. The velocity distribution is uniform upwind of the leading edge of the plate. A very thin boundary layer develops near the plate surface where the air velocity is considerably less than the main airstream velocity. The thickness of the velocity boundary layer,  $d_u$ , increases along the plate (from zero at the leading edge) in the downstream direction as increasing quantities of fluid are affected, until reaching a so-called critical Reynolds number. At this point instabilities in the boundary layer result in a breakdown in the laminar structure and cause turbulence to begin (Vennard, 1965). The transition from laminar to turbulent flow occurs at a critical Reynolds number whose value varies from  $10^4$  to  $10^6$ , according to the specific experimental conditions, particularly the amount of turbulence in the mainstream airflow.



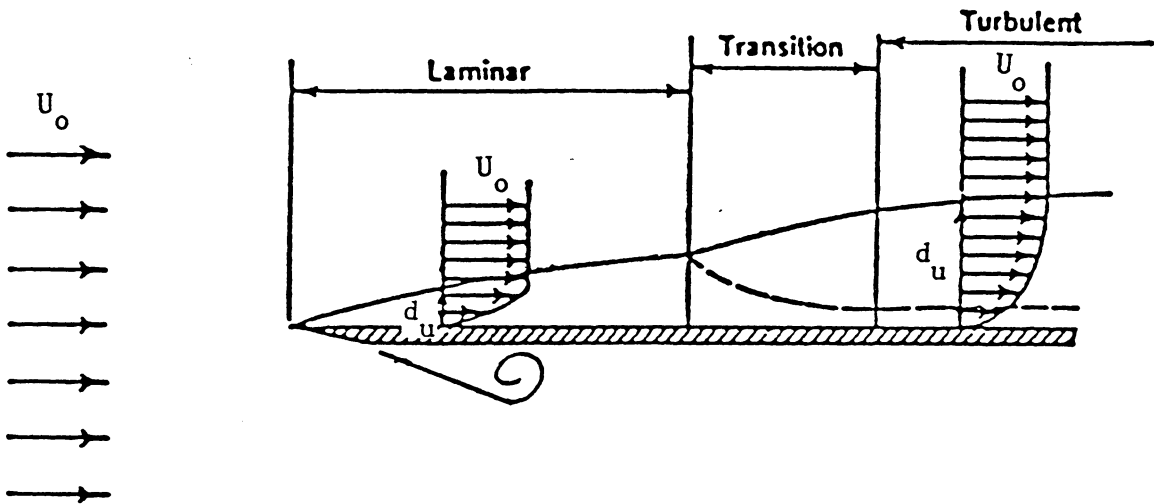


Figure II-1. Velocity Boundary Layer Development over a Flat Plate in a Laminar Airflow after Vennard (1965).

The transition boundary layer then thickens and develops into a turbulent boundary layer. A viscosity-dominated sublayer persists very close to the surface beneath the turbulent outer boundary layer flow, but its thickness is greatly reduced. This is the classical description of the development of a boundary layer.

The dimensionless Reynolds number is used to characterize the boundary layer flow regime :

$$\text{Re} = U L / \nu \quad (\text{II-3})$$

where  $U$  is the fluid velocity,  $L$  is the distance along the plate (characteristic length), and  $\nu$  is the kinematic viscosity of the fluid (absolute viscosity  $\div$  the fluid density).

The velocity boundary layer over a flat plate may be turbulent due to the flow separation at the leading edge. A truly laminar boundary layer may develop only at low airspeeds (or for fluids with a high kinematic viscosity).

At large Reynolds numbers the frictional shearing stress in the boundary layer is large due to the large velocity gradient across the airstream, while the shearing stress in the free airstream is quite small. Thus, one should consider at least two regions of airflow: a boundary layer near the wall where friction forces must be considered, and the region outside the boundary layer where friction forces are small and for which perfect fluid theory is a good approximation (Schlichting, 1955).

### Laminar Flow

Fluid elements are constrained to move in parallel paths in true laminar flow. All agitation of the fluid particles is on the molecular level. For a flat plate at zero incidence to a laminar airflow, the static pressure remains constant for the entire field of flow. The thickness of the velocity boundary layer,  $d_u$ , for flow which has not separated may be estimated by equating the friction forces per unit volume to the inertial forces (Schlichting, 1955) :

$$\mu U/d_u^2 \cong \rho U^2/x \quad (\text{II-4})$$

The empirical solution for  $d_u$  is :

$$d_u \sim 5 (v x/U_o)^{0.5} = 5 x/Re_x^{0.5} \quad (\text{II-5})$$

where  $x$  is the distance from the leading edge and  $Re_x$  is the Reynolds number based on this distance,  $Re_x = U_o x/v$ . The numerical factor of 5 is a correlation coefficient necessary to define the boundary layer thickness as the distance from the boundary to the point where the velocity is 99 % (some choose 95%) of the mainstream velocity (Schlichting, 1955). This definition of boundary layer thickness is somewhat arbitrary as the velocity transition from the boundary flow to the mainstream occurs asymptotically.

The diffusion (or concentration) boundary layer,  $d_d$ , is much thinner than the velocity boundary layer, as shown in Figure II-2.

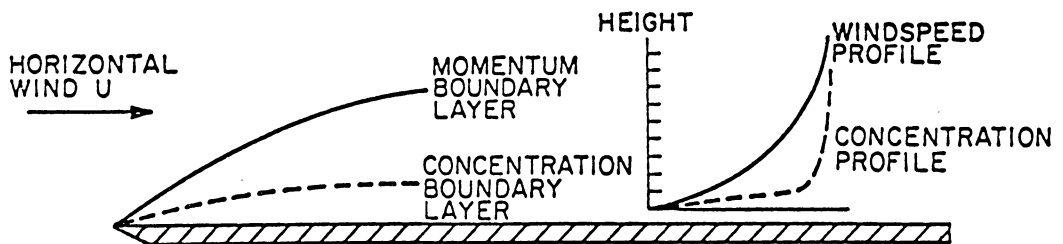


Figure II-2. The Relationship of the Momentum and Concentration Boundary Layers over a Flat Plate in a Laminar Airflow after (Davidson,1977).

Most of the resistance to mass transport is close to the boundary surface. Davies (1966) estimated the thickness of the diffusion layer for a laminar velocity boundary layer. The conservation equation for concentration of a trace material diffusing in the airflow along a flat plate is (Davies, 1966) :

$$\partial C / \partial t = D \partial^2 C / \partial z^2 - U \partial C / \partial x \quad (\text{II-6})$$

An approximate solution may be obtained if the concentration and velocity gradients are assumed to be linear from the boundary to mainstream. The thickness of the diffusion layer, as shown in Figure II-3, may be approximated as :

$$\partial^2 C / \partial z^2 \sim C_0 / d_d^2 \quad (\text{II-7})$$

where  $C_0$  is the mainstream concentration. The rate of change in the diffusion layer concentration along the boundary in the  $x$  direction, as shown in Figure II-4, is approximately :

$$\partial C / \partial x \sim C_0 / x \quad (\text{II-8})$$

It was assumed in this equation that all the diffusing substance has been captured at the surface. Figure II-5 illustrates the relationship of the velocity and the diffusion boundary layers such that :

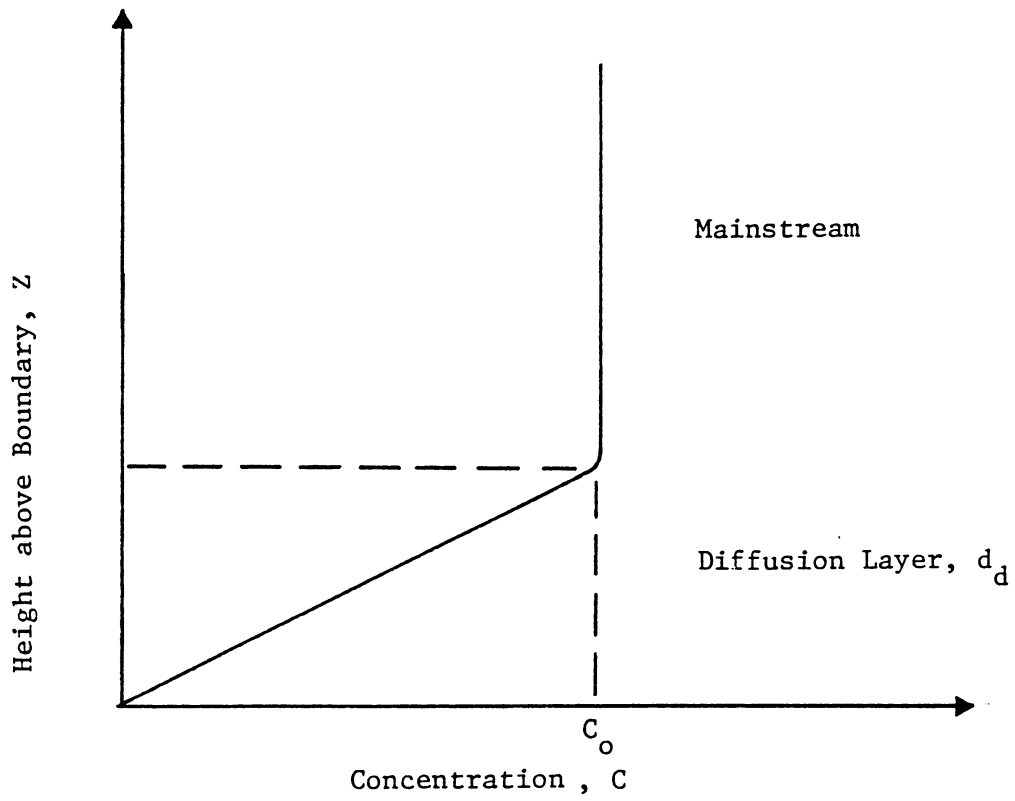


Figure II-3. The Diffusion Layer Thickness,  $d_d$ , after Davies (1966).

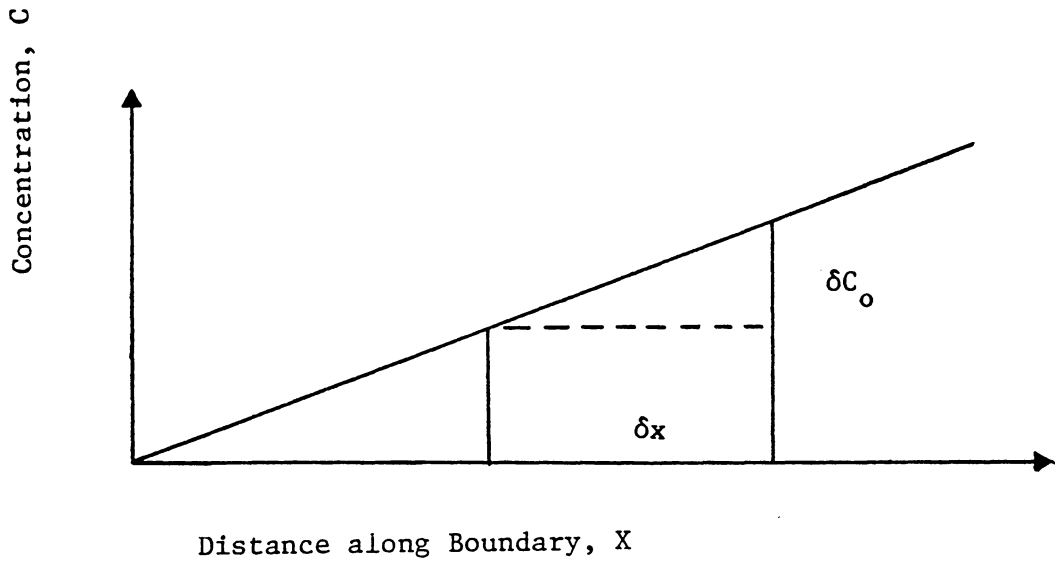


Figure II-4. The Rate of Change ( $\delta C_0 / \delta x$ ) of the Concentration along the Boundary after Davies (1966).

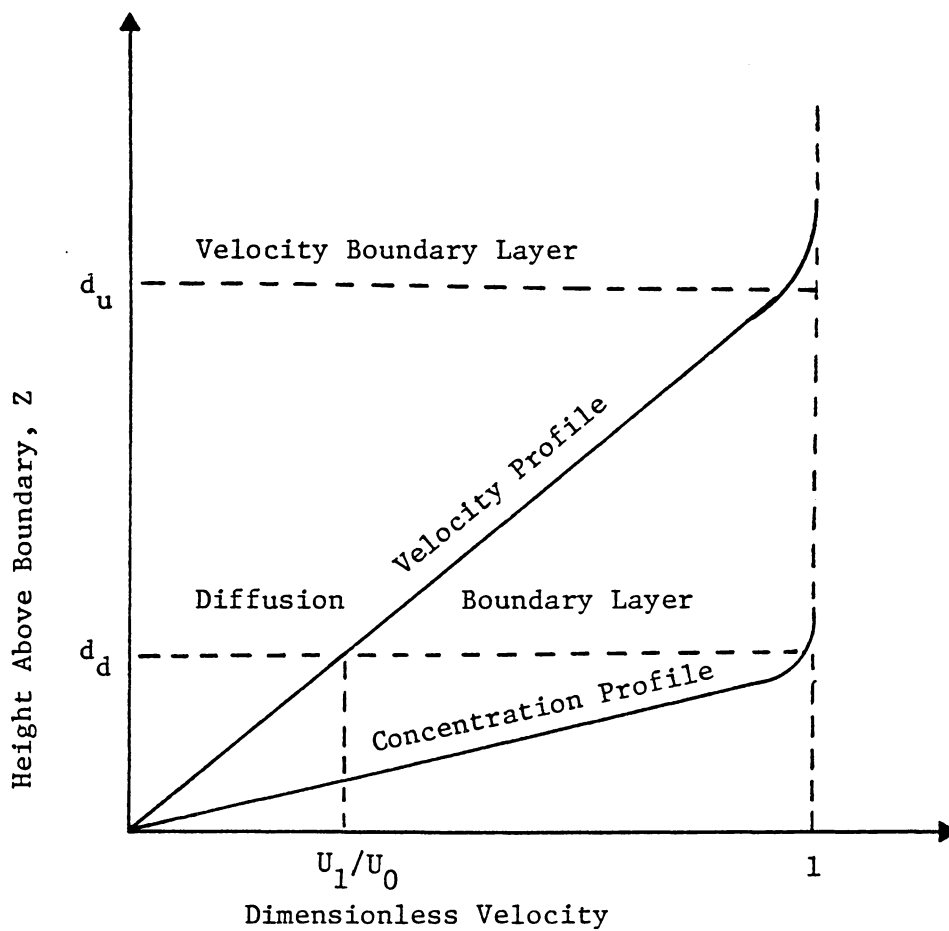


Figure II-5. The Relationship of the Velocity and Diffusion Boundary Layers after Davies (1966).



$$U_1 \sim U_o d_d/d_u \quad (\text{II-9})$$

For steady-state conditions ( $\partial C/\partial t = 0$ ), at the edge of the diffusion layer the diffusion equation becomes :

$$D \partial^2 C/\partial z^2 - U_1 \partial C/\partial x = 0 \quad (\text{II-10})$$

Substituting the estimates for  $\partial C/\partial x$  and  $U_1$  into Equation (II-6) gives :

$$D C_o/d_d^2 - (C_o U_o d_d)/(x d_u) = 0 \quad (\text{II-11})$$

and solving for  $d_d$  :

$$d_d^3 = D x d_u/U_o \quad (\text{II-12})$$

or:

$$d_d = (D x d_u/U_o)^{0.333} \quad (\text{II-13})$$

Table II-1 lists the theoretical thicknesses of the velocity boundary layer and the diffusion boundary layer for one micron diameter particles in laminar flow over a smooth, flat plate.

TABLE II-1. THE THEORETICAL THICKNESSES OF THE LAMINAR  
VELOCITY AND PARTICLE DIFFUSION BOUNDARY LAYERS OVER  
A SMOOTH FLAT PLATE

Distance from leading edge, x (cm)	Reynolds number, $Re_x$ (dimensionless)	Approximate thickness, $d_u$ ( $\mu\text{m}$ )	Approximate thickness, $d_d$ ( $\mu\text{m}$ )
1	1,333	1369	5.7
5	6,667	3062	13
10	13,333	4330	18
20	26,667	6124	25
50	66,667	9682	40

The assumed mean airspeed is 2.0 m/s, and the mean particle diameter is 1.0  $\mu\text{m}$  for which the diffusion coefficient,  $D$ , is  $2.7 \times 10^{-7} \text{ cm}^2/\text{s}$ .

### Flow Separation

The decelerated fluid elements do not always remain within the boundary layer along the entire length of the boundary. The boundary layer may increase in thickness to the point that a balance of the friction and pressure gradient forces causes the flow in the boundary layer to reverse; as a result the decelerated fluid elements are forced outside the boundary layer. Boundary layer separation occurs when the fluid particles become separated from the solid boundary.

Flow separation (i.e., boundary layer separation) occurs primarily in the airflow near bluff bodies, such as cylinders, spheres, or blunt-edged flat plates. However, flow separation may occur on a sharp-edged flat plate if the plate is rotated so that the angle of incidence with the airflow is greater than approximately ten degrees (Schlichting, 1955). When flow separation occurs on a flat plate, a region of decelerated airflow (a wake) exists in which vortices are formed and the pressure distribution is no longer constant. Flow separation creates a large amount of turbulence and drastically alters the flow lines.

### Turbulent Flow

Turbulent flow occurs when the fluid elements stop moving in straight lines and develop irregular fluctuations in their streamlines. The fluid elements collide with each other and disperse throughout the fluid. This causes mixing to occur.

The thickness of the turbulent velocity boundary layer,  $d_v$ ,

near a flat plate at zero incidence may be approximated by the following equation (Schlichting, 1955):

$$d_v = 0.37 x / Re_x^{0.2} \quad \text{for } 5 \times 10^5 < Re_x < 10^7$$

(II-14)

Estimation of the thickness of the diffusion boundary layer in turbulent flow is discussed in a following section on eddy diffusion.

CHAPTER III  
DRY DEPOSITION MECHANISMS

There are three types of forces acting on solid particles which cause them to deposit from a moving fluid: external forces (such as gravity), fluid resistance forces, and the forces resulting from particle interaction. There are also numerous other factors influencing dry deposition as shown in Table III-1. However, the primary dry deposition mechanisms for particles are generally regarded to be gravitational settling, inertial impaction, Brownian diffusion, and eddy diffusion. Although electrostatic attraction has not been identified as a primary mechanism, it has been included in the following descriptions of dry deposition mechanisms.

Gravitational Settling

Gravitational settling or sedimentation occurs when the earth's gravitational attraction for a particle is greater than the aerodynamic drag on the particle. Sedimentation is an important dry deposition mechanism for particles which are dense or have large diameters (greater than approximately 10 microns). Acidic aerosol particles generally do not settle appreciably due to their small individual size.

Spherical particles falling through air rapidly attain a terminal velocity,  $V_t$ , that may be predicted by Stokes' law:

$$V_t = ((\rho_p - \rho_f) g D_p^2) / (18 \mu_f) \quad (\text{III-1})$$

TABLE III-1. SOME FACTORS AFFECTING DRY DEPOSITION

Micrometeorological	Surface	Depositing Material	
		Particles	Gases
Stability	Boundary Layer	Agglomeration	Reactivity
Turbulence	Biotic Growths	Density	Diffusivity
Zero-plane Height	Canopy Growth	Shape	Solubility
Flow Separation	Physical Structure	Electrostatics	
Friction Velocity	Chemical Structure	Resuspension	
Relative Humidity	Senescence	Hygroscopicity	
Temperature	Leaf Flutter	Diffusivity	
Seasonal Variation	Water		
Surface Heating	Prior Deposition		
Terrain	Electrostatic Properties		
Wind Velocity			

After Sehmel (1980).

where  $\rho_p$  and  $\rho_f$  are the particle and fluid densities,  $g$  is the acceleration of gravity,  $\mu_f$  is the absolute viscosity of the fluid, and  $D_p$  is the particle diameter.

Terminal settling velocities for particle diameters from 0.001 to 100 microns are listed in Table III-2. The error in using the Stokes equation will not exceed one percent for particle diameters up to approximately thirty microns (BGI, Inc., 1980).

As the particle size increases, the inertial effect becomes important. The dimensionless particle Reynolds number,  $Re_p$ , is the ratio of the inertial forces to the viscous forces:

$$\begin{aligned} Re_p &= (\rho_f v_t^2 / D_p) / (\mu_f v_t / D_p^2) = (\rho_f v_t D_p) / \mu_f \\ &= v_t D_p / \nu_f \end{aligned} \quad \text{(III-2)}$$

where  $\nu_f$  is the kinematic viscosity of the fluid ( $\mu/\rho$ ).

At large  $Re_p$ , Stokes' law overestimates the terminal settling velocity. Davies (1966) has developed a lengthy formula based on the particle drag coefficient to predict the terminal velocity for  $Re_p$  up to 4.0 .

Particle mobility increases as the size of a particle approaches that of the air molecules. Stokes' law underestimates the settling velocity for aerosols with a diameter less than approximately one micron and must be modified by the Cunningham slip correction factor (Dennis, 1976).

Most deposition theory has been developed for spherical particles;

TABLE III-2. DYNAMIC CHARACTERISTICS OF PARTICLES \*

Diameter ( $\mu\text{m}$ )	0.001	0.01	0.1	1.0	10.0	100
Slip Correction						
Factor .....	217	22.2	2.87	1.16	1.02	1.001
Terminal Gravitational Settling Velocity						
(cm/s) .....	6.53-07	6.69-06	8.63-05	3.50-03	3.06-01	2.48
Diffusion Coefficient						
( $\text{cm}^2/\text{s}$ ) ....	5.11-02	5.23-04	6.75-06	2.74-07	2.39-08	2.36-09
Mobility						
(s/g) .....	1.27+12	1.30+10	1.68+08	6.82+06	5.96+05	5.87+04
Relaxation						
Time (s) ...	6.66-10	6.82-09	8.80-08	3.57-06	3.12-04	3.07-02

\* Unit density spheres.

After BGI, Inc. (1980).



non-spherical particles may be characterized by how their behavior deviates from the behavior of spherical particles through the use of a shape factor. Airborne particles may also be classified according to their "aerodynamic diameter" to overcome the variability in shape and density. Thus "aerodynamic diameter" is defined as a unit density sphere that has the same impaction performance as that of the particle in question (Ellenbecker, 1982).

### Inertial Impaction

Inertial deposition or impaction occurs when particles are unable to change their direction as rapidly as the fluid streamlines around an obstacle, and the particles instead impact on the object due to their inertia. Impaction is an important dry deposition mechanism for particles with diameters greater than approximately one micrometer (Friedlander, 1977). Significant particle impaction may result from the velocity imposed on a particle by the eddy turbulence of the atmosphere (Belot and Gauthier, 1975).

The Stokes' number (I) is used to characterize the impaction phenomenon and is defined as follows (Dennis, 1976) :

$$I = (C_c \rho_p D_p^2 U) / (18 \mu_f L) \quad (\text{III-3})$$

where U is the mean airstream velocity,  $C_c$  is the Cunningham slip correction factor, and L is the characteristic length, such as the obstacle diameter or the viscous sublayer thickness. The theoretical efficiency of impaction increases with increasing

particle diameter or windspeed but particle rebound also increases. Surface characteristics, such as stickiness or protrusions, are especially important in limiting particle bounce-off and resuspension of deposited particles.

Interception is usually considered as a subcase of inertial impaction. Interception occurs when a particle streamline approaches within one particle radius of the collector surface, so the particle touches and sticks to the collector.

### Brownian Diffusion

Microscale diffusion is due to Brownian motion, the random movement exhibited by small particles in a fluid as a result of the forces exerted on them by the surrounding fluid molecules. The intensity of the Brownian motion increases as the particle size decreases and is especially important for particles less than approximately one micrometer in diameter. The Brownian diffusion coefficient,  $D$ , of a particle is related to the properties of the fluid and may be determined by the following equation (Fuchs, 1964).

$$D = k B T_a \quad (\text{in cm}^2/\text{sec}) \quad (\text{III-4})$$

where  $k$  is the Boltzmann constant and  $T_a$  is the absolute temperature. The particle mobility,  $B$ , after Dennis (1976) is :

$$B = C_c / (3 \pi \mu_f D_p) \quad (\text{III-5})$$

where  $C_c$  is the Cunningham slip correction factor. Thus, the diffusion coefficient (and rate of diffusion) increases as the particle diameter decreases. Table III-2 also lists diffusion coefficients for particle diameters from 0.001 to 100 microns.

The deposition velocity due to Brownian diffusion may be estimated by dividing the diffusion coefficient value by the thickness of the diffusion layer, although it is sometimes quite difficult to determine a precise value for the diffusion layer thickness.

### Eddy Diffusion

The transfer mechanism resulting from turbulent eddies in a flowing fluid is called eddy diffusion. Particles may deposit due to eddy diffusion at a rate much greater than would be predicted by sedimentation or Brownian diffusion theory.

The particle momentum diffusivity is frequently assumed equal to the fluid momentum diffusivity. This is a good assumption for very small particles, when the dimensionless Schmidt number ( $v_f/D_p$ ) is approximately one. However, this assumption becomes questionable as the particle diameter increases above one micron (Rouhiainen and Stachiewicz, 1970). El-Shobokshy and Ismail (1980) have shown that assuming particle diffusivity equal to the momentum diffusivity underestimates particle deposition velocity.

The investigations of eddy diffusivity by von Karman resulted in the use of dimensionless expressions for mean velocity and length by defining the friction velocity,  $u_*$  :

$$u_* = - (\tau_0 / \rho_f)^{0.5} \quad (\text{III-6})$$

where  $\tau_0$  is the tangential shearing stress. The friction velocity is comparable to the mean turbulent velocity value where the turbulence is greatest (Davies, 1966).

Dimensionless variables are used to generalize the analysis of turbulent boundary layers :

$$Z_+ = z u_* / \nu \quad \text{and} \quad U_+ = u / u_* \quad (\text{III-7})$$

where  $z$  is the distance normal to the surface and  $u$  is the mean fluid velocity parallel to the surface.

The value of the friction velocity  $u_*$  (and thus the eddy diffusivity) depends on the airspeed, distance from the leading edge, and the surface roughness. El-Shobokshy and Ismail (1980) have determined that the deposition of particles with diameters up to five microns is significantly affected by boundary surface roughness even though the surface may be considered smooth.

The velocity profile may not be described by a single equation involving  $Z_+$  throughout a turbulent boundary layer. Thus, the surface boundary layer was divided into three flow regimes by von Karman.

- the viscous sublayer, where  $Z_+ < 5$
- the buffer or transition region, where  $5 < Z_+ < 30$
- the main boundary layer, where  $Z_+ > 30$

These regimes were developed for pipe flow but are valid for flow over a flat plate as well.

Lin et al. (1953) developed the following empirical formulas for the eddy diffusion coefficient,  $K$ , by experimentation.

$$K = v \left( Z_+ / 14.5 \right)^3 \quad \text{viscous sublayer} \quad (\text{III-8})$$

$$K = v \left[ (Z_+ / 5) - 0.959 \right] \quad \text{transition region} \quad (\text{III-9})$$

The turbulence decreases as the boundary is approached; thus the magnitude of the eddy diffusion coefficient decreases.

### Electrostatic Attraction

The electrostatic charge associated with an aerosol consists of an excess or deficiency of electrons attached to the aerosol. The excess charge is assumed to reside on the aerosol surface (Harper, 1967). Most aerosol production mechanisms, such as combustion, result in a highly charged aerosol (Bricard and Pradell, 1966). Aerosols may also have naturally acquired charges as the result of electron transfer during contact or separation (i.e., nebulization), or as the result of free ion diffusion in the atmosphere.

The net charge on an aerosol cloud may be quite small even if the individual particles are highly charged. Whitby and Liu (1966) calculated the charge distribution for particles with diameters between 0.01 and 0.1 microns. The larger particles

generally had a higher charge associated with them than the smaller particles. The number of charges acquired by a particle is limited by the breakdown strength (i.e., discharge) of the surrounding air, which is about  $1.7 \times 10^{10}$  electrostatic units/cm for dry air.

Natural background radioactive or cosmic radiations produce bipolar ions in the atmosphere (Bricard and Pradell, 1966). After some time, ambient aerosols will acquire an equilibrium charge distribution as predicted by Boltzmann's Law :

$$N_n / N_0 = \exp [(-n^2 e^2)/(D_p k T_a)] \quad (\text{III-10})$$

where  $N_n$  and  $N_0$  are the relative number of particles carrying  $n$  and 0 units of charge,  $D_p$  is the particle diameter,  $k$  is Boltzmann's constant,  $T_a$  is the absolute temperature, and  $e$  is the elementary unit of charge.

Table III-3 shows the predicted charge distribution following Boltzmann's Law. The majority of the particles less than one micron are neutral or singly charged (Agarwal and Sem, 1978).

When an aerosol or a stationary object in an air stream is electrostatically charged (or when both are charged) the trajectory of the aerosol past the object may be affected such that it will collide with the stationary object (Moore, 1976). Electrostatic attraction may therefore be an important mechanism for transporting particles across the viscous sublayer. The force of attraction (or repulsion) of electrostatic charges follows Coulombs Law :

TABLE III-3. CHARGE DISTRIBUTION ON AEROSOLS \*

Diameter ( $\mu\text{m}$ )	Percent of Particles Carrying, $n_p$ , Elementary Electrostatic Charge Units								
	$n_p = -4$	-3	-2	-1	0	+1	+2	+3	+4
0.01				0.34	99.32	0.34			
0.04		0.23	16.22	67.10	16.22	0.23			
0.10		0.26	4.39	24.09	42.52	24.39	0.26		
0.40	2.19	5.92	12.05	18.44	21.26	18.44	12.05	5.92	2.19
1.0	5.42	8.06	10.71	12.70	13.45	12.70	10.71	8.06	5.42

\* According to Boltzmann's Law.

After Agarwal and Sem (1978).

$$F \propto (Q_p Q_o) / r^2 \quad (\text{III-11})$$

where  $Q_p$  and  $Q_o$  are the magnitude of the electrostatic charges on the particle and object and  $r$  is the distance separating the charges on the particle and object.

Five different relevant electrostatic attraction and repulsion situations have been identified and mathematically characterized by Ranz and Wong (1952) :

- 1) A charged particle and an unlike point charge on the collector.
- 2) A charged particle and its image in the collector.
- 3) A point charge on the collector and its image in the aerosol.
- 4) A repulsion of the aerosol being collected by the aerosol cloud of which it is a part.
- 5) A charged particle attraction to a collector having a charge induced by the aerosol cloud surrounding the collector.

The so-called "image charge" is a phenomenon whereby a surface without a net charge (i.e., neutral) has a surface charge redistribution induced by a nearby concentrated point charge. The surface develops an area of negative charge and an area of positive charge. The induced electrostatic surface charge occurs more readily for conductors as their electrons are more mobile.

The coulombic attraction force is the simplest to describe mathematically, and its magnitude is generally greater than the image attraction force (Kraemer and Johnstone, 1952). Image



attraction may be important in the situation where the collector charge has been neutralized. The image force term considerably complicates the mathematical expression for the attraction of aerosols to a surface (Kraemer and Johnstone, 1952).

Brock and Marlow (1975) compared the deposition velocity resulting from an electric field,  $V_e$ , to that due to Brownian diffusion,  $V_d$  :

$$V_e / V_d \sim Q e d_d E / kT \quad (\text{III-12})$$

where  $d_d$  is the thickness of the diffusion boundary layer,  $Q$  is the number of elementary charges on the particle,  $e$  is the elementary unit of charge,  $E$  is the electric field strength,  $k$  is Boltzmann's constant, and  $T$  is the absolute temperature.

Brock and Marlow (1975) considered the case when  $d_d$  might be large ( $0.001 \text{ cm} < d_d < 1 \text{ cm}$ ), which might occur in a stable atmosphere (i.e., a temperature inversion with low wind speed). They used a value of  $T = 300$  Kelvin,  $Q = 1$ , and  $E$  ranged from 200 to 400 volts/m, such that the ratio of  $V_e / V_d$  was :

$$0.1 < V_e / V_d < 160 \quad (\text{III-13})$$

Brock and Marlow (1975) concluded that even weakly charged ( $Q = 1$ ) small particles (diameter  $< 0.1$  micron) may be electrostatically deposited during inversion conditions when the deposition due to diffusion is minimal.

## CHAPTER IV

### PARTICLE DEPOSITION THEORY

The development of a general model to quantify particle deposition is difficult. The conversion from one primary deposition mechanism to another primary mechanism may occur very rapidly. For example, a satisfactory theory to predict the transition from deposition by Brownian diffusion to deposition by inertial impaction has not yet been developed (Friedlander, 1977).

Rouhiainen and Stachiewicz (1970) believe that some researchers have made assumptions that cannot be theoretically defended in order that their atmospheric deposition models agree with the experimental results. Many of the deposition theories do not consider particle bounce or re-entrainment. This may be significant for particles with diameters greater than approximately one micrometer.

Several theories for the deposition of monodisperse particles are presented here. In the most significant studies of particle deposition in turbulent pipe flow, the theory and experimental results did correlate. Particle deposition in pipe flow is analogous to deposition on a flat plate.

#### Stagnant Film Theory

This theory describes steady-state particle transport in an isothermal, stationary gas. A one-dimensional equation is derived from Fick's second law of diffusion and the terminal settling velocity (Friedlander, 1977). The total flux,  $J$ , to a surface is :

$$J = \int_0^b -D \left( \frac{dC}{dz} \right) - V_t C \quad (\text{IV-1})$$

The flux is considered negative when it is toward the surface. The mathematical equivalent to the surface collecting all the particles within one particle radius is  $C = 0$ , even though there are particles collected on the surface. When the previous equation is integrated from concentration  $C = 0$  at  $z = 0$  at the surface to  $C = C_\infty$  at  $z = b$  (where  $b$  is the diffusion layer thickness) :

$$J = -(V_t C_\infty) / [1 - e^{(-V_t b/D)}] \quad (\text{IV-2})$$

where  $C_\infty$  is the mean particle concentration in the main airstream measured at some distance  $b$  from the surface (i.e., diffusion layer thickness). If the gravitational settling term is much larger than the Brownian diffusion term ( $V_t \gg D/b$ ), the particle flux is due primarily to sedimentation. If the gravitational settling term is much less than the diffusion term, the particle flux is due primarily to diffusion.

This theory is presented as a method of predicting particle deposition in calm conditions where an aerodynamic boundary layer is not developed.

### Deposition Across a Laminar Boundary Layer

Friedlander (1977) has also presented the theory to predict the diffusion rate of small particles across a laminar boundary layer based on the following steady-state equation for convective diffusion:

$$U(\partial C/\partial x) + W(\partial C/\partial Z) = D(\partial^2 C/\partial Z^2) \quad (\text{IV-3})$$

The transfer of matter across a boundary layer is quite similar to the transfer of heat in forced convection. Chamberlain (1960) applied this principle in order to solve the equation for convective diffusion. The total flux of particles to the surface between the leading edge and the point  $x$  is :

$$\begin{aligned} J &= (0.678 D^{0.666} U^{0.5} C_{\infty}) / (x^{0.5} \mu^{0.125}) \\ &= 0.678 (D/x) \text{Re}^{0.5} \text{Sc}^{0.333} C_{\infty} \quad (\text{IV-4}) \end{aligned}$$

where  $x$  is the horizontal distance from the leading edge,  $U$  is the mainstream air velocity, and  $C_{\infty}$  is the mainstream particle concentration. The factor 0.678 changes with the surface characteristics, and the angle of incidence of the flat plate to the airflow.

For example, Davidson (1977) found this factor to be 0.661 for a flat plate normal to the air flow. Davidson's predictions of the particle flux to a flat plate parallel and to a flat plate normal

to the air flow were almost identical.

This theory considers only the diffusion mechanism and would be most applicable to small particles or gases which have no significant settling velocity. A laminar boundary layer will occur at low Reynolds numbers (i.e., near the leading edge or at low windspeeds).

### Deposition Across a Turbulent Boundary Layer

The characterization of a turbulent boundary layer is more difficult than for a laminar boundary layer due to the varying degrees of turbulence. Turbulence is a function of the tangential shear stress,  $\tau_0$ . The tangential shear stress for the viscous sublayer is at the boundary surface while the tangential shear stress in a turbulent boundary layer is based on the rate of momentum transfer perpendicular to the surface.

Momentum transfer across the streamlines of the mean flow results primarily from the turbulence; this causes an enhanced drag between adjacent layers of the fluid (Davies, 1966). However, the final transfer of the longitudinal stress to a smooth surface occurs in the viscous sublayer. Turbulence exists in this layer in both the normal and longitudinal directions but the normal turbulence (which promotes eddy diffusion) is smaller and dies away more quickly as the surface is approached.

The rate of deposition is enhanced in a turbulent flow since the diffusion layer adjacent to the surface is much thinner and the eddy turbulence maintains the mainstream particle concentration

near to the viscous sublayer (i.e., closer to the boundary surface).

Friedlander and Johnstone (1957) and Sehmel (1971) developed a theory for particle deposition in turbulent flow based on a one-dimensional steady-state equation for mass flux density to a smooth surface. The instantaneous particle flux,  $J$ , to a flat surface may be predicted by the following equation :

$$J = -(D + K)dC/dZ - V_t C \quad (\text{IV-5})$$

where  $D$  is the Brownian diffusion coefficient,  $K$  is the eddy diffusion coefficient, and  $V_t$  is the terminal settling velocity.

The basic assumptions of this model are: particles diffuse at a constant flux from a uniform particle concentration, agglomeration or reentrainment does not occur, and the terminal settling velocity describes the gravitational effects (Sehmel, 1971). The particle flux is considered negative when it is toward the surface; the particle deposition velocity,  $V_d$ , is always considered positive.

The theory for particle deposition in turbulent flow is quite controversial. There have been numerous revisions and additions to the original Friedlander and Johnstone (1957) theory. Owen (1960) considered particle diffusivity to depend only on the characteristics of the airflow. Liu and Agarwal (1974) assumed a particle would be eddy transported within one stopping distance of the boundary after which inertia would transport it to the boundary. Liu and Ilori (1973) considered an additional

particle diffusivity, analogous to Brownian diffusion, such that the total effective particle diffusivity,  $K_t$ , is given as the sum of the fluid eddy and the particle diffusivities :

$$K_t = K + U_n^2 \tau \quad (\text{IV-6})$$

where the dimensionless form of  $U_n$ , the normal component of the turbulent velocity has been defined by Davies (1966) :

$$U_{n+} = U_n / u_* = Z_+ / (Z_+ + 10) \quad (\text{IV-7})$$

The particle relaxation time,  $\tau$ , is given as :

$$\tau = (C_c \rho_p r_p^2) / (4.5\mu) \quad (\text{IV-8})$$

The dimensionless relaxation time,  $\tau_+$ , is then defined as :

$$\tau_+ = (\tau u_*^2) / \nu \quad (\text{IV-9})$$

Equation (IV-6) may written in a dimensionless form with the dimensionless eddy diffusivity,  $K_+$ , and the dimensionless effective particle diffusivity,  $K_{t+}$ , which will be used in later formulations :

$$K_{t+} = K_+ + U_{n+}^2 \tau_+ \quad (\text{IV-10})$$

Browne (1974) considered surface roughness and predicted

that at a distance from the boundary equal to the particle stopping distance,  $S$ , a particle would be unable to stop before it touches and remains at the boundary, as shown in Figure IV-1. El-Shobokshy and Ismail (1983) have shown that the surface roughness coefficient is approximately zero for a smooth surface, such as acrylic. Therefore, surface roughness was not considered in developing this model. The particle stopping distance is defined as :

$$S = (\rho_p d_p^2 U_n) / 18 \mu = \tau U_n \quad (\text{IV-11})$$

El-Shobokshy and Ismail (1980) followed the surface roughness approach of Browne (1974) and the approach of Lin, Moulton, and Putnam (1951) to define the eddy diffusivity with separate Equations (III-8 and III-9) for the sublayer ( $0 < Z_+ < 5$ ) and transition regions ( $0 < Z_+ < 30$ ).

The following equation for mass transfer to a flat surface is derived from the Equation (IV-5) :

$$J + V_t C = - (D/v + K_t/v) dC/dZ_+ \quad (\text{IV-12})$$

where  $Z_+ = zu_* / v$ , and  $S_+ = Su_* / v$ . Equation (IV-12) may then be rearranged as :

$$- \int_{C_0}^0 (u_* dC) / (J + V_t C) = \int_{Z_+}^{S_+} dZ_+ / (D/v + K_t/v) \quad (\text{IV-13})$$

The integration limits are inverted due to the negative sign.



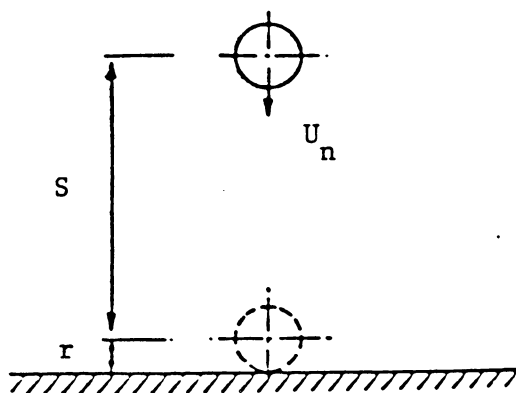


Figure IV-1. The Relationship of the Particle Stopping Distance,  $S$ , to the Smooth Surface, after Browne (1974).

The upper limits of integration are such that particle concentration would be  $C = 0$  at one particle stopping distance from the surface,  $Z_+ = S_+$ . At the lower limits of integration  $C = C_0$ , the mainstream concentration, and  $Z_+ = 30$ , the upper boundary of the transition region. The following equation is the result after Equations (III-8 and III-9) are substituted into Equation (IV-10) and then into Equation (IV-13) :

$$\begin{aligned}
 -\int_{C_0}^0 (u_*^* dC / J + V_t C) &= \int_5^{S_+} dz_+ / [(D/v + (Z_+/14.5)^3 \\
 &+ (Z_+/Z_+ + 10)^2 \tau_+ ] + \int_{30}^5 dz_+ / [(Z_+/5) - 0.959 \\
 &+ (Z_+/Z_+ + 10)^2 \tau_+ ] \qquad \qquad \qquad (IV-14)
 \end{aligned}$$

Brownian diffusion is considered insignificant compared to the eddy diffusion in the transition region and was eliminated from this term in Equation (IV-14). After integration Equation (IV-14) reduces to the particle flux :

$$J = (V_t C_0 A) / (1 - A) \qquad \qquad \qquad (IV-15)$$

$$\text{where } A = \exp (-V_t \text{INT} / u_*^*) \qquad \qquad \qquad (IV-16)$$

and where INT is the right side of Equation (IV-14),  $\text{INT} = I_s + I_t$ . The integral for the sublayer region is  $I_s$ , and the integral for

the transition region is  $I_t$ . After substitution of the appropriate values for  $D$ ,  $v$ , and  $\tau_+$ , the integrals  $I_s$  and  $I_t$  may be solved by a numerical computation method (Hewlett-Packard Company, 1979). When Equation (IV-15) is rearranged, the deposition velocity may then be calculated from the following equation :

$$V_d = J/C_0 = V_t / (1-1/A) \quad (IV-17)$$

The lower limit for the predicted particle deposition velocity is the terminal gravitational settling velocity. If the diffusional resistance is high ( $INT$  is a large negative number,  $A$  would approach infinity and  $1/A$  would approach zero), the deposition velocity will be equal to the gravitational settling velocity. If the diffusional resistance is low, the deposition velocity will be greater than the gravitational settling velocity.

### Intermittent Turbulence Theory

Rouhianen and Stachiewicz (1970) suggest that a proper theory of particle deposition must be based on a mathematical description of the turbulent motion of the fluid and the response of the particle to the fluid motion.

Recent investigations have redefined the problem of particle deposition in turbulent flow with a "surface renewal" or intermittent turbulence theory, whereby particles are transported rather than diffused to the surface by an unsteady, inhomogeneous transport mechanism resulting from vortex formation and shedding on the

boundary surface (Slinn, 1974). Slinn believes the following equation for deposition velocity correlates best with previous experimental results for turbulent flow :

$$V_d = C_d \bar{U} (v/D)^{-n} \quad (\text{IV-18})$$

where  $n$  may vary from 0.5 to 1.0 depending on the turbulence, surface structure, and particle size (Hicks and Slinn, 1982). Slinn used a value of  $n = 0.6$  for smooth surfaces,  $n = 0.66$  for rough surfaces in turbulent flow, and  $n = 0.5$  for the stagnant film theory. The drag coefficient,  $C_d$ , must be experimentally determined. This theory stresses the inverse proportionality of the deposition velocity with the particle diffusion coefficient.

## CHAPTER V

### PARTICLE RESUSPENSION

Although the major thrust of this study is to investigate deposition, particle resuspension can not be completely ignored. One must remember that the net dry deposition flux to a surface is in fact the gross particle deposition minus particle resuspension. In most dry deposition models the prediction of particle capture is based almost entirely on the transport mechanism (Dahneke, 1971). It is frequently assumed that a particle will always be captured upon contact with a surface. This assumption has proven correct in many applications to pipe flow (Esmen, Ziegler, and Whitfield, 1978). However, additional investigation of this subject is necessary (Davidson, Miller, and Pleskow, 1982).

A brief review of particle adhesion and resuspension is presented.

#### Particle Adhesion

The phenomenon of a particle attaching to a surface or to another particle is called adherence; the strength of the bond is the force of adhesion (Corn, 1966). This force of adhesion can be quite large for small particles. For example, dust collects on the ceiling of a room; the force of adhesion is greater than the gravitational settling force.

A discussion follows of the factors affecting particle adhesion, such as: London-van der Waals forces, electrostatic attraction,

relative humidity, contact area, and surface characteristics. Several of these factors are interrelated, such as electrostatic attraction and relative humidity; temperature and relative humidity.

#### London-van der Waals Forces

The London-van der Waals force is the force between two atoms or molecules due to the attraction of the charged subatomic particles. Atoms or molecules which are electrically neutral may be attracted to each other. This force is atomic in nature and should not be confused with electrostatic attraction which is entirely a surface phenomenon. The magnitude of the van der Waals force,  $F$ , is strongly inversely dependent on the distance of separation,  $r$ , of the surfaces (Corn, 1966) :

$$F \propto r^{-7}$$

The magnitude of this force decreases much more rapidly than the electrostatic force as the separation distance increases. Gases or liquids absorbed to a surface may prevent close particle-surface contact and reduce the van der Waals force. This force becomes less important as an adhesion mechanism as particle size increases.

#### Electrostatic Forces

A particle may be attracted to another particle or surface due to the attraction of opposite electrostatic charges . The

electrostatic force may serve to attract particles across the viscous sublayer as well as to ensure particle retention. As previously discussed, the magnitude of the attractive force is dependent on the number of the electrostatic charges and on the inverse square of the separation distance. Large particles generally have a greater electrostatic charge, so the magnitude of the electrostatic attractive force increases with particle size.

The greatest electrostatic charge build-up occurs at low humidities (less than 40 percent). At high humidities a thin layer of water only a few molecules thick may coat the surface, conduct electrostatic charge, and serve as an effective grounding mechanism.

Corn (1961) reported that particles and surfaces may hold electrostatic charge for some time. The effect of contact on charge redistribution is not well known. "As soon as a charged particle touches another charged particle or surface, charge may or not be reduced by conduction or neutralization, or further charge can develop by contact charging" (Corn, 1966).

#### Relative Humidity and Temperature

Relative humidity is a measure of the water vapor content of air at a specific temperature. Particle adhesion generally increases with relative humidity due to the greater possibility of the development of a surface water film. The surface tension resulting from the thin surface film enhances particle adhesion

(Corn, 1961). For example, most individuals have experienced the difficulty of separating two smooth plates sandwiching a thin water film.

The amount of water vapor that air may contain increases with temperature; however, the surface tension of a liquid generally decreases with temperature. A quantitative theory of the effect of relative humidity or temperature on particle adhesion has not been presented in the literature, probably because these effects are so dependent on the nature of the specific substances in question.

#### Contact Area

It has been found in experimental studies that increased surface roughness resulted in decreased particle adhesion (Corn and Stein, 1965). The greater surface roughness decreased the area between the contacting surfaces and the adhesion force was reduced. Esmen, Ziegler, and Whitfield (1978) found that particle flattening on impact was a major factor in particle adhesion; particle flattening was also a major factor in particle bounce-off.

#### Resuspension

A particle will become resuspended in an airstream when the aerodynamic drag and lift forces exceed the force of particle adhesion. A brief description of particle resuspension is presented in the three following subcases: bounce-off, re-entrainment, and agglomerates.



### Bounce-off

When a particle strikes a surface it may stick or bounce-off. The particle may bounce a short or long distance from the surface into the airstream depending on the rebound force (Sehmel, 1971). A particle may also slide or roll before becoming resuspended (Corn, 1966). The particle which rebounds only a short distance may soon collide with the surface again and adhere after this collision.

Sehmel (1971) reported that particle deposition velocity increases with particle diameter and Reynolds number if the surface is a perfect sink for particles. However, the prediction of the deposition velocity is generally more difficult; most surfaces do not behave as a perfect particle sink. Particle rebound increases as the particle diameter increases. As a result the particle concentration may be greater just above the viscous sublayer than in the main airstream (Sehmel, 1971). This higher concentration may enhance particle diffusion toward the surface so that particle deposition increases, but deposition may decrease if particle diffusion away from the surface increases. A high particle concentration just above the sublayer will not develop if particles bounce great distances from the surface.

Small particles generally adhere to a surface if they collide at a low velocity; particles usually bounce-off after high velocity collisions (Dahneke, 1973). Chamberlain and Little (1981) reported that the deposition efficiency was quite low when the approach velocity exceeded one m/s for five micron diameter particles

and 0.5 m/s for ten micron particles. This study is primarily interested in small particles (diameter less than 2 microns), however, there is little information on the resuspension of this size particle.

Particle bounce is also increased by previously-deposited particles and other protuberances. A particle may strike a previously deposited particle at such an angle of approach that it is deflected back into the airstream (the particle might also be deflected to the surface). Leaf hairs may increase the sublayer thickness and reduce bounce-off by cushioning the particle collision (Chamberlain and Little, 1981). When leaf hairs are numerous, a particle is likely to impact on another leaf hair as it bounces-off.

The theory for particle bounce-off is well developed; Dahneke (1972) has theoretically described the influence of flattening on particle adhesion and bounce-off.

#### Re-entrainment

Sehmel (1971) found that even two micron particles could be re-entrained from untreated surfaces. Re-entrainment was always greater for untreated surfaces than sticky surfaces, apparently the surface film absorbed a portion of the particle impact force and also increased particle adhesion.

When the particle diameter is less than the viscous sublayer thickness, the possibility of re-entrainment is lessened. Sehmel (1971) hypothesized that the re-entrainment of 14 micron diameter

particles resulted from turbulent eddies which penetrated the viscous sublayer closer than 14 microns. Corn and Stein (1965) found that a much higher air velocity was required to penetrate and dislodge particles within the sublayer. An example of the difficulty of removing a particle embedded in the viscous sublayer is that dust collects on the surface of a recently washed automobile and adheres regardless of how fast the automobile is driven.

### Agglomerates

The deposition-resuspension mechanism may change the physical properties of a particle (Slinn, 1975). Small particles may become attached to larger previously-deposited particles. If re-entrainment occurs, the small particles may become resuspended in one group.

Belot and Gauthier (1975) also reported on the tendency of small particles to become attached to larger particles on a surface and form agglomerates from three to 100 microns in diameter. The agglomerates appeared to be more easily removed from the surface than individual particles. They also hypothesized that the individual particles were imbedded within the viscous sublayer whereas the larger agglomerates extended into the turbulent boundary layer. Agglomerates extending above the viscous sublayer are subject to contact with a greater number of particles, but the greater aerodynamic lift force increases the probability of particle resuspension.

Corn (1961) hypothesized that the adhesion force for an agglomerate to a surface was different than that for a particle;

an agglomerate will contact the surface differently than a particle. The density of an an agglomerate is also likely to be different than that for the individual particle (Corn, 1961).

Payatakes (1977) developed a theoretical model to predict particle agglomeration during particle deposition to fibrous filters, but it is not known if this theory is applicable to agglomerate formation on a flat plate.

CHAPTER VI  
PREVIOUS EXPERIMENTAL DEPOSITION STUDIES

Literature reviews of numerous particle deposition studies have been presented by McMahon and Denison (1979), Sehmel (1980), and Hosker and Lindberg (1982). Particle deposition studies may be classified in two general categories :

1. Modeling studies utilizing controlled wind tunnel studies with monodisperse particles.
2. Experimental field studies with limited data on particle size or collection surface characteristics.

A brief description of the experimental studies most pertinent to this research are listed in Table VI-1.

Chamberlain investigated the deposition of iodine isotopes from an airstream onto flat surfaces of various materials as early as 1953. Chamberlain (1960) found that the velocity of deposition decreased as the the distance from the sharp leading edge increased due to the increasing boundary layer thickness. Chamberlain (1960) also compared the deposition of iodine isotope aerosols onto flat plates electrified with an applied voltage of 11,000 volts (electrostatic field of 2200 volts/centimeter) to the deposition onto grounded flat plates without an electrostatic field. The charged plates collected 2 to 13 times more particles than the grounded

TABLE VI-1. DRY DEPOSITION STUDIES RELEVANT TO THIS RESEARCH

Reference	Particle Diameter, micrometer	Deposition Velocity, cm/s	Surface type
Chamberlain (1960)	gas	0.07-0.71 2.1 1.2	copper foil filter paper bean leaf
Chamberlain (1974)	gas	0.17-1.0 0.2 -1.0	copper foil bean leaf
Rosinski (1957)	0.5-5.0	*	adhesive paper
Rosinski <u>et al</u> (1965)	0.5-5.0	*	coniferous tree
Langer (1965)	0.5-5.0	*	coniferous needle
Rosinski <u>et al</u> (1967)	0.5-5.0	*	brass polystyrene
Davies (1960)	28- 34	*	glass slide
Wedding <u>et al</u> (1975)	3.3 6.8	* *	poplar leaf sunflower leaf
Little (1979)	2.75, 5.0,& 8.5	*	numerous species leaves and stems
Grace <u>et al</u> (1976)	*	*	poplar leaf
Davidson (1977)	ambient aerosol	*	oat grass glass slide

\* not reported in the literature.

plates. Most of the aerosols were collected on the negatively charged plate. Chamberlain concluded that most of the aerosols were positively charged, and that the earth's surface would tend to attract positively charged aerosols.

Chamberlain (1974) investigated lead isotope transfer to bean leaves at an airspeed of 1.15 m/s. The deposition velocity again decreased with distance from the leading edge but increased with an increasing angle of incidence between the leaves and the airflow.

Rosinski (1957) tested the efficiency of adhesive paper as a collection device, and found that fluorescent particles (0.5 to 5.0 micron diameter) were electrostatically attracted to filter paper at humidities less than 24% and at low air speeds (<4 m/s). However, impaction was the primary removal mechanism at high humidities and high airspeeds. The effects of angle of incidence and humidity on particle rebound were also investigated.

Rosinski and Nagamoto (1965) investigated fluorescent particle (0.5 to 5.0 micron) deposition and reentrainment from small trees at airspeeds of 1.95 to 4.1 m/s. A tree connected to an electrometer developed a voltage (-250 volts in 5 minutes) only when the tree was electrically isolated from the ground. Electrostatic charge build-up was effectively prevented by grounding the tree roots in moist soil.

Langer (1965) investigated the same type particle deposition onto and re-entrainment from individual coniferous needles and wires in a 1.8 cm diameter wind tunnel. When a potential of -2000 volts was applied to a wire in an air flow of 30 cm/sec, particles deposited in the wake region (rear surface) of the wire. Charged dust particles were not collected on an uncharged surface by an image charging mechanism. The theoretical electrostatic collection was less than 0.1% and was considered insignificant at the Reynolds numbers tested (1140 and 2000), corresponding to airspeeds of 1.2 and 1.6 m/s. Inertial impaction was the primary deposition mechanism.

Rosinski and Langer (1967) later investigated the deposition of the same type particles onto flat plastic and metal surfaces. It appeared that electrostatic attraction affected deposition on both the upper and lower surfaces at low (1.25 to 3.9 m/s) as well as high air speeds (7.3 m/s), although uneven particle deposition and size separation occurred. The plastic surfaces were found to develop randomly distributed regions of high electrostatic charge.

Davies (1960) investigated the deposition of Lycopodium spores (28 to 34 micron diameter) onto glass microscope slides. Deposition of these large particles at an airspeed of 0.5 m/s was due primarily to gravitational settling. Impingement on the blunt leading edge of the slide limited deposition on the horizontal surfaces as the air speed increased. At the highest air speeds (9.5 m/s), deposition on the horizontal surfaces resulted from eddy diffusion



and impaction in the turbulent boundary layer.

Wedding et al. (1975) compared the deposition of lead chloride (3.36 microns diameter) and fluorescent uranine (6.77 microns) aerosols onto leaf surfaces at an airspeed of 2.68 m/s. Rough, pubescent (hairy) sunflower leaves collected ten times more particles than smooth, waxy tulip poplar leaves. They concluded the difference in deposition was due to leaf surface characteristics. The air flow characteristics were different between the groups of flapping leaves and a single trailing leaf with little motion. However, they found that the functional form and value of the results were similar.

Little (1977) investigated the deposition of 2.75, 5.0, and 8.5 micron diameter polystyrene aerosols at different plant locations (leaf lamina, stem, and petiole) at airspeeds of 1.5 to 5.0 m/s. The presence of leaf hairs increased the deposition velocity of the 5.0 micron particles; perhaps the hairs projected above the leaf boundary layer enhanced particle impaction. Particle deposition was heaviest at the leaf tip and along the leaf margins where a turbulent boundary layer developed. Increased particle size and airspeed resulted in increased deposition velocities due to the greater particle momentum and turbulence in the boundary layer. The deposition velocities to the petiole and stem were much greater than for the leaf lamina, but the leaf lamina collected the majority of the particles due to its greater surface area. Significant particle deposition to bare twigs may occur,

especially at high wind speed.

Grace and Wilson (1976) investigated the air flow over a poplar leaf at airspeeds of 0.5 to 10.2 m/s. The boundary layer on the rough, under surface was turbulent while the boundary layer of the smooth, upper surface was laminar at low air speeds. The boundary layer for the leaf became turbulent at a Reynolds number (930) much lower than that required for a flat plate (by approximately a factor of 10).

Grace (1980) investigated air flow over a leaf surface at 1 m/s. When the leaf boundary layer was laminar, the transfer of aerosols to the leaf surface occurred by diffusion. If the boundary layer was turbulent, then aerosol transfer resulted from eddy diffusion or inertial impaction. The boundary layer over a leaf was usually turbulent or partly turbulent due to the leaf shape, orientation, and turbulent atmospheric conditions, but a portion of the boundary layer was sometimes laminar near the leading edge and on the flatter parts of the leaf. The entire boundary layer may be laminar at very low wind speeds or when leaves are small. Even in a turbulent boundary layer there was a viscous sublayer close to the surface where air flow remained laminar. This sublayer was only a few tens of micrometers thick but it was thought to be much thicker in pubescent leaves.

Davidson and Friedlander (1978) developed a filtration model to predict aerosol dry deposition to a plant canopy. The deposition

of trace metals was also measured in the field on teflon plates and on wild oat grass. These data were used to test the filtration model and to determine trace metal transport mechanisms. Photographs show that particles accumulated along the fine hairs of the wild oat seed husks.

CHAPTER VII  
MATERIALS AND METHODS

Wind Tunnel Modeling

Wind tunnel modeling of atmospheric phenomena, such as particle deposition, is often desirable since the most important variables, such as air speed, temperature, sunlight, humidity, and turbulence can be controlled. The expense and time are much less than that required in a full scale atmospheric study.

Snyder (1981) has prepared some guidelines for fluid modeling. For complete similarity between the model and the prototype (full scale) conditions there must be geometric, kinematic, and dynamic similarity:

- For geometric similarity, all the relevant linear dimensions of the model must have the same direct proportionality to the full size dimensions.
- For kinematic similarity, there must be a constant ratio between the two sets of corresponding velocities.
- For dynamic similarity between a model and prototype, there must be a constant ratio between the corresponding sets of fluid inertia forces (i.e., gravity, pressure, surface tension, elasticity, and viscosity).

All the similarity requirements will be rigorously satisfied only when the model is as large as the prototype. This study sought

to characterize the particle deposition onto a flat plate in order to better understand the deposition process as it occurs in the wind tunnel. The boundary layer development was modeled in order to use the previously mentioned turbulent flow particle deposition model. In this case, dynamic similarity is dependent on the viscous forces and would occur if the Reynolds number ( $U L/\nu$ ) is the same for the experimental plate and the deposition model boundary layers. This study would be the first step toward characterization of the more complex atmospheric deposition process.

Descriptions of the materials and methods used in this study follow.

### Wind Tunnel

A low-speed wind tunnel with a 30 cm x 30 cm cross section was constructed in the ATDL Applied Fluid Dynamics Laboratory. Its design was based on a scaled-down version of the ATDL wind tunnel; details are shown in Figure VII-1. The maximum air speed is 5.0 m/s for a laminar mainstream airflow. The front flow straightener consists of a high efficiency particle filter (Astrocel I, American Air Filter); the rear flow straightener consists of three layers of fine-mesh screen. Access to the wind tunnel is through a hinged door just in front of the plate support system. The 18 inch diameter tube-axial fan is driven by a 0.75 Hp variable speed motor. The fan and motor were mounted so as to minimize vibration in the wind tunnel. The wind tunnel also has a window along one wall and is vented through the building wall

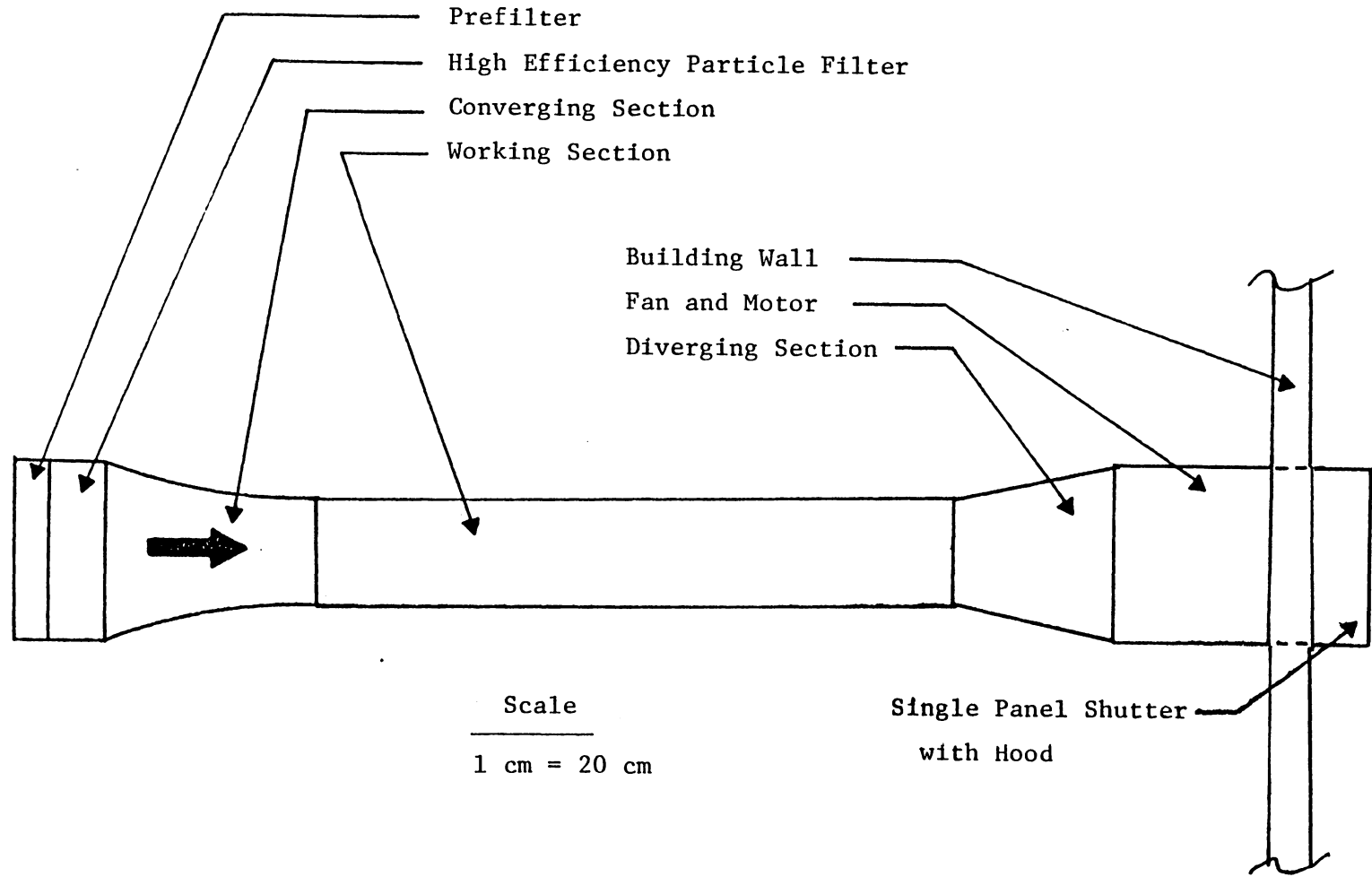


Figure VII -1. Low-Speed Wind Tunnel Constructed for Particle Deposition Studies.

to the exterior to prevent inhalation of its exhaust.

### Aerosol Generation System

Monodispersed aerosols were generated by pneumatically dispersing (or nebulizing) a water-based suspension of uniform-size microspheres (Duke Scientific Corp., 1982). The nebulizer construction, as shown in Figure VII-2, was based on a small particle generator designed by Leong, Wang, Stukel, and Hopke (1982). This dispersion method produces a monodisperse aerosol and is frequently used as a standard for the calibration of optical particle counters (Berglund and Liu, 1973).

Compressed nitrogen from a high pressure cylinder passed through an absolute filter (MSA Airline Filter No. 85759), before entering the nebulizer, as shown in Figure VII-3. The high velocity jet created by the gas flowing through the 0.04 cm orifice results in a low pressure near the outer jet region. This reduced pressure drew the microsphere suspension droplets through a 0.16 cm tube from the reservoir toward the air jet. The droplets disintegrated into aerosols when they contacted the high velocity gas. The aerosols were rapidly accelerated to the speed of the gas stream (Dennis, 1976). The larger aerosols had sufficient momentum that they impacted on the wall directly in front of the jet and then drained down into the reservoir. However, the smaller aerosols had less momentum and followed the gasflow upward and out of the nebulizer.

The aerosol was subsequently mixed with dry gas to evaporate

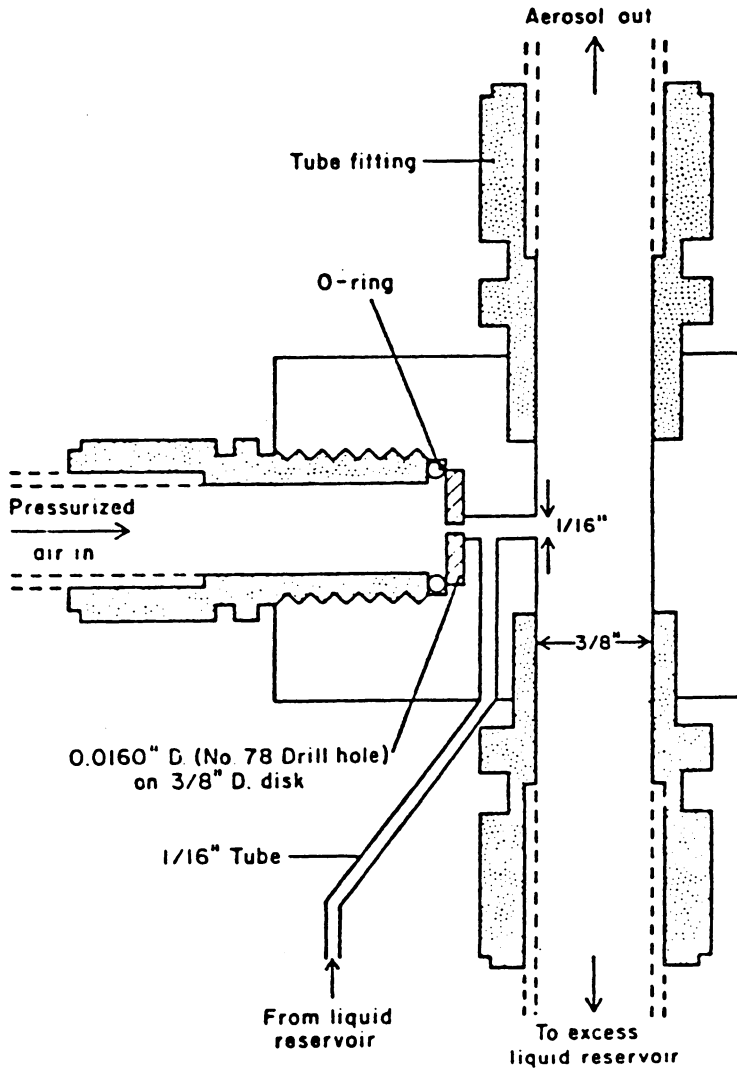


Figure VII -2. Nebulizer Design after Leong, Wang, Stukel, and Hopke (1982).



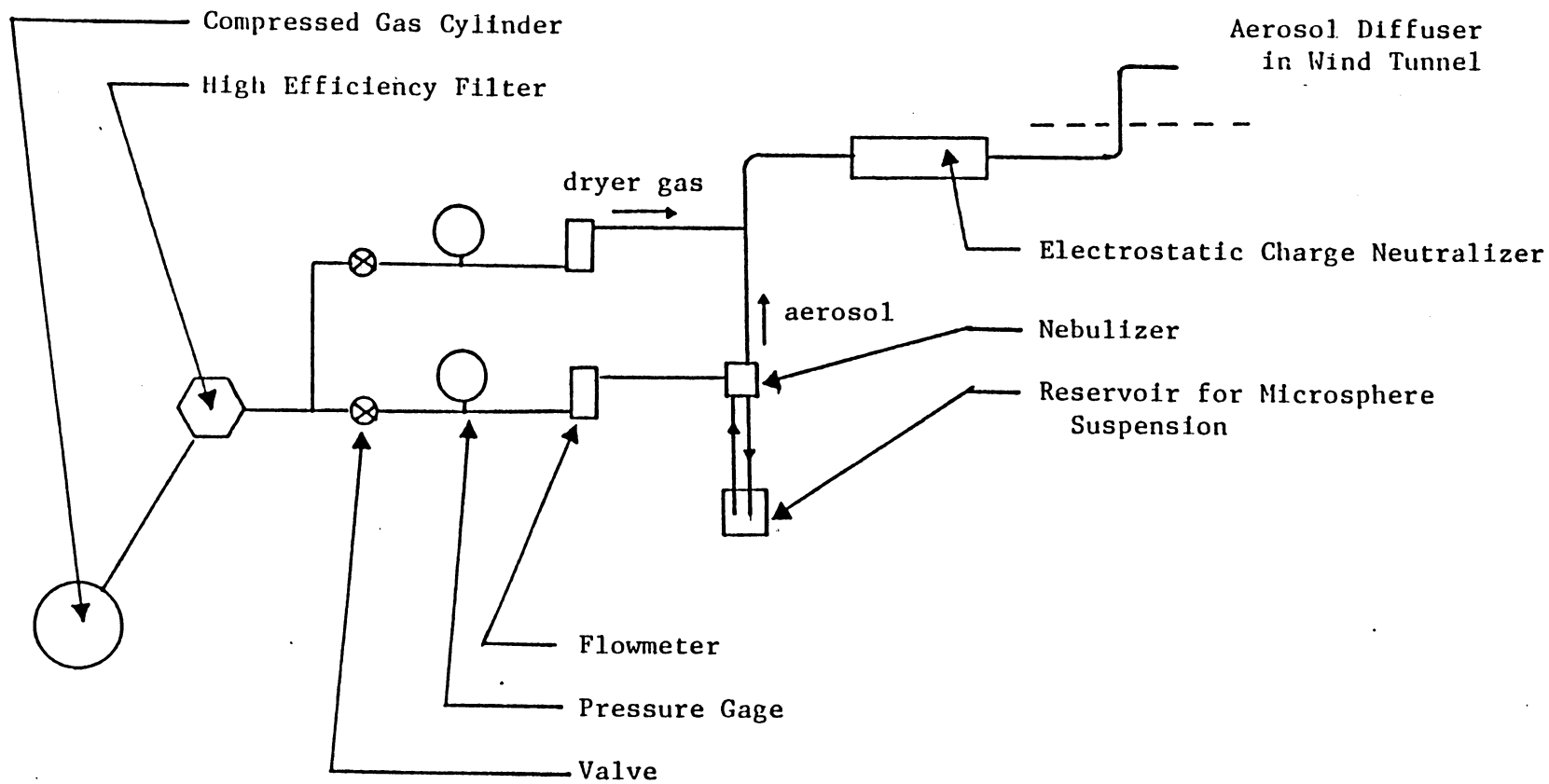


Figure VII -3. A Schematic Illustration of the Monodisperse Aerosol Generation System.

the water attached to the microspheres. The dry gas also served to increase the velocity so that microspheres passed through the charge neutralizer. Both the aerosol and dry gas lines had valves, pressure gauges, and flowmeters in order to maintain a relatively constant aerosol output.

The 0.8, 0.9, 1.0, 1.1, and 2.0 micron diameter microspheres had diameter standard deviations of 0.6, 9.9, 1.0, 0.8 and 0.7 percent, respectively. They were purchased in a concentrated suspension of approximately  $10^{10}$  particles/ml with a density of 1.05 g/ml. The 0.9 and 1.0 micron diameter microspheres are fluorescent to improve the optical contrast between the microspheres and the background; their excitation ranges are 225 - 320 nanometer (nm), 390 - 400 nm, and 440 - 490 nm. An incandescent lamp will cause the microspheres to fluoresce. Their emission range is 500 - 600 nm which is in the spectrum of visible light.

Stabilizing chemicals prevented the coagulation of the microsphere suspension. Any dissolved substances, including the stabilizing chemicals, result in the formation of very small secondary particles (diameters < 0.3 microns) upon dispersion. The suspension was diluted from the original concentration as supplied by approximately 500 to 1 to prevent the formation of double particles (i.e., two particles in one drop). Triple-distilled deionized water was used for dilution in order to minimize the production of secondary particles.

### Electrostatic Charge Neutralizer

The aerosol generation system produces aerosols that have a high electrostatic charge which must be neutralized to prevent unwanted electrostatic deposition (Liu and Pui, 1974). The charge "neutralizer" actually reduces the electrostatic charge to that approximated by the Boltzmann distribution rather than completely neutralizing the charge as its common name infers.

The most common, effective method to reduce the electrostatic charge is to use a source of ionizing radiation (Liu and Pui, 1974). Polonium 210 (Nuclear Products Company, El Monte, CA) releases high energy alpha particles as it decays. The alpha particles ionize into positive and negative ions any air molecules with which they collide. Ions of the opposite charge are captured by the aerosols as they flow through the neutralizer chamber containing Polonium 210, thus reducing their electrostatic charge.

The aerosol particles must be in contact with the bipolar ions for a length of time sufficient for the Boltzmann charge distribution to develop in order to be "neutralized". The characteristic time of neutralization,  $t_n$ , for the charge neutralizer was calculated as 0.005 seconds utilizing the method presented by Cooper and Reist (1973) as listed in Appendix B. The average residence time,  $t_r$ , of the particles in the neutralizer chamber was calculated by dividing the volume of the chamber by the aerosol flowrate. For a flowrate of 4.6 l/m,  $t_r$  was calculated as 8.0 seconds.

The ratio of  $t_r/t_n$  is an approximation of the completeness of charge neutralization and should be much greater than one

(Cooper and Reist, 1973). The ratio was approximately 1600, which is an order of magnitude higher than that used by others (Cooper and Reist, 1973). However, the activity of Polonium 210 decreases more rapidly due to its short half-life than that for the Krypton 85 sources used in the other studies. Billard, Madelaine, and Delhaye (1970) also successfully used a two millicurie Polonium 210 source for aerosol charge neutralization.

The range of the alpha particles in air is approximately four cm. The chamber diameter was 4.8 cm so the Polonium sources (20 at 100 microcuries each) were positioned at 2 cm intervals longitudinally, as shown in Figure VII-4. This positioning of the sources was to insure aerosol contact with the bipolar ions.

### Aerosol Analyzer System

A Climet Model CI-226 high resolution particle analyzer was employed with dual EG&G ORTEC Model 550 discriminators and dual Model 449 counters in a two-channel system.

The CI-226 serves as the sensor to detect aerosols over a size range of 0.3 to 10 microns. Aerosols are sampled at a rate of 0.25 ft<sup>3</sup>/m. The viewing volume is small enough to detect individual particles. The particle sensing zone is located at the primary focal point of the elliptical mirror, a photomultiplier tube is located at the secondary focal point, as shown in Figure VII-5. Each particle is illuminated by the quartz halogen lamp when it enters the sensing zone. The photomultiplier tube detects

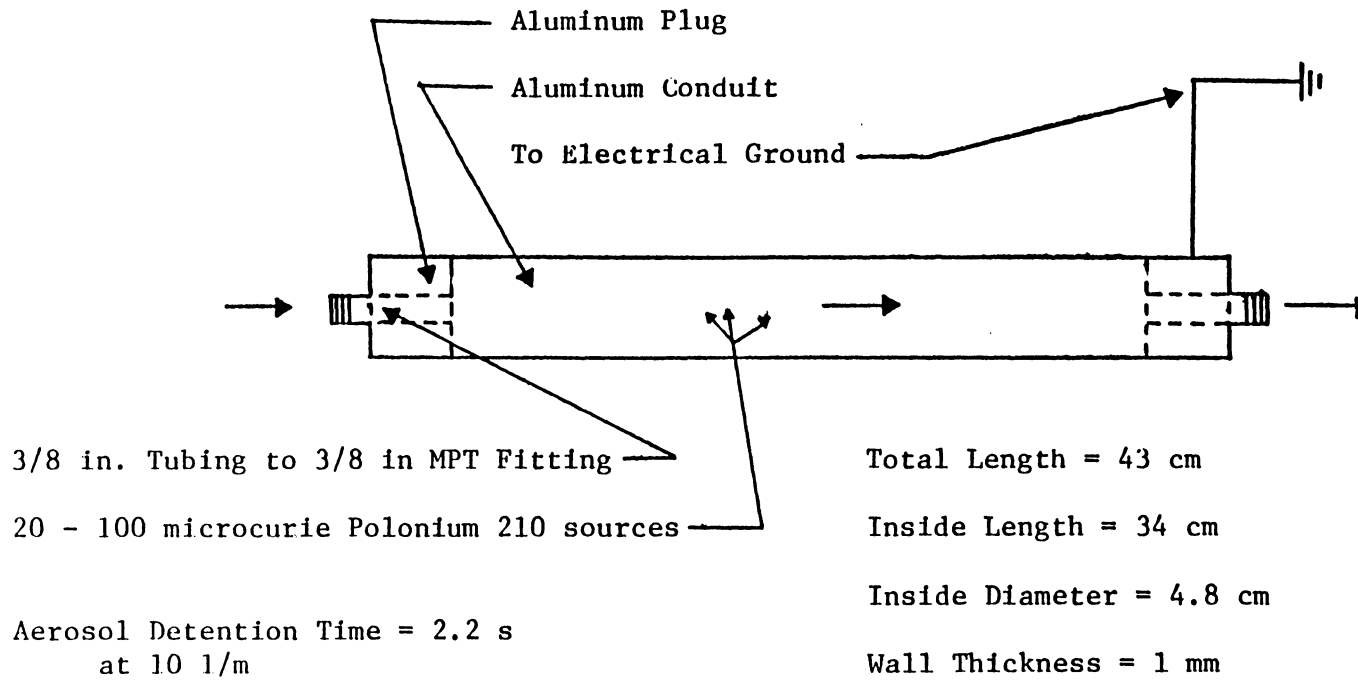


Figure VII -4. A Schematic Illustration of the Aerosol Electrostatic Charge Neutralizer

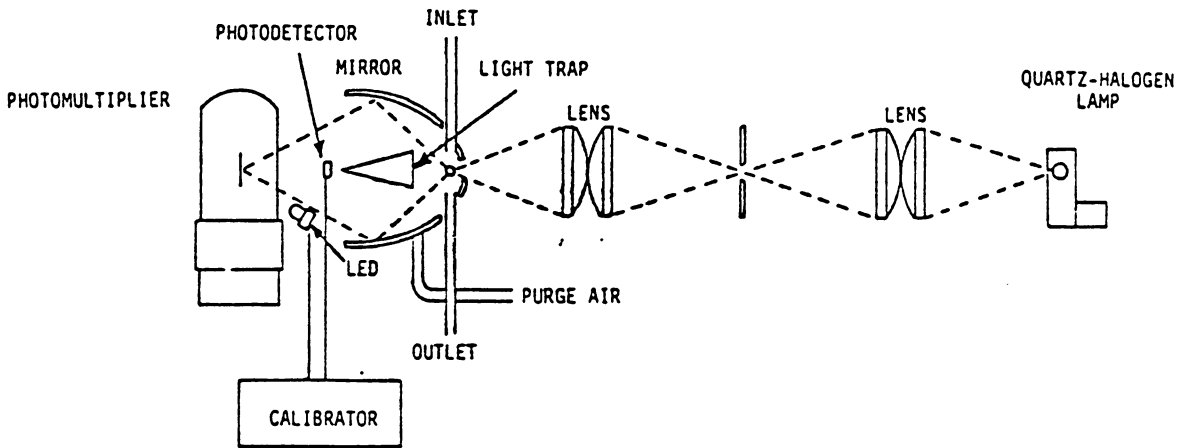


Figure VII -5. Climet Model CI-226 Optical System.

the light scattered by each particle and converts it into an electrical pulse. The Climet output is proportional to the particle diameter, as shown in Table VII-1.

The analog output pulses from the CI-226 sensor are monitored by the ORTEC Model 550 high resolution pulse height analyzer. It has adjustable lower and upper voltage levels (windows) which allow one to count particles in a specific voltage range (i.e., particle diameter range).

The analog output pulses from the discriminator are then monitored by the ORTEC Model 449 Log/Lin ratemeter (counter). It measures the average count rate of the input pulses over a wide selection of averaging times (time constants of 0.03, 0.1, 0.3, 1, 3, 10, 30 seconds and also on a log scale) for a selection of ranges (10, 30, 100, 300,  $10^3$ ,  $3 \times 10^3$ ,  $10^4$ ,  $3 \times 10^4$ ,  $10^5$ ,  $3 \times 10^5$ ,  $10^6$  counts/s and also on a log scale).

The ORTEC Models 550 and 449 do not contain an integral power supply but are used in conjunction with an ORTEC Model 401/402 Series Bin and Power Supply.

The ORTEC Model 449 was interfaced with the Hewlett-Packard 3052A data acquisition system (scanner) so the output voltages could be sampled and stored on a diskette by the HP 9836 microcomputer. The particle sampling program for the HP 9836 was written by Pendergrass (1983). The output voltage was also recorded simultaneously by a Heathkit Model 204 strip chart recorder.

TABLE VII-1. CLIMET MODEL CI 226 PARTICLE COUNTER  
OUTPUT VOLTAGE VERSUS PARTICLE DIAMETER

---

Output Voltage	Diameter ( $\mu\text{m}$ )
28 millivolts	0.3
44	0.4
65	0.5
80	0.6
118	0.8
160	1.0
270	1.5
460	2.0
1.0 volt	3.0
1.7	4.0
2.6	5.0
3.75	6.0
5.0	7.0
6.5	8.0
8.2	9.0
10.0	10.0

---

After Climet Instrument Company (1982).



### Air Velocity Measurement

The instantaneous air velocity,  $U$ , was measured over the experimental plate with a TSI (Thermal Systems Inc.) Model 1054A anemometer with TSI Model 1056 variable decade resistance unit and TSI Model 1057 signal conditioner incorporating a TSI Model 1218-20 hot-film boundary layer probe.

The hot-film probe was calibrated against a Pitot tube system (MKS Instruments Inc., Baratron type 170M-6B with a range multiplier and digital readout unit type 170M-25B) in laminar air flow in the wind tunnel.

The boundary layer probe had a single 50 micron diameter hot film 1.0 mm long. The hot-film probe was selected over a hot-wire type because of its durability in contaminated air flow and its long term calibration stability. The probe was supported by a carriage system which could be lowered within 0.13 mm of the flat plate or raised to any desired height.

The TSI anemometer system was interfaced with the HP 3052A scanner so the velocity values could be sampled and stored on diskette by the HP 9836 microcomputer. The velocity sampling program was written by Pendergrass (1983).

The hot-film anemometer has several inherent limitations. It can not be accurately calibrated at airspeeds less than approximately 0.5 m/s. At low airspeeds the heat loss from the hot-film occurs partly by natural convection so the sensor may over estimate the air velocity (Grace and Wilson, 1976). The probe may also disturb the airflow when it is near the surface.

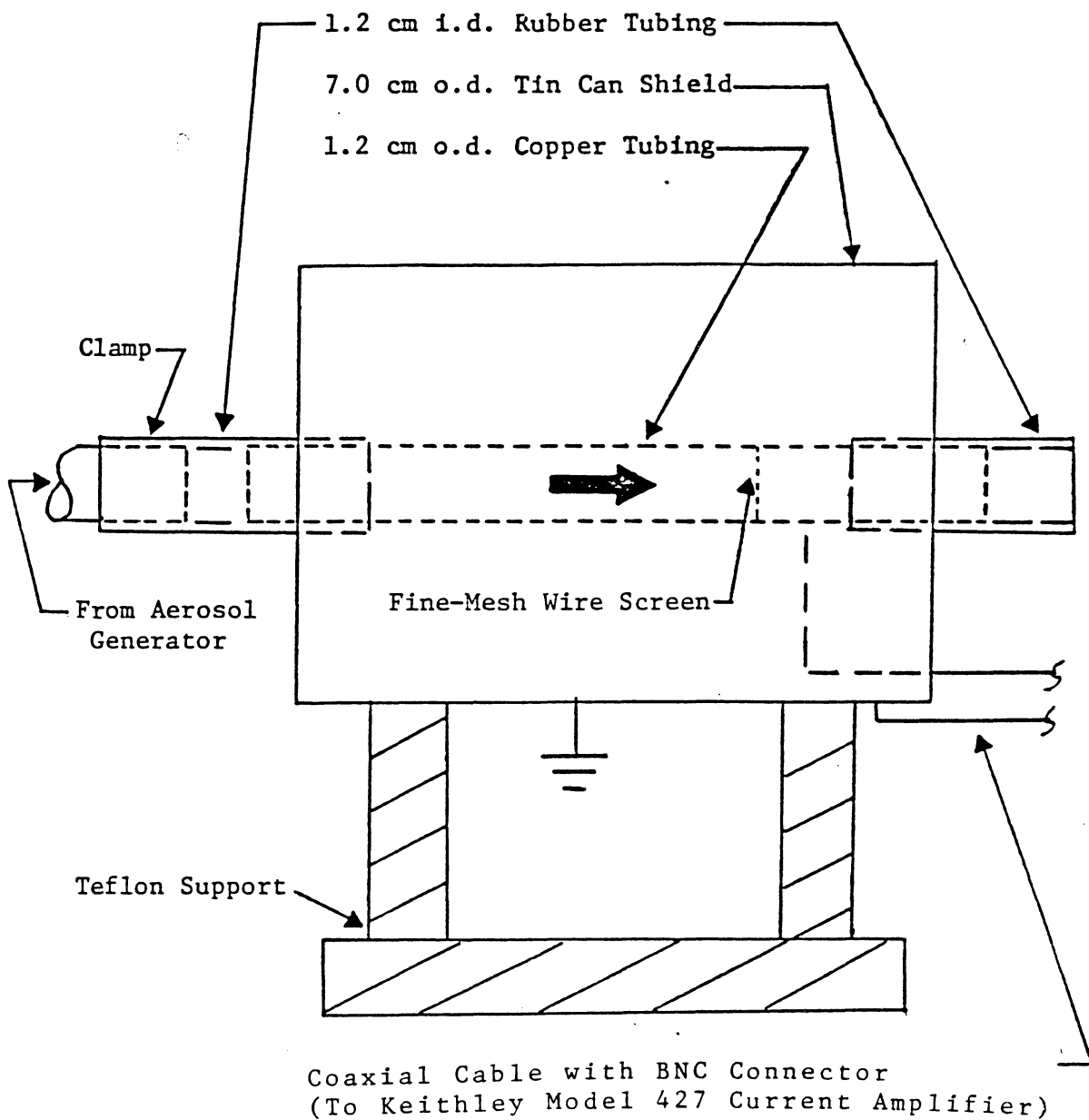
The probe can not accurately measure the velocity when the turbulence intensity is greater than 0.25.

### Electrostatic Charge Measurement System

The total electrostatic charge on the aerosol produced by the nebulizer system was measured to determine if the Polonium 210 charge neutralizer was effective in reducing the electrostatic charge. The preferred method is to measure the electrostatic charge on each particle exiting from the charge neutralizer, however the required equipment (an electrostatic classifier and an aerosol electrometer) were unavailable and too expensive to purchase.

The Faraday cup, as shown in Figure VII-6, was based on a design by John (1980). The copper tubing was surrounded by a tin can shield which insulated the tubing from any stray atmospheric electrostatic charges. The end of a 1/8-inch diameter braided copper cable was soldered to the tin can shield. The other end of the cable was clamped to a copper-coated steel rod driven into the ground. The copper tubing was electrically isolated from the tin can shield by the rubber tubing. The Teflon stand in turn insulated the tin can from the supporting table. Shielded coaxial cable was used for all the electrical connections.

The instant a charged aerosol entered the cup, an equal induced charge appeared on the copper tubing inside the Faraday cup as required by Gauss' Law (John, Reischl, Devor, and Weslowski, 1978). This induced current was then measured with a Keithley Model 427 Current Amplifier. The Keithley output voltages were monitored




---

Not To Scale

---

Figure VII -6 . The Faraday Cup.

with an oscilloscope and plotted on a strip chart recorder. A schematic illustration of the charge measurement system is shown in Figure VII-7.

A standard microsphere suspension was nebulized for all the electrostatic charge measurement experiments.

### Experimental Deposition Plate

The experimental deposition plate was cut from an Acrylite cast acrylic sheet (du Pont Polymer Products Division) and was 27 cm long x 12 cm wide x 1.7 mm thick with a sharp leading edge (less than a ten degree angle). A transparent plate was used in order to directly count the deposited microspheres with a microscope. The use of microscope slides as deposition surfaces was considered, but rejected; it is questionable if a near-equilibrium turbulent boundary layer develops over such a short length (Hosker, 1983).

Pau U and Reifsnyder (1980) have shown that a coated surface considerably reduced reentrainment for 30 micron diameter particles; a thin film greatly increased particle adhesion. Thus the experimental plate was considered an "ideal" deposition surface when it was coated with a thin film of microscope lens immersion oil (Cargille Laboratories, Inc.). Likewise, the experimental plate was considered a non-ideal surface when it was not coated with oil.

The flat plate support system consisted of three horizontal 1/4-inch diameter threaded steel rods. The rods were positioned 14 cm apart in slots in the sides of the wind tunnel, so the

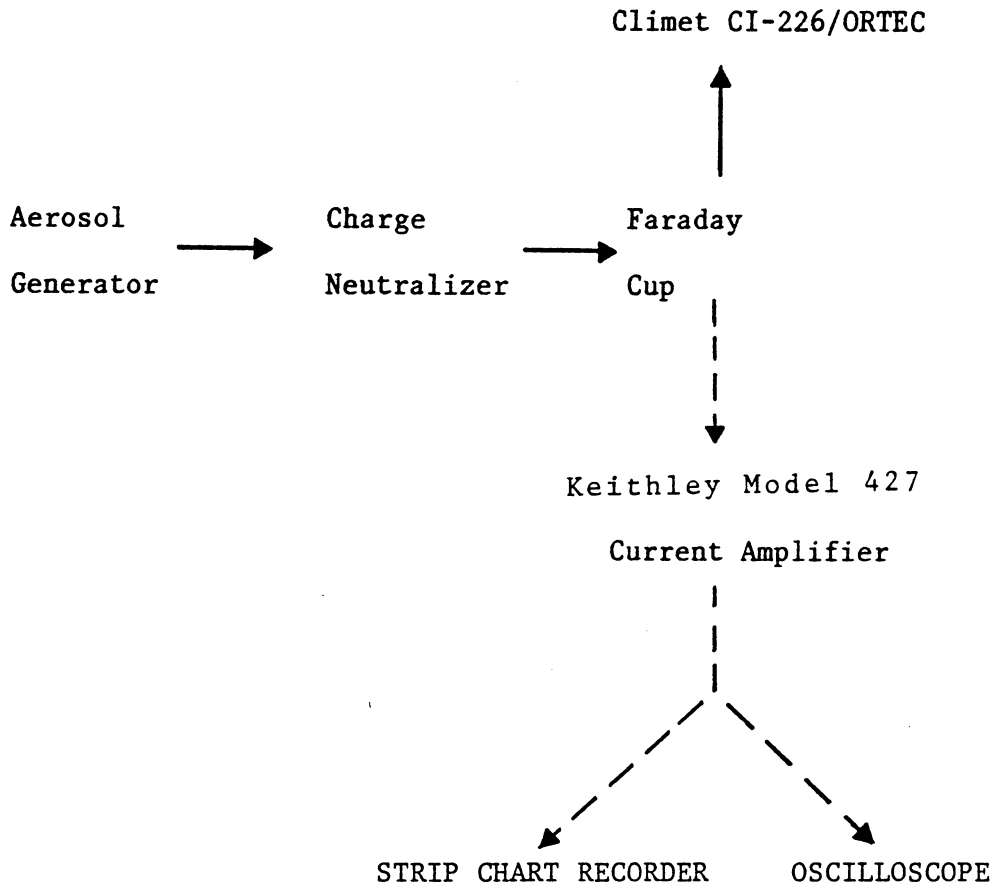


Figure VII -7. A Schematic Illustration of the Aerosol Electrostatic Charge Measurement System.

elevation of the plate could be varied. The flat plate was held in place when nuts on the threaded rods were tightened against the sides of the plate. The support system did not extend above the flat plate surface. The leading edge of the plate extended at least 3 cm upstream of the support system.

### Quantification of Particle Deposition

Particle deposition was quantified by direct counting with a Bausch and Lomb DynaZoom microscope with ten power wide field eyepieces and a 97 power oil immersion objective. The total magnification was 970.

Glass slide covers (18 mm x 18 mm x 0.17 mm) were placed over an 18 mm wide strip in the center of the plate along the longitudinal axis. The slide covers were used to prevent the particles from floating in the immersion oil. The microspheres were more distinct than other particles, especially for the fluorescent microspheres. Only the microspheres on the upper surface were counted; sizing was unnecessary due to the measured (and observed) uniformity of the microsphere diameters.

The diameter of the field of vision was 190 microns at a magnification of 970, as measured with a stage micrometer. At each point particle counts were made in 190 micron wide traverses extending across the deposit at intervals of 1 mm. Five traverses were made at each point and each traverse was repeated. Microscopic examination of each plate required approximately four days. The number of particles counted on each plate ranged from 400

to 2000 depending on the experiment.

The intent was that a sufficient number of particles should be deposited to make counting easy but to prevent particle build-up to such an extent that it would modify the physical characteristics of the surface.

#### Aerosol Generation and Deposition System

A schematic illustration of the entire aerosol generation and deposition system is shown in Figure VII-8.

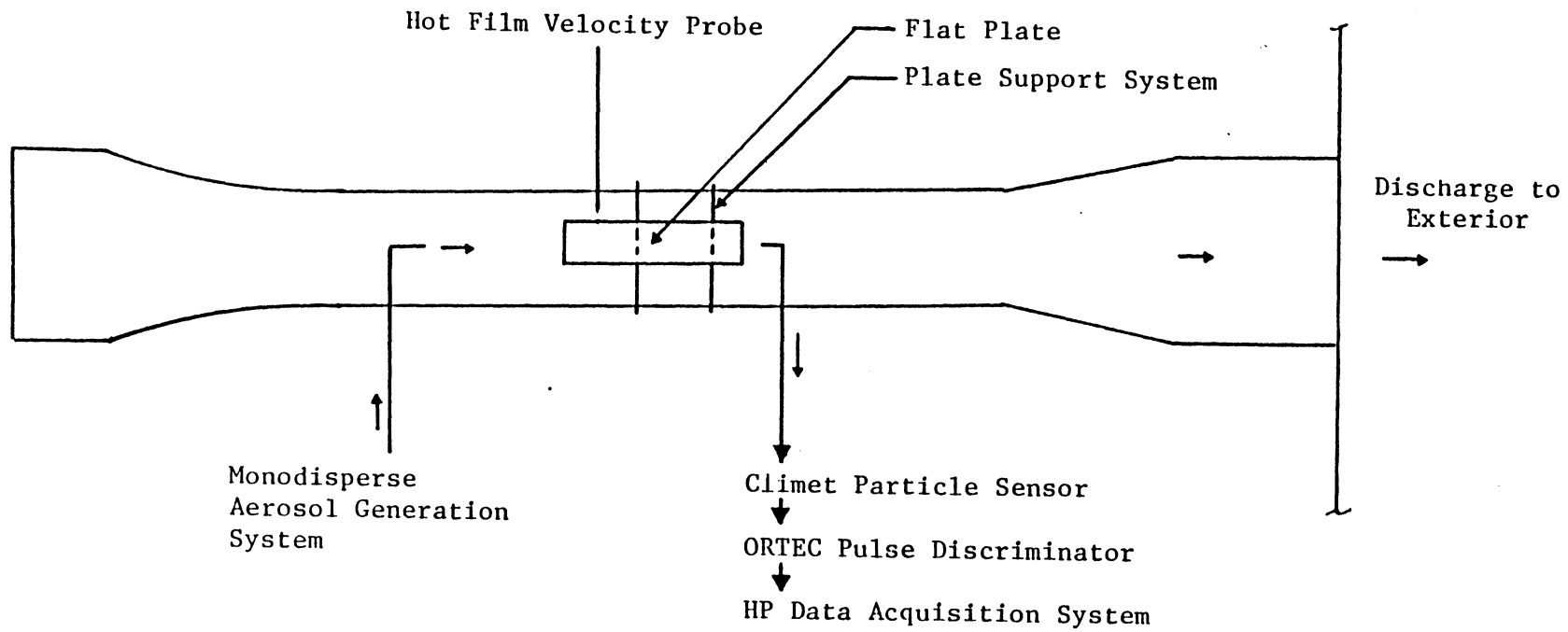


Figure VII -8. Particle Generation and Deposition System.



CHAPTER VIII  
CALIBRATION RESULTS

Wind Tunnel Test Section Calibration

The first set of calibration tests was to determine if the airflow was laminar in the wind tunnel test section. The motor and fan were allowed to warm-up before calibration of the hot-film anemometer was begun. Measurements were performed when the atmosphere was relatively stable. The wind tunnel exhausted to the exterior; when operated at low speeds it was somewhat affected by atmospheric turbulence. The wind tunnel airflow surged when an exterior door was open; exterior doors were locked during experimentation.

The local turbulence intensity,  $T_i$ , (also the velocity coefficient of variation) was calculated using the following equation (Grace and Wilson, 1976):

$$T_i = \left[ \frac{1}{N} \sum (\bar{U} - U)^2 \right]^{0.5} / \bar{U} \quad \text{(VIII-1)}$$

where  $\bar{U}$  is the local mean velocity and  $U$  is the local instantaneous velocity. The turbulence intensity times the mean velocity is equal to the standard deviation of the mean velocity. The mean velocity and turbulence intensity values were calculated from 6000 consecutive hot-film records ( $N$ ); the sampling rate was 100 Hertz for 60 seconds.

The locations of the horizontal and vertical velocity profiles

in the wind tunnel cross section are shown in Figure VIII-1. A vertical velocity profile was made from  $z = 3$  to 10 cm above the floor of the wind tunnel at  $y = 16$  cm from the rear wall; where  $y$  is the crosswind coordinate and the rear wall is the wind tunnel wall farthest from the operator. The mean velocities are shown plotted versus location ( $z$ ) in Figure VIII-2. The boundary layer is shown developing over the wind tunnel floor from  $z = 3$  to 6 cm, but the velocity was constant from  $z = 6$  to 10 cm. The velocities which ranged from to 2.54 m/s are shown in Table VIII-1 with the respective standard deviations and turbulence intensities. In the test section for the experimental flat plate ( $z = 7$  to 8 cm) the mean velocity varied by approximately 1 % from 2.43 to 2.46 m/s.

The probe support was moved, the hot-film anemometer was recalibrated, and a horizontal velocity profile was made at  $y = 11$  to 20 cm from the rear wall of the wind tunnel at  $z = 7$  cm above the wind tunnel floor. The mean velocities were quite constant, as shown in Figure VIII-3. The velocities which ranged from 2.14 to 2.26 m/s are shown in Table VIII-1 with the respective standard deviations and turbulence intensities. In the experimental test section for the flat plate at  $y = 14$  to 16 cm from the rear wall, the velocity was quite uniform at 2.2 m/s.

The probe was placed at  $y = 16$  cm and  $z = 15$  cm, the hot-film anemometer was recalibrated and the wind tunnel airspeed was increased in steps. The wind tunnel mainstream turbulence intensity decreased from 1.8 % at 1.2 m/s to 1.0 % at 4.9 m/s, as shown in Table VIII-2. The turbulence intensity was less at the high velocities

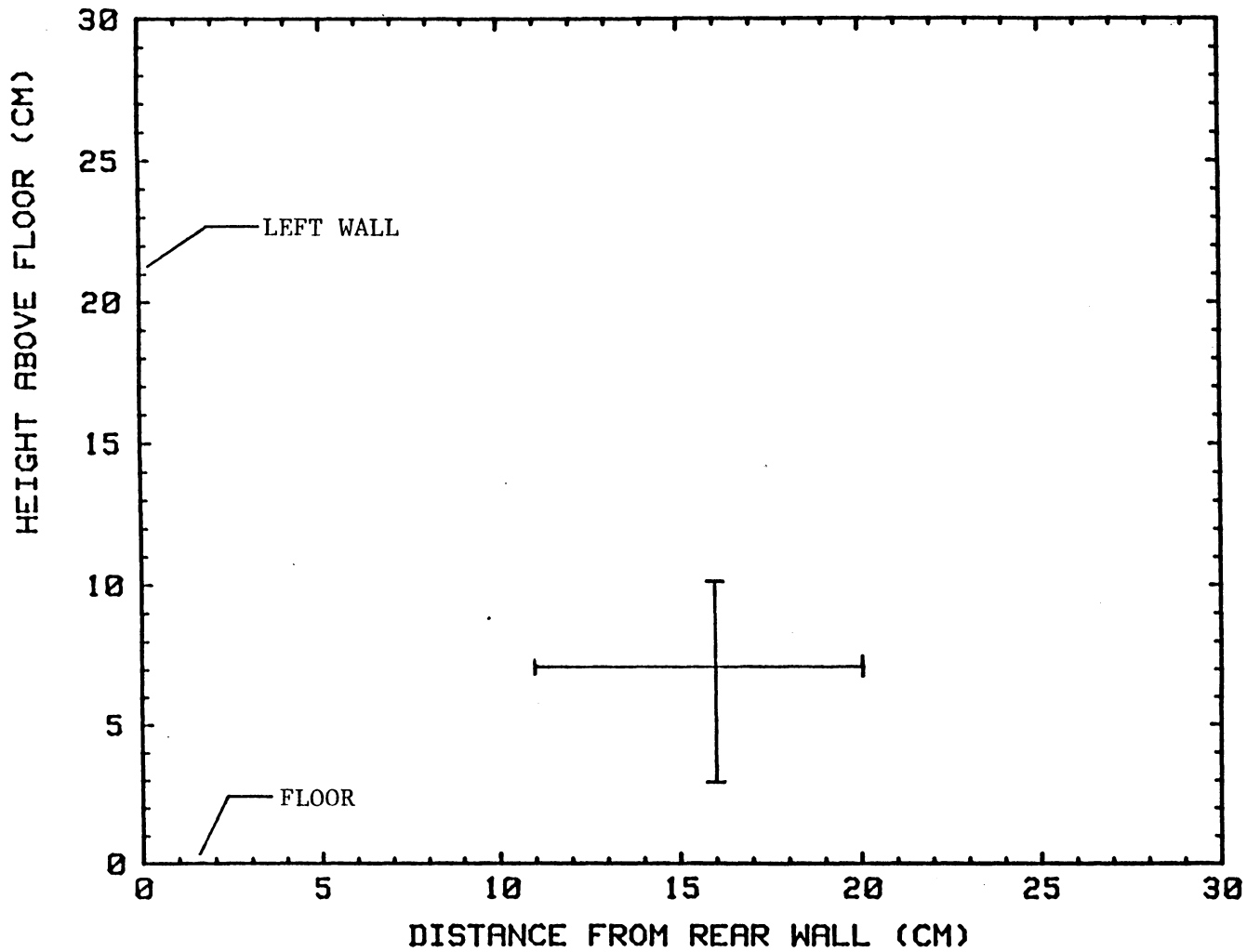


Figure VIII-1. Locations of the Vertical and Horizontal Velocity Profiles in the Wind Tunnel.

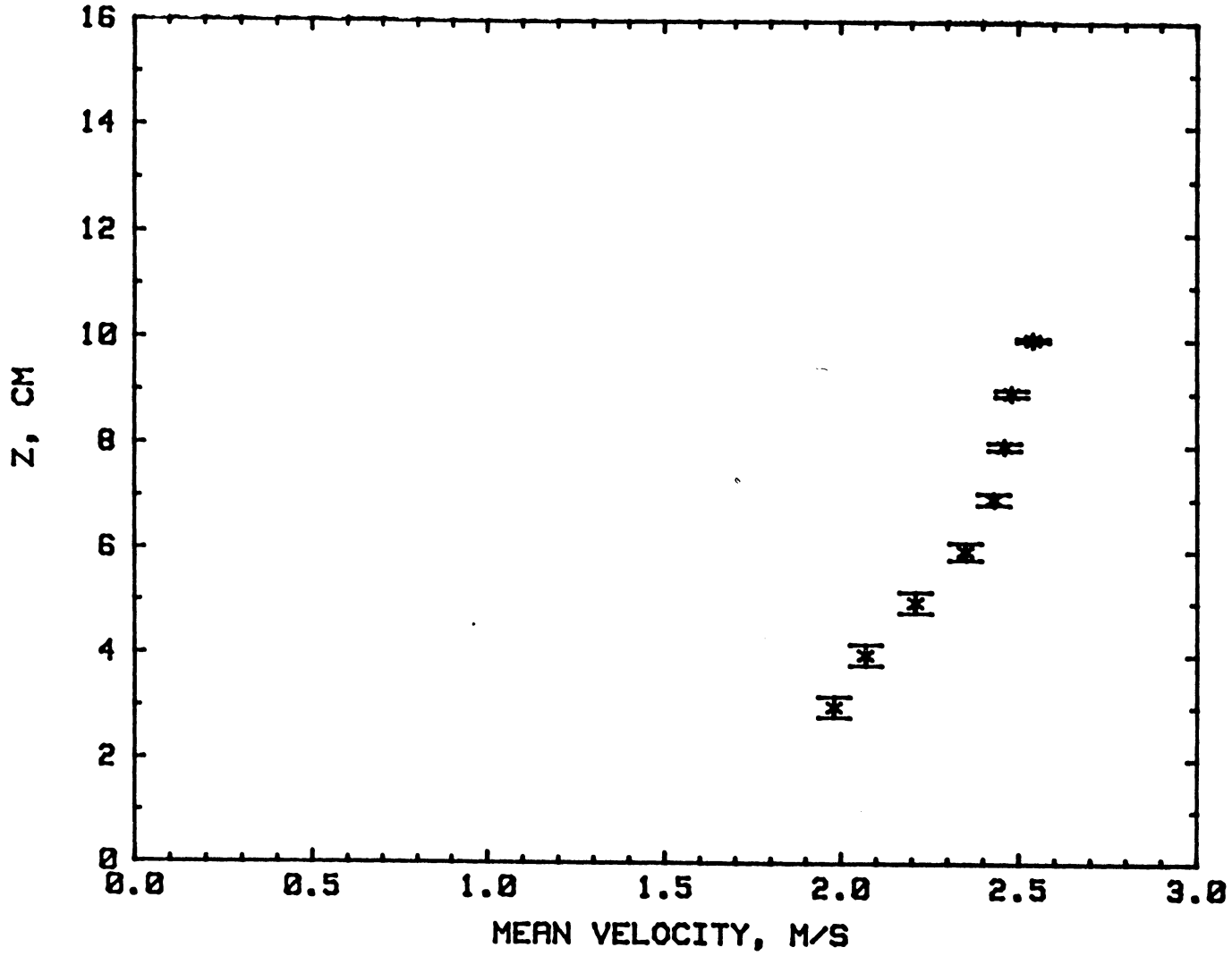


Figure VIII-2. Vertical Velocity Profile at Y = 16 cm in the Wind Tunnel.

TABLE VIII-1. WIND TUNNEL TEST SECTION CALIBRATION

Distance (cm)	Mean Velocity (m/s)	Turbulence Intensity (%)	Velocity Standard Deviation
Vertical Profile at Y = 16 cm			
Z = 3	1.98	10	0.20
4	2.07	10	0.20
5	2.21	10	0.20
6	2.35	7	0.17
7	2.43	5	0.11
8	2.46	3	0.07
9	2.48	2	0.06
10	2.54	1	0.03
Horizontal Profile at Z = 7 cm			
Y = 11	2.26	3	0.06
12	2.23	3	0.07
13	2.22	3	0.07
14	2.21	3	0.07
15	2.21	3	0.07
16	2.20	3	0.07
17	2.20	4	0.07
18	2.20	3	0.07
19	2.16	4	0.08
20	2.14	4	0.08

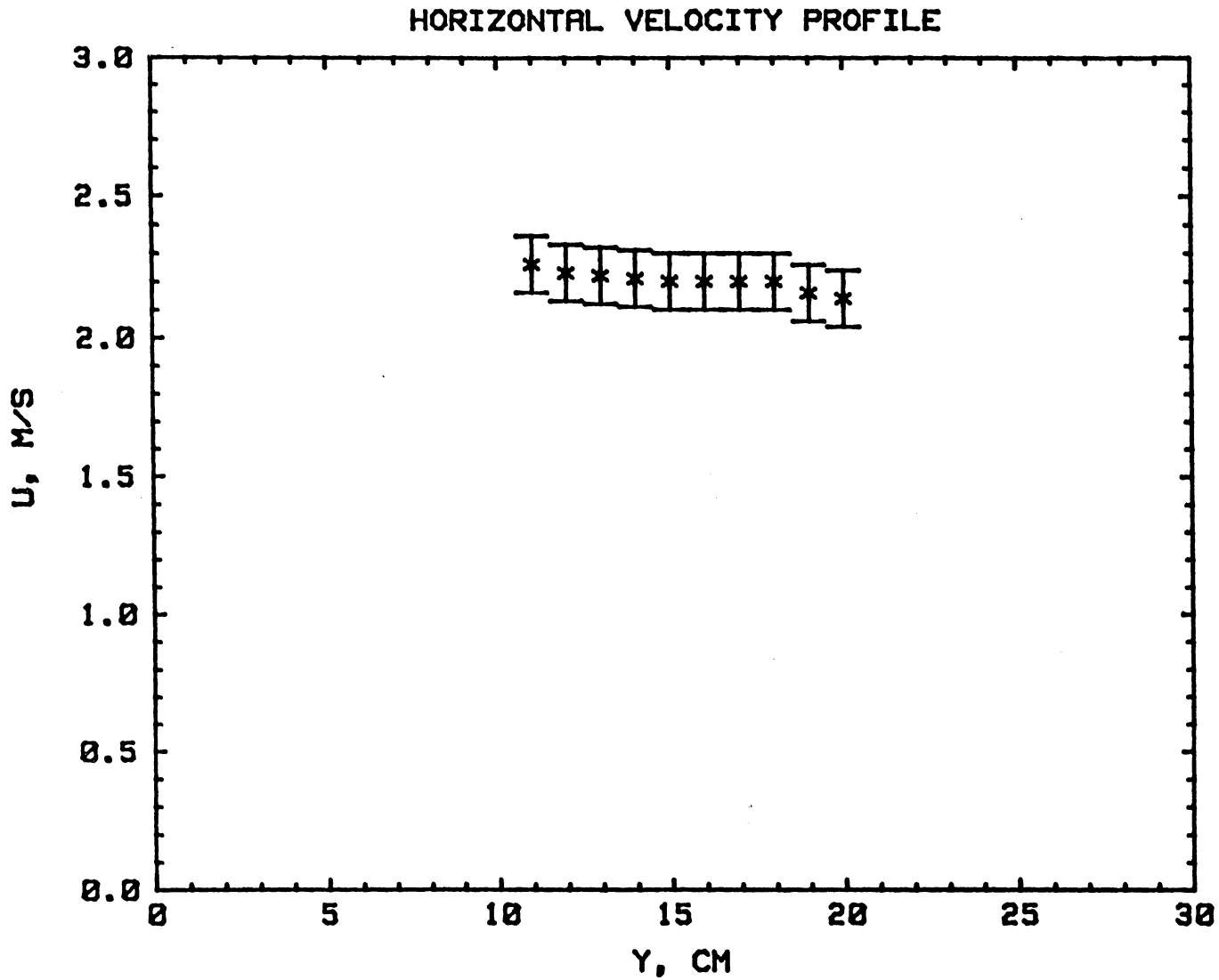


Figure VIII-3. Horizontal Velocity Profile at  $Z = 7$  cm in the Wind Tunnel.

TABLE VIII-2. THE MAINSTREAM TURBULENCE INTENSITIES  
AT VARIOUS WIND TUNNEL VELOCITIES

	Mean Velocity (m/s)	Turbulence Intensity (%)	Velocity Standard Deviation
Laminar Mainstream	1.2	1.8	0.02
	1.7	1.5	0.03
	2.2	1.5	0.03
	2.6	1.2	0.03
	3.0	1.1	0.03
	3.5	1.1	0.04
	4.0	1.0	0.04
	4.4	1.0	0.04
	4.9	1.0	0.05
Turbulent Mainstream	1.3	9.5	0.12
	1.9	10.7	0.20
	2.2	11.0	0.24
	2.5	11.0	0.28
	2.7	11.0	0.30
	3.1	11.0	0.33
	3.3	12.0	0.38

The sampling rate at each velocity was 100 Hertz for 60 seconds.

due to the greater compression of the turbulent eddies in the converging section of the wind tunnel. The turbulence intensity at 2.2 m/s was less than that for the vertical and horizontal velocity profiles as the probe was in the center of the wind tunnel and less affected by the boundary layers which developed over the floor, top, and sides. The experimental flat plate was positioned low in the wind tunnel to increase the visibility of the flat plate and the velocity probe during experimentation.

In the following experiment turbulence was induced by placing a grid in the wind tunnel approximately 40 cm upstream of the flat plate. The individual elements were 6 mm x 6 mm x 29 cm, spaced 6 mm apart, and were positioned horizontally and vertically in a grid. The sharp edges on the individual grid elements induced flow separation with subsequent vortex formation; the vortex formation and shedding created a turbulent mainstream.

The probe was again placed at  $y = 16$  cm and  $z = 15$  cm, the hot-film was recalibrated, and the wind tunnel airspeed was increased in steps. The wind tunnel mainstream turbulence intensity increased from 9.5 % at 1.3 m/s to 12.0 % at 3.3 m/s, as shown in Table VIII-2. The vortex formation and shedding increased with the air speed so the mainstream turbulence also increased.

One would conclude that the mean air velocity was quite uniform both vertically and horizontally at an airspeed of 2 m/s in the experimental test section for the flat plate. The low turbulence intensity indicates the mainstream airflow was indeed laminar.



### Surface Flow Visualization

The flow of an oil film on a flat plate will closely follow the boundary layer air flow (Merzkirch, 1974). A visual flow pattern of the surface flow may be obtained except where there is flow separation (Maltby and Keating, 1962). Although the original flow conditions in the thin boundary layer are slightly altered due to the presence of the oil film, this effect may be ignored for flow visualization purposes (Merzkirch, 1974).

The intent of this flow visualization study was to qualitatively characterize the air flow over the surface of the experimental plate. It was desired to identify any regions where the airflow was disturbed as particle deposition would be significantly affected there.

A spray-painted black aluminum plate (13cm x 36cm x 1.5 mm) with a sharp leading edge was airbrushed with an oil/pigment mixture (3 parts by weight titanium dioxide, 12 parts diesel fuel, and 1 part partially hydrogenated soybean oil). The titanium dioxide pigment provided a fine pattern of high contrast.

The experimental plate was then tested at wind tunnel airspeeds of 2 m/s and 5 m/s under conditions simulating those for the particle deposition studies. The airflow moved the oil/pigment mixture over the surface in filaments. The pigment was deposited in wake regions and continued to build-up into long streaks in the direction of flow until all of the oil had been blown away or evaporated.

Figure VIII-4 is a photograph of oil/pigment flow on the experimental plate after 90 minutes (zero angle of incidence and

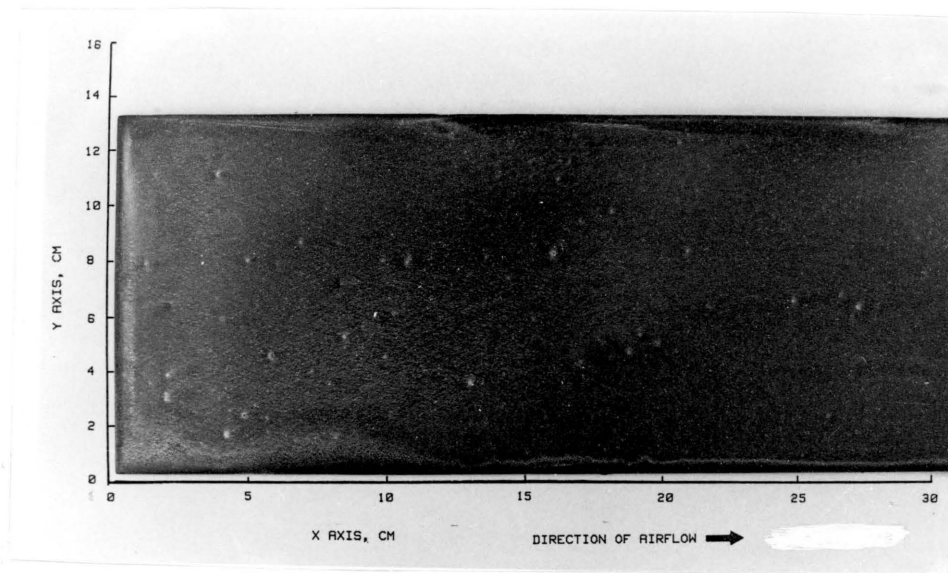


Figure VIII-4. Oil/Pigment Flow at 5 m/s.

airspeed of 5 m/s). Vortex formation is indicated by the build-up of the white titanium dioxide pigment approximately 0.7 cm from the leading edge (along the y axis) and 0.7 cm from the side edges (x axis). There was no indication of airflow being disturbed elsewhere on the experimental plate. The random white spots are the result of spattering of the oil/pigment mixture during the airbrushing procedure.

Figure VIII-5 is a photograph of the oil/pigment flow for 160 minutes at an airspeed of 2 m/s. Vortex formation is indicated by the pigment build-up approximately 0.5 cm from the leading and side edges. The wake regions are not as distinct as in Figure VIII-4; there was less vorticity in this experiment due to the lower airspeed.

Figure VIII-6 is a photograph of the oil/pigment flow on the experimental plate after 80 minutes at an airspeed of 2 m/s. The flat plate was positioned at an angle of incidence of seven degrees to the airflow (i.e., the leading edge was lower than the trailing edge). Vortex formation is indicated by the build-up of pigment approximately 0.3 cm from the leading and side edges. This experiment indicates there was somewhat less flow disturbance at the edges with the experimental plate rotated slightly rather than positioned at a zero angle of incidence with the airflow. Thus, the results would not be significantly effected, if the experimental plate was not positioned exactly parallel to the airflow.

One may conclude that the airflow was disturbed in a region less than one centimeter from the leading and side edges of the

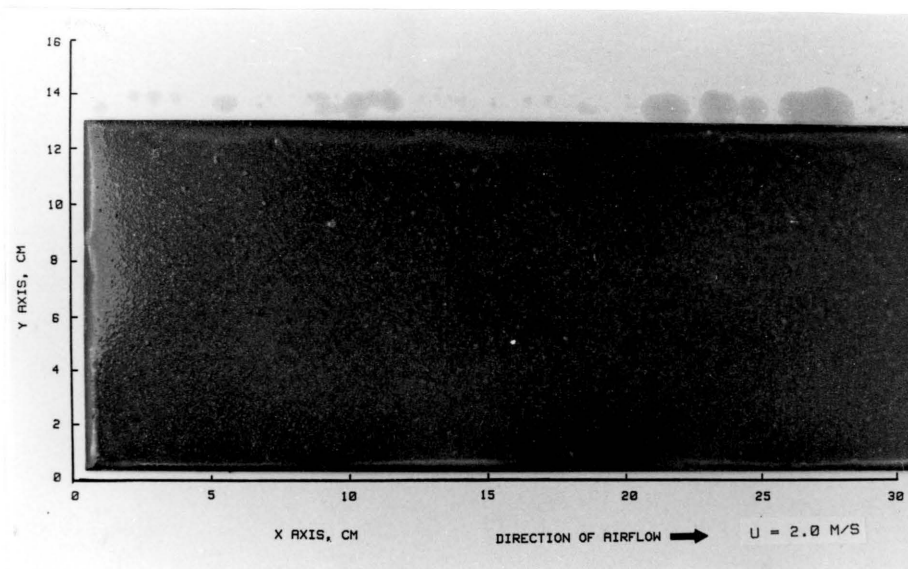


Figure VIII-5. Oil/Pigment Flow at 2 m/s.

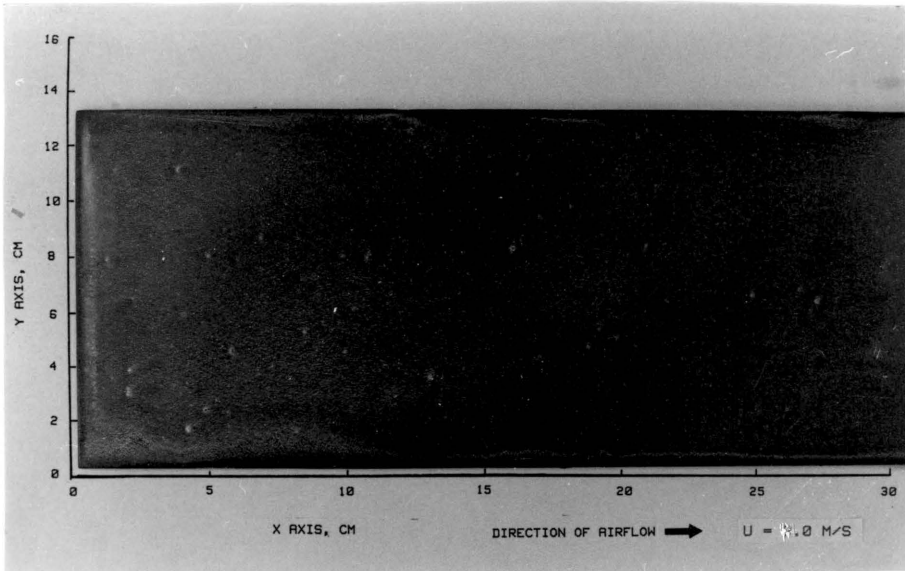


Figure VIII-6. Oil/Pigment Flow on a Flat Plate at a Seven Degree Angle of Incidence with the 2 m/s Airflow.

experimental plate. The airflow over the rest of the plate appeared to be undisturbed.

### Aerosol Generation

The aerosol outputs for nebulizer pressures of 30, 40, 50, and 60 psig are shown plotted versus time in Figure VIII-7. The aerosol generation system had a relatively constant short-term output of one micron diameter microspheres of 400 per second at 50 psig. The exhaust flowrates were measured with a soap bubble flow meter at 30, 40, and 50 psig as 3.1, 3.8, and 4.6 liters per minute, respectively.

Solvent evaporation with a subsequent increase in the microsphere suspension concentration was observed by Liu and Lee (1975) during long-term operation of a pneumatic nebulizer. However, an increase in the microsphere concentration is minimized in the present system through the use of a large reservoir volume.

High pressure nitrogen cylinders were used through a double pressure regulator to operate the nebulizer because of availability and low cost. Compressed air cylinders were much more expensive; the available air compressor was limited to a maximum output pressure of 40 psig and was very noisy.

Ambient air is approximately 78 % nitrogen. The kinematic viscosities,  $\nu$ , of air and nitrogen are 0.148 and 0.158 cm<sup>2</sup>/s, respectively, at 20 C and one atmosphere. The difference in the viscosities of air and nitrogen is 6.3 %. This small difference was not considered to significantly affect the nebulizer

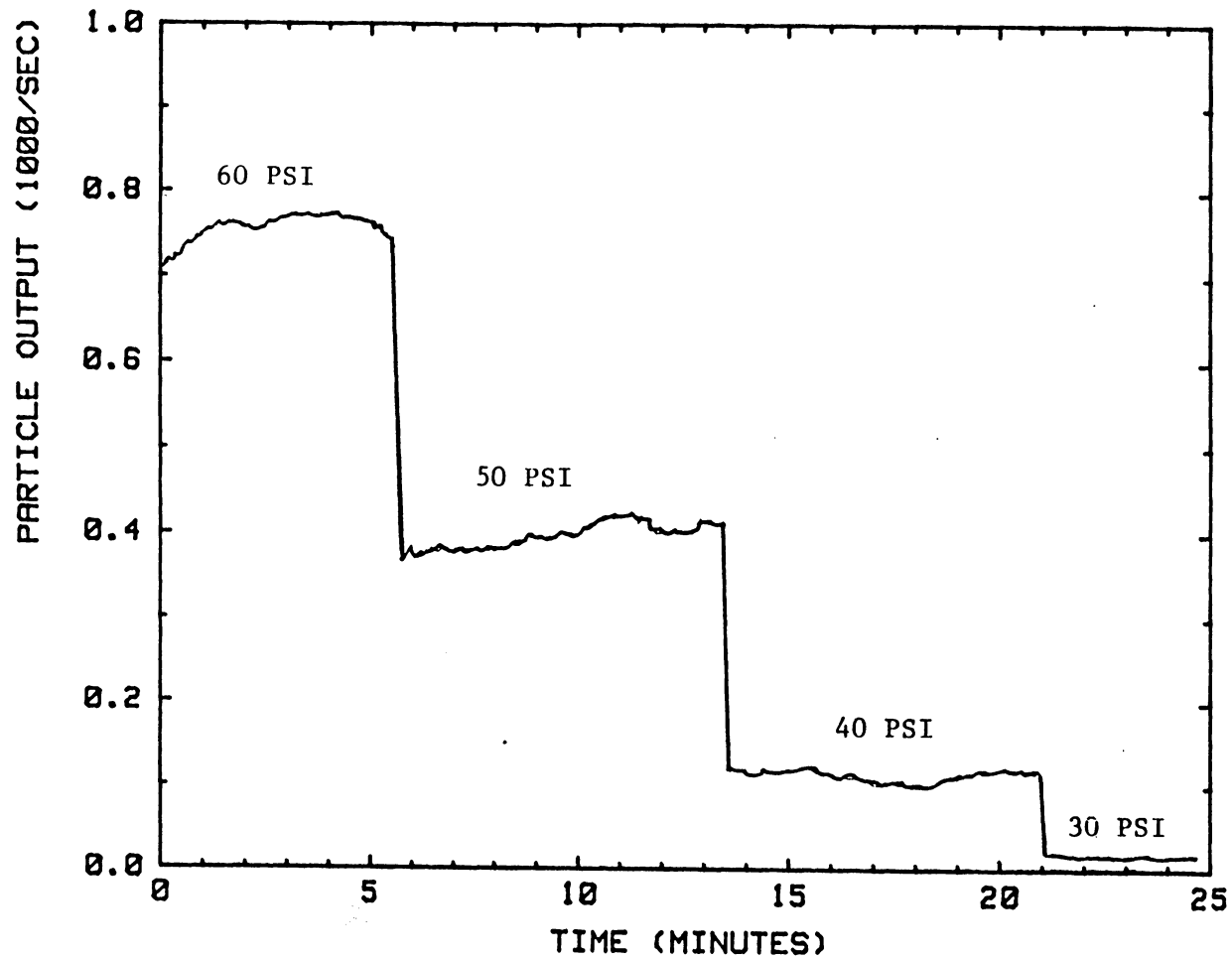


Figure VIII-7. Nebulizer Particle Output Versus Time for Various Pressures.

performance, aerosol diffusion, or aerosol deposition.

### Aerosol Dispersion

The intent of this test was to characterize the dispersion of aerosols from the generator outlet in the laminar wind tunnel airflow. Aerosols were dispersed into the airstream 18 cm upstream of the leading edge of the experimental plate. The locations of the horizontal and vertical aerosol concentration profiles in the wind tunnel are shown in Figure VIII-8.

The aerosol concentration was measured in a vertical traverse at  $z = 4$  to 11 cm above the wind tunnel floor at  $y = 16$  cm from the rear wall, as shown the semi-log plot Figure VIII-9. Each point represents the 30 second average particle concentration from the strip chart record. The maximum particle concentration of 5000 particles per liter occurred at 6.5 cm to 7.5 cm (i.e., the centerline of the plume). The shape of the vertical concentration profile indicates that particle diffusion may be approximated by a Gaussian distribution function. The vertical standard deviation,  $\sigma_z$ , (a measure of the position of the point of inflection on either side of the curve) was calculated as 0.767 cm. One may conclude that a flat plate located near the centerline of the plume would have a relatively constant boundary layer aerosol concentration in the vertical direction for approximately one centimeter.

The aerosol concentration was measured in a horizontal traverse at  $y = 13$  to 18.5 cm from the rear wall at  $z = 8.0$  cm



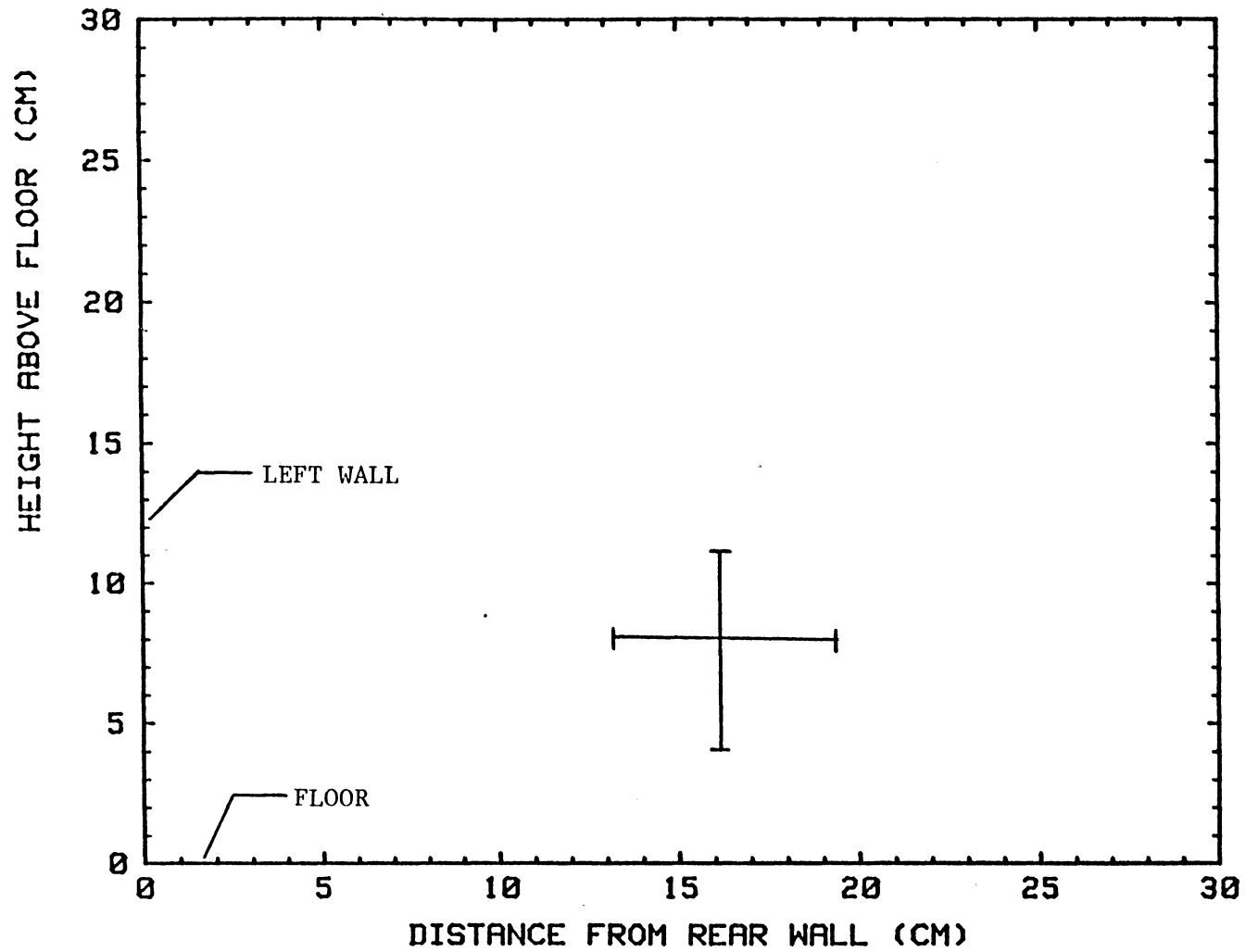


Figure VIII-8. Locations of the Horizontal and Vertical Particle Concentration Profiles.

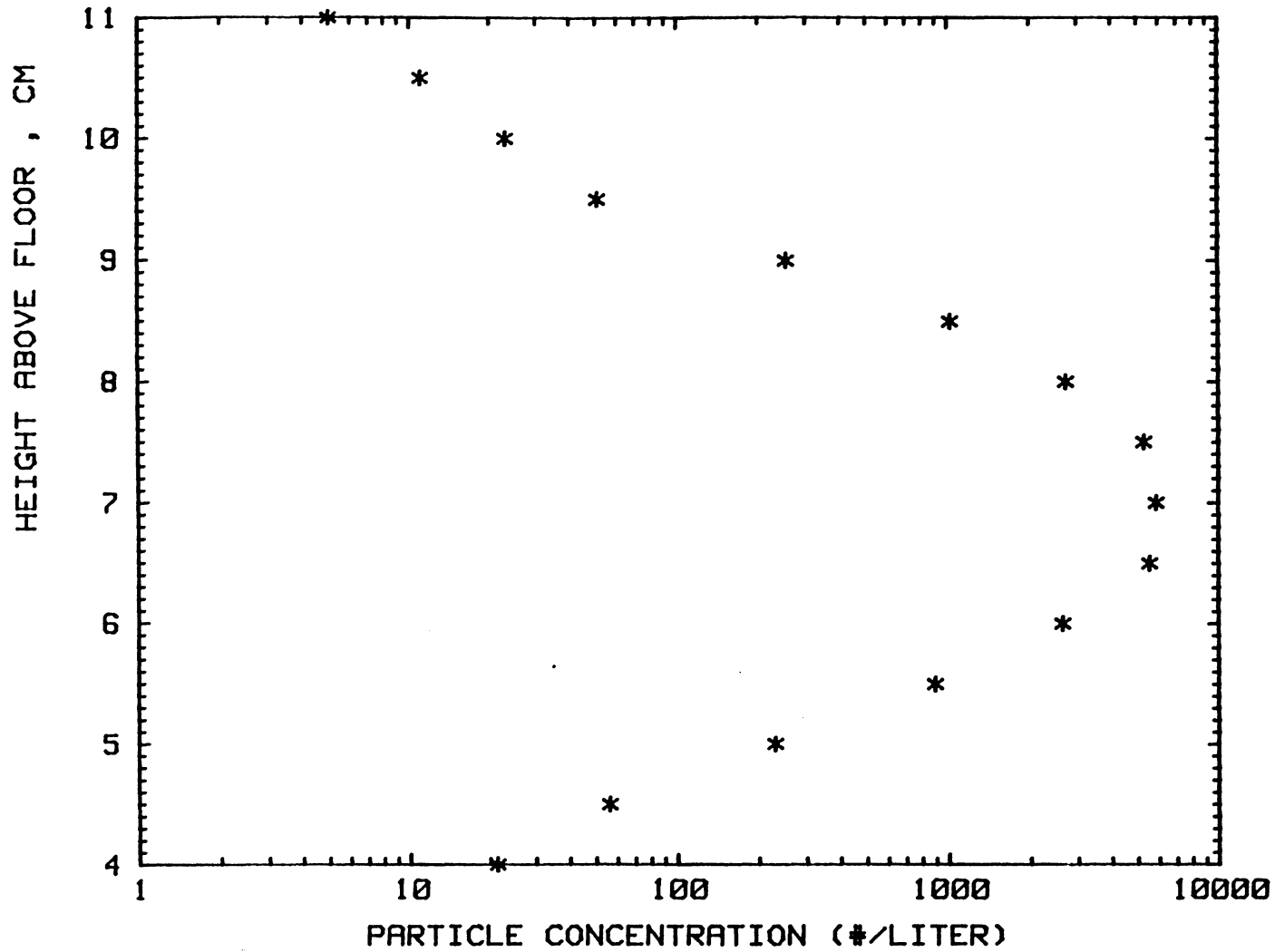


Figure VIII-9. Typical Vertical Particle Concentration Profile.

above the floor of the wind tunnel, as shown in the semi-log plot Figure VIII-10. The maximum particle concentration of 2500 particles per liter occurred at  $y = 15$  cm to 15.5 cm from the rear wall. The maximum aerosol concentration for the horizontal traverse was less than that for the vertical traverse as the horizontal traverse was about one centimeter above the plume centerline. The shape of the horizontal aerosol concentration profile indicates that particle diffusion in the crosswind direction may also be approximated by a Gaussian distribution function. The horizontal standard deviation,  $\sigma_y$ , was calculated as 0.767 cm. Thus, the horizontal and vertical aerosol plume dispersion were very nearly equal. One may conclude a flat plate located near the aerosol plume centerline would have a relatively constant aerosol concentration in the horizontal direction for approximately one centimeter.

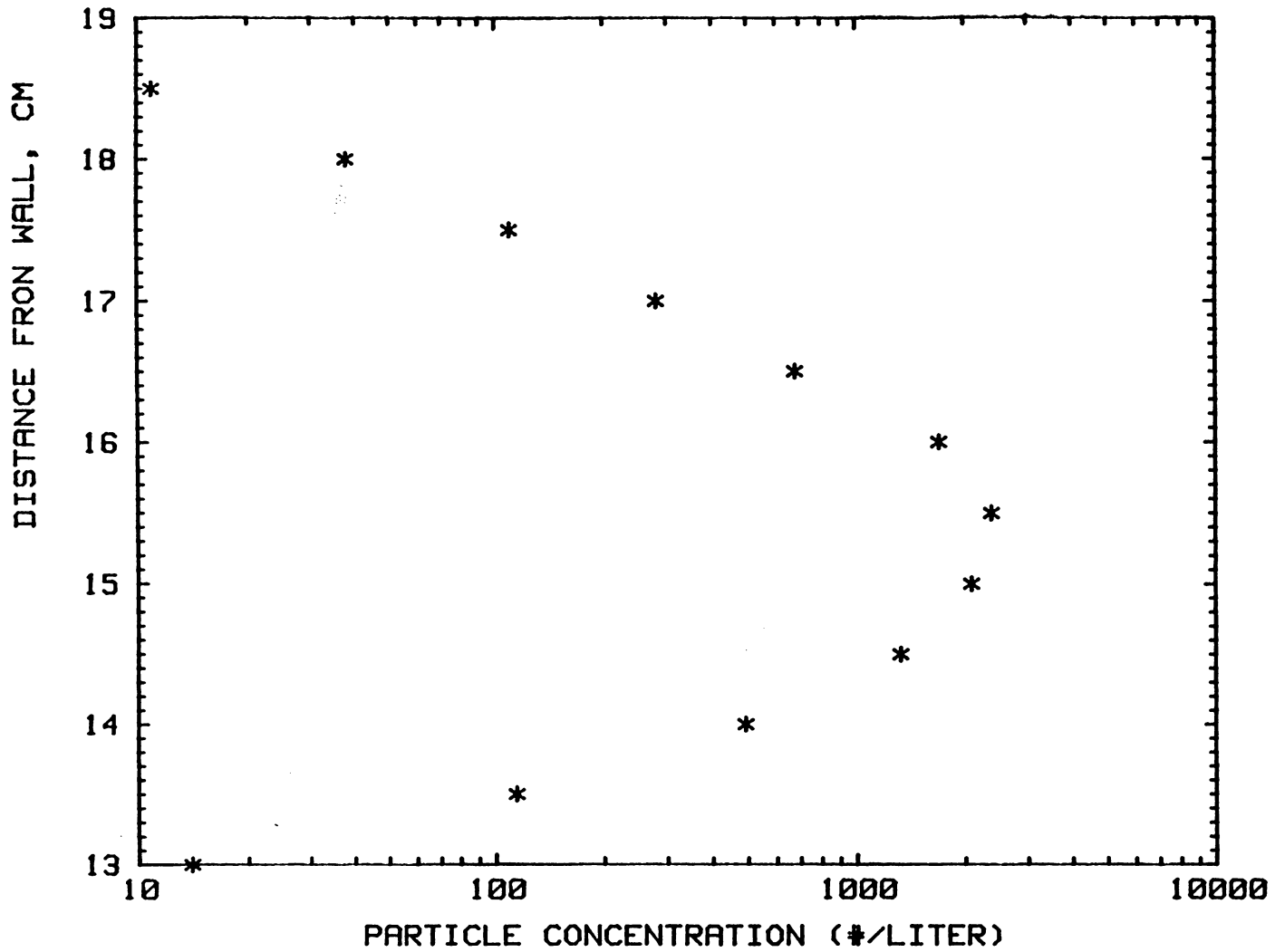


Figure VIII-10. Typical Horizontal Particle Concentration Profile.

### Background Aerosol Concentrations

The background aerosol concentration in the wind tunnel was measured to determine if background particle concentration might affect the deposition of the latex microspheres.

Figure VIII-11 shows a semi-log plot of the background particle concentrations in both the Applied Fluid Dynamics Laboratory ambient atmosphere and in the wind tunnel. The small particle (diameter less than 0.6 microns) counts were quite high in the laboratory atmosphere. Small particle counts were about a factor of 10 lower in the wind tunnel due to the high efficiency filter at the wind tunnel entrance. The background measurements were made in a "clean" atmosphere. Small particle counts were significantly higher when tobacco smoke or automobile exhaust were present in the atmosphere.

There was only a small difference in the number of 1.0 micron particles in the laboratory and wind tunnel atmosphere. The particle concentration values ranged from 10 to 15 particles per liter. This was much less than the 5000 particles per liter measured at the centerline of the aerosol generator exhaust plume. Particles larger than 1.5 microns were only occasionally measured in the laboratory atmosphere and were effectively removed by the high efficiency particle filter.

Thus, the background concentration of one micron diameter particles would not significantly affect the deposition of the latex microspheres.

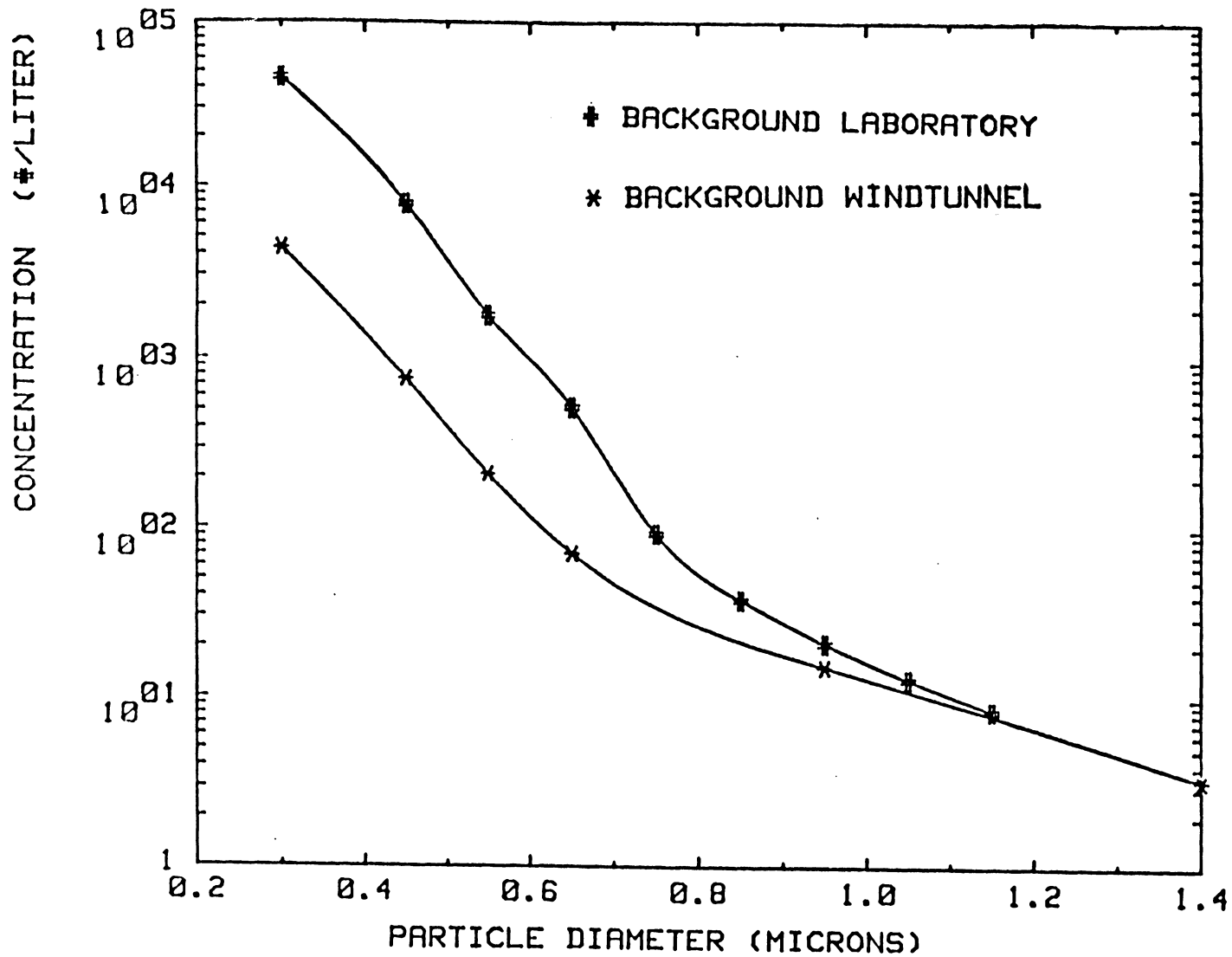


Figure VIII-11. Wind Tunnel and Laboratory Background Particle Concentrations.

### Electrostatic Charge Measurements

The original intent of this test was to measure an average electrostatic charge per particle (total electrostatic charge ÷ total particle count) in the aerosol generator exhaust. The Climet/ORTEC system counts only those particles greater than 0.3 microns in diameter. However, a large number of particles less than 0.3 microns in diameter were present in the aerosol generator exhaust. It appears that they contributed significantly to the total electrostatic charge. These small particles were either small particles from the compressed gas cylinder or secondary aerosols produced from nebulization of the microsphere stabilizing chemicals. One could only measure the total electrostatic charge on all the particles passing through the Faraday cup.

The total electrostatic charge, I, was calculated as follows:

$$I = V \div G \quad (\text{IX-2})$$

where V is the Keithley current amplifier output voltage and G is the current amplifier gain ( $10^{-11}$  volts per ampere). The current amplifier was operating at its limits (i.e., maximum gain and suppression). A relatively slow current amplifier rise time of 300 milliseconds was required to reduce the noise from 60 Hertz alternating currents.

The total electrostatic charge was measured on the aerosol generator exhaust (at 50 psi) with and without the charge neutralizer. The current amplifier output (without the nebulizer)

was relatively constant at 3.2 volts for the six seconds shown in Figure VIII-12. The current was calculated as  $3.2 \times 10^{-11}$  amperes (coulombs per second). One electrostatic charge unit (electron charge) has a value of  $1.6 \times 10^{-19}$  coulombs.

The current amplifier output was reduced 94% to 0.2 volts after the charge neutralizer was installed, as shown in Figure VIII-13. The current flow was calculated as  $2.0 \times 10^{-12}$  amperes with an RMS current noise of approximately  $2 \times 10^{-15}$  amperes (Keithley Instruments Inc., 1975).

Thus, the total electrostatic charge in the aerosol generator exhaust was significantly reduced by the Polonium 210 source.



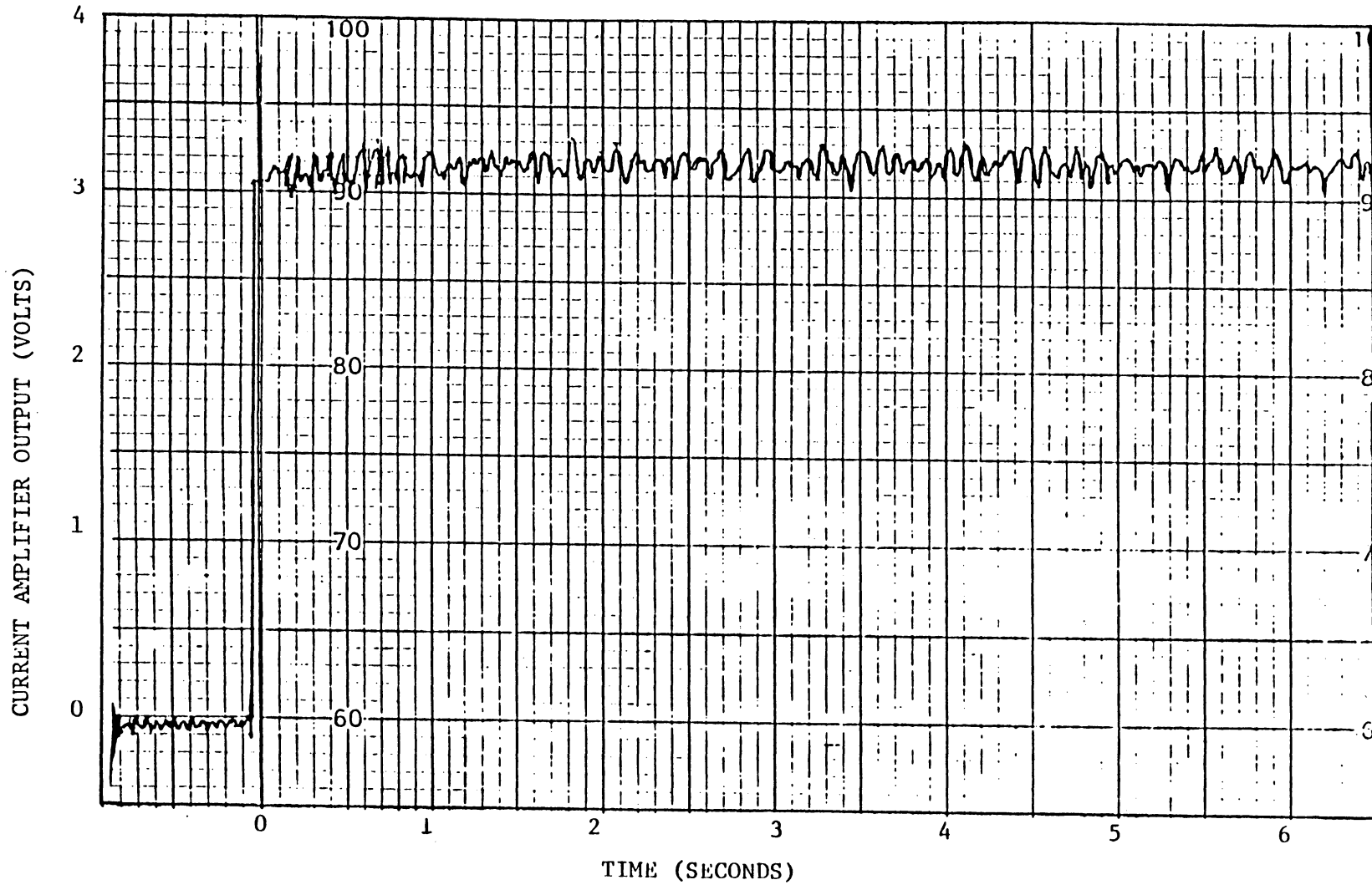


Figure VIII-12. Current Amplifier Output Voltage Versus Time Without Charge Neutralizer.

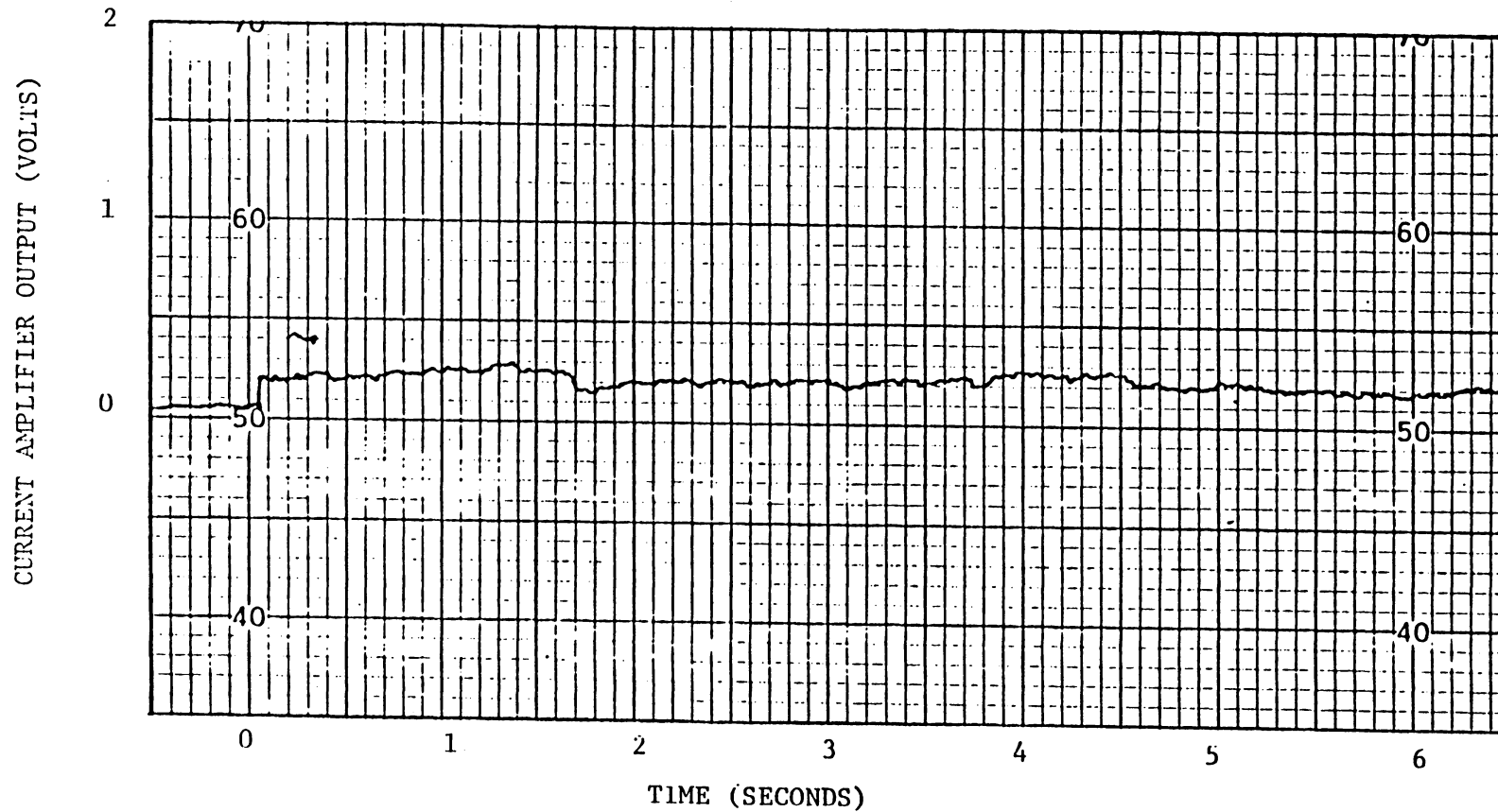


Figure VIII-13. Current Amplifier Output Voltage Versus Time with Charge Neutralizer.

### Experimental Plate Velocity Boundary Layers

The intent of this test was to characterize the velocity boundary layer over the experimental deposition surface in a laminar mainstream airflow (turbulence intensity of 0.015 and a mean velocity of 2 m/s).

The boundary layer over the experimental plate was initially characterized without the aerosol generator outlet in place. Consequently, the effect of the turbulence from the outlet on the boundary layer development was not realized. The boundary layer for the entire length of the experimental plate was more turbulent with the outlet in place. It was important to keep the aerosol outlet close to the experimental plate in order to maintain a high particle concentration in the boundary layer. Another experiment was performed to characterize the increased boundary layer turbulence due to the outlet. The results were most relevant; only the results with the outlet in place are presented.

Vertical velocity profiles were made from  $z = 1$  to 20 mm  $\pm 0.25$  mm above the horizontal plate at distances of  $x = 1$  cm to 26.5 cm  $\pm 0.1$  cm from the leading edge. The mean velocity and turbulence intensity for each point on the profile were calculated from 6000 consecutive hot-film anemometer records; the sampling rate was 100 Hertz for 60 seconds. Measurements were not made closer to the surface than 1 mm because of the previously mentioned limitations of the hot-film anemometer. The experimental data are listed in Appendix C.

Figure VIII-14 shows that the velocity profiles were similar

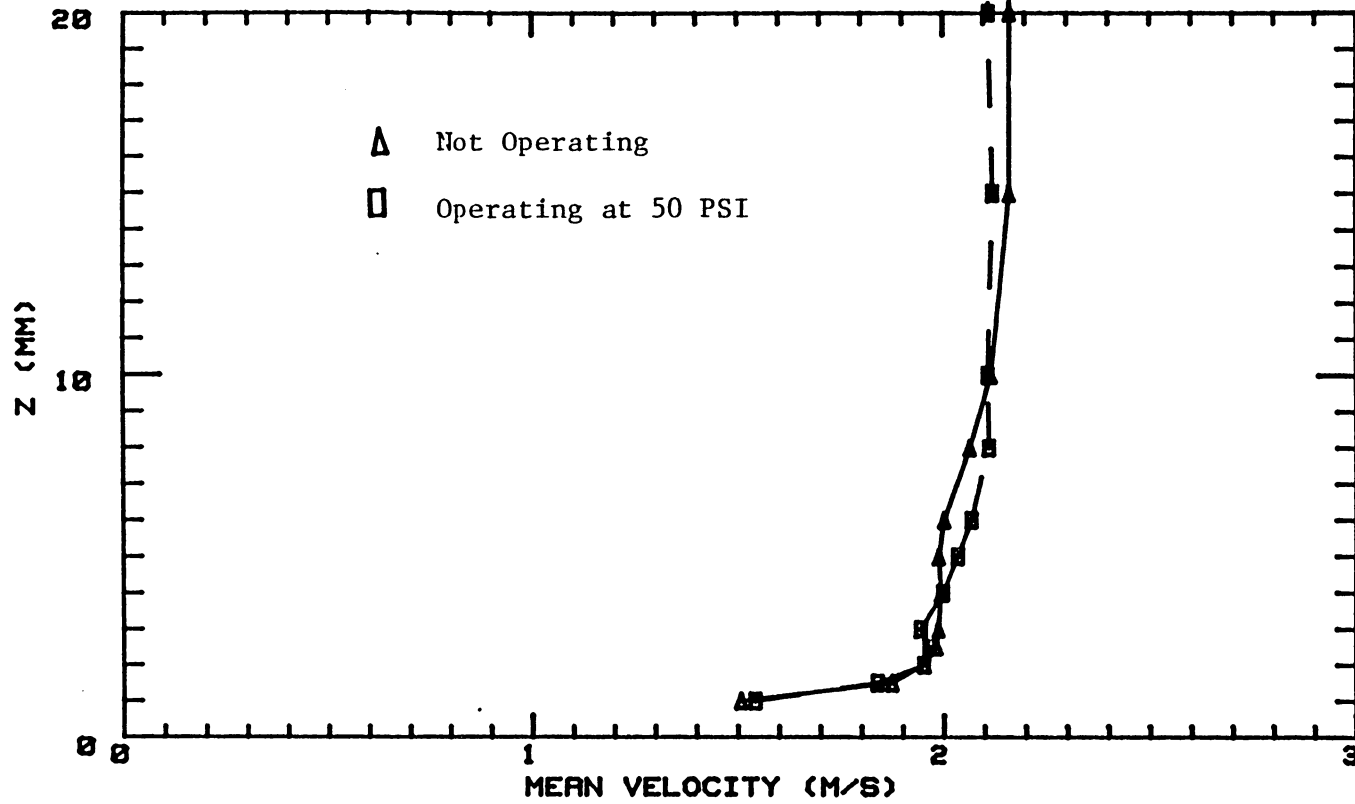


Figure VIII-14. Velocity Profiles With Aerosol Generator Operating and Not Operating.

at  $x = 1$  cm for the aerosol generator operating at 50 psi and for the aerosol outlet in place but not discharging aerosols. It appears that the boundary layer development on the surface of the aerosol generator outlet was responsible for creating the turbulence and not the jet from the aerosol generator outlet. Subsequent experiments were performed with the aerosol outlet in place but not discharging.

The velocity increased with  $z$  as shown in the velocity profiles in Figures VIII-15 and 16. The boundary layer velocity gradient ( $\Delta U/\Delta Z$ ) generally increased with  $x$  and also with Reynolds number. The shapes of the profiles were similar; the deviation of the shape of the profile at  $x = 12$  cm can not be explained. However, the airflow was slightly altered by the converging flow at the trailing edge of the experimental plate. This resulted in a decreased velocity gradient at  $x = 26.5$  cm (0.5 cm from the trailing edge). The mainstream velocity increased slightly from 2.15 to 2.25 m/s over the seven hour sampling period. This would account for a slight shift to the right of the velocity profiles. Due to the decreased airflow at the boundary the airflow at the outer boundary layer region speeded-up to maintain flow continuity. The mean velocity values at  $z = 20$  mm were slightly greater than the mainstream mean velocity.

The flat plate presented a bluff body to the oncoming airstream, consequently the airstream was diverted from its original path at the leading edge. The flow separation resulted in vortex formation there. In the core region of the vortex the

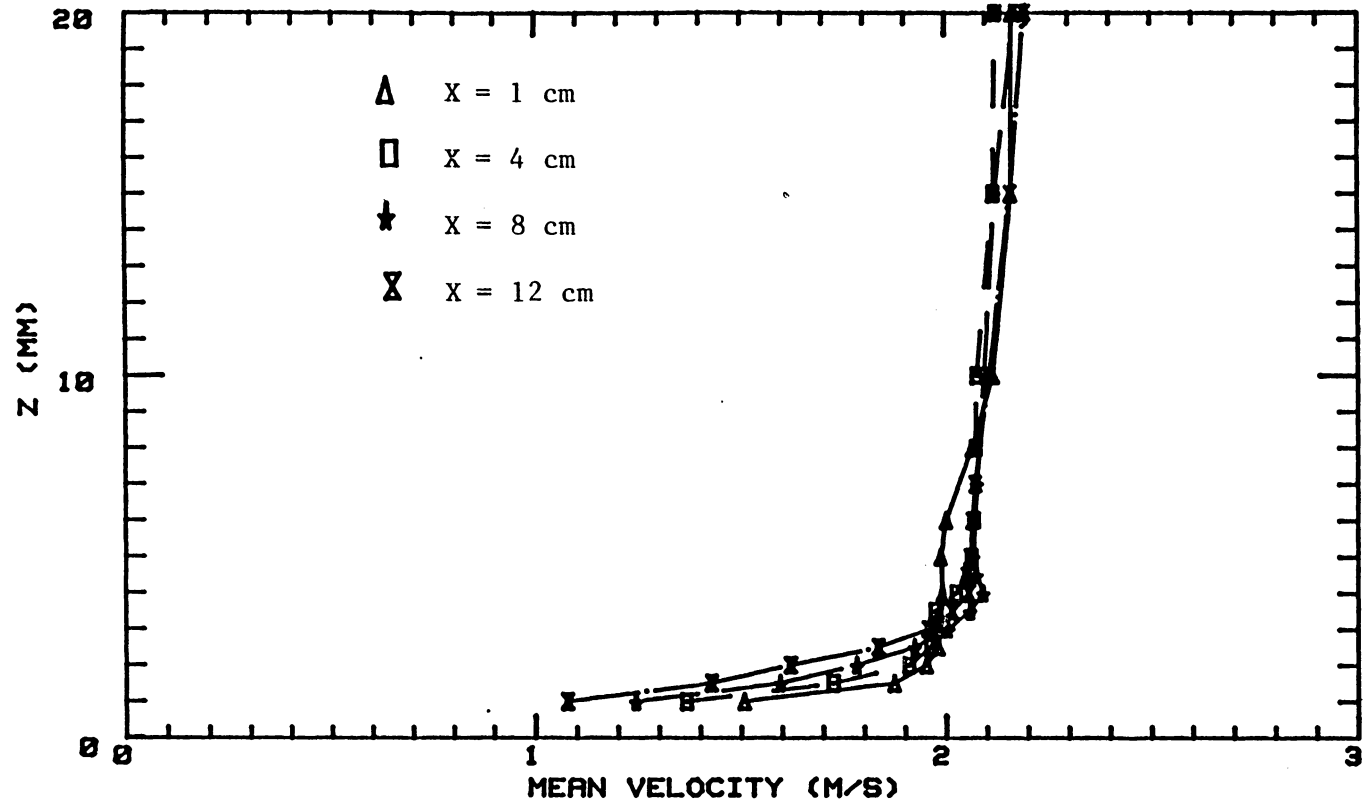


Figure VIII-15. Velocity Profiles at X = 1, 4, 8, and 12 Centimeters From the Leading Edge.

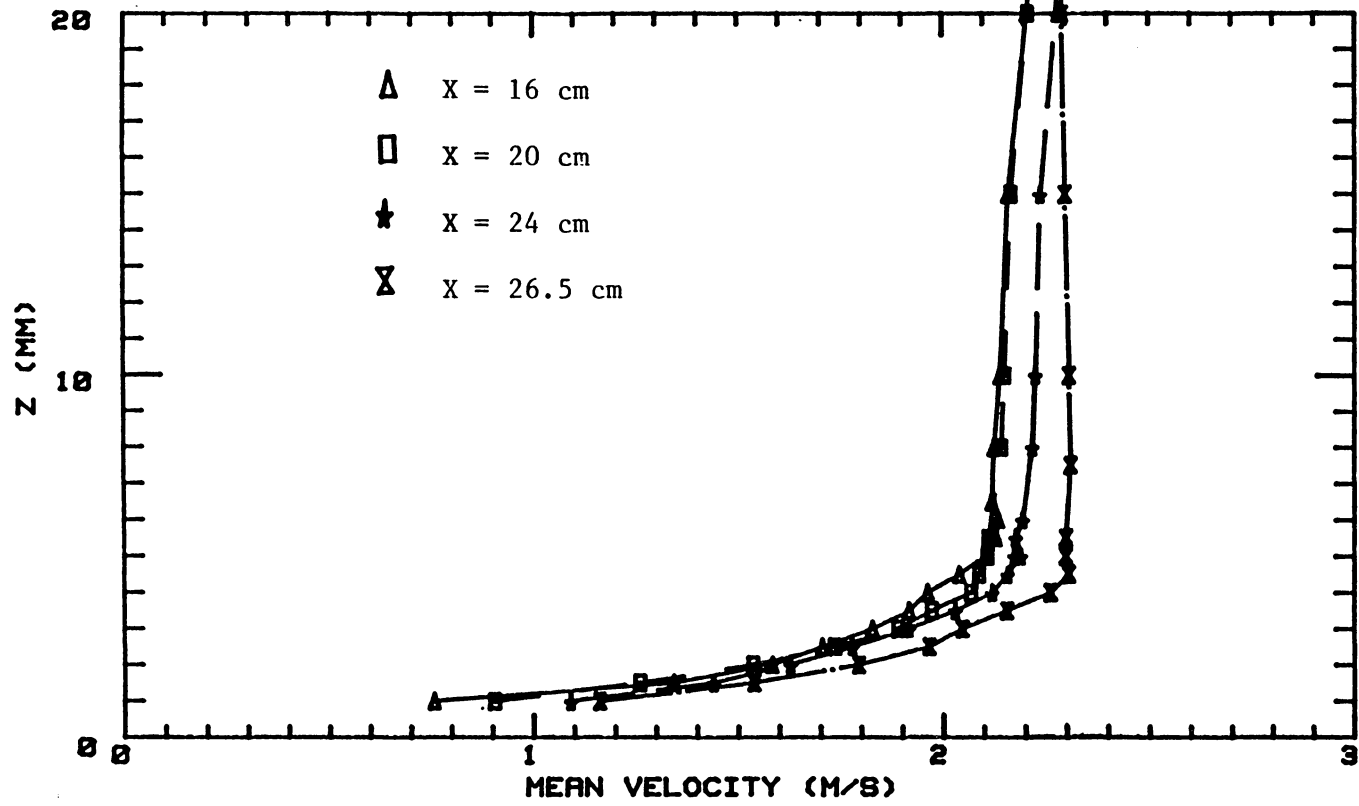


Figure VIII-16. Velocity Profiles at X = 16, 20, 24, and 26.5 Centimeters From the Leading Edge.

velocity was reduced, but at its extremes the velocity was increased. It appears that the velocity was greatest at  $z = 1$  mm near the leading edge due to the location of the probe in the region of increased velocity. However, the velocity at  $z = 1$  mm decreased with distance from the leading edge up to  $x = 20$  cm due to the vortex dissipation. The velocity at  $z = 1$  mm began to increase at  $x = 20$  cm as the boundary layer development began.

The mean velocity profiles, their locations, and the velocity boundary layer are shown in Figure VIII-17. Table VIII-3 lists the theoretical and experimental velocity boundary layer thicknesses at various distances and Reynolds numbers along the plate. The theoretical thicknesses were calculated using Equation (II-5) for laminar flow. The experimental thicknesses were determined from the mean velocity profiles. The experimentally determined thicknesses did not correlate well with the theoretical predictions. When the aerosol generator outlet was removed, the experimental and theoretical thicknesses correlated better. The deviation from the boundary layer theory appears to be due to the increased turbulence in the boundary layer.

The turbulence intensity profiles are shown in Figures VIII-18 and 19. Although the turbulence intensity varied, the shapes of the profiles were similar especially at distances up to 12 cm from the leading edge. The variation of the turbulence intensities was probably due to the intermittent vortex shedding from the leading edge. The turbulence intensity was greatest at the boundary and tended to decrease with an increase in the distance above



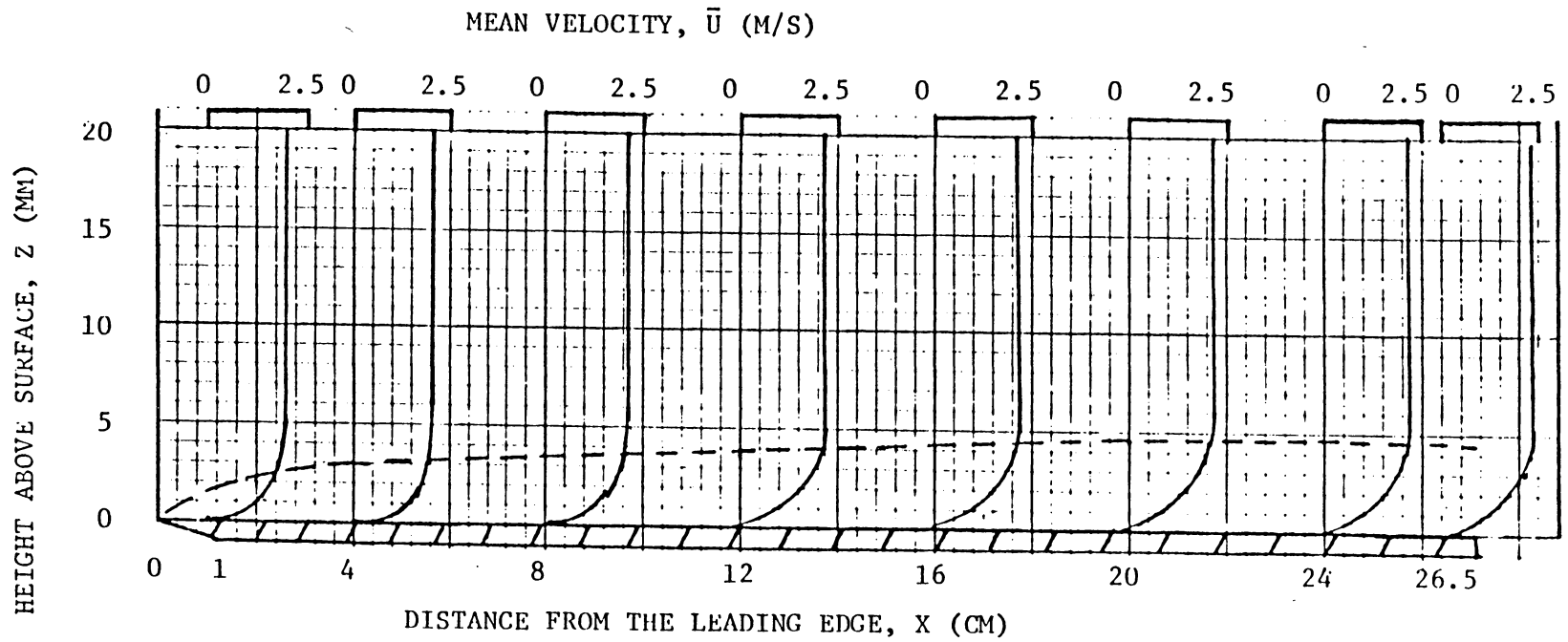


Figure VIII-17. The Mean Velocity Profiles along the Experimental Plate and Velocity Boundary Layer.

TABLE VIII-3. THEORETICAL AND EXPERIMENTAL  
VELOCITY BOUNDARY LAYER THICKNESSES

Distance from Leading Edge, X (cm)	Theoretical Thickness, (mm)	Experimental Thickness, (mm)	Plate Reynolds Number *
1	1.4	2.0	1467
4	2.6	3.0	5867
8	3.7	3.5	11733
12	4.5	3.5	17600
16	5.1	4.0	23467
20	5.6	4.5	29333
24	6.1	4.5	35200
26.5	6.8	4.0	38867

\* U = 2.2 m/s

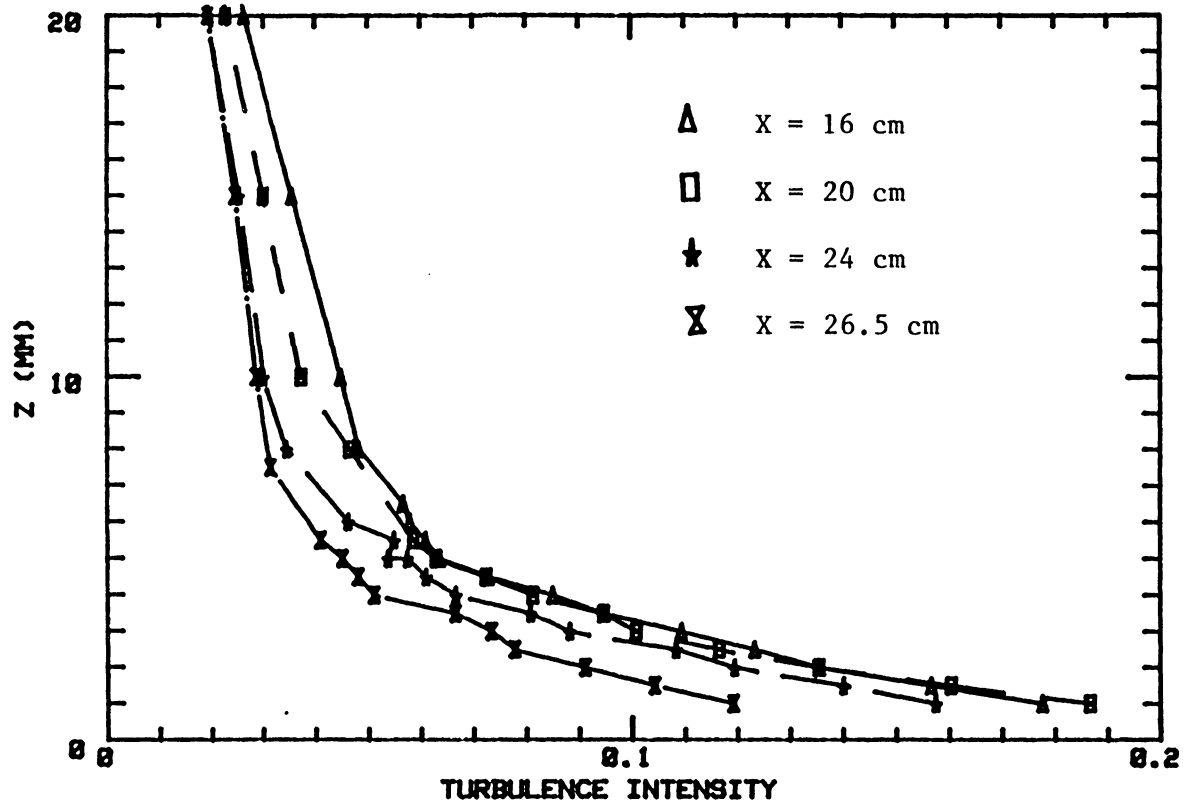


Figure VIII-18. Turbulence Intensity Profiles at X = 16, 20, 24, and 26.5 Centimeters From the Leading Edge.

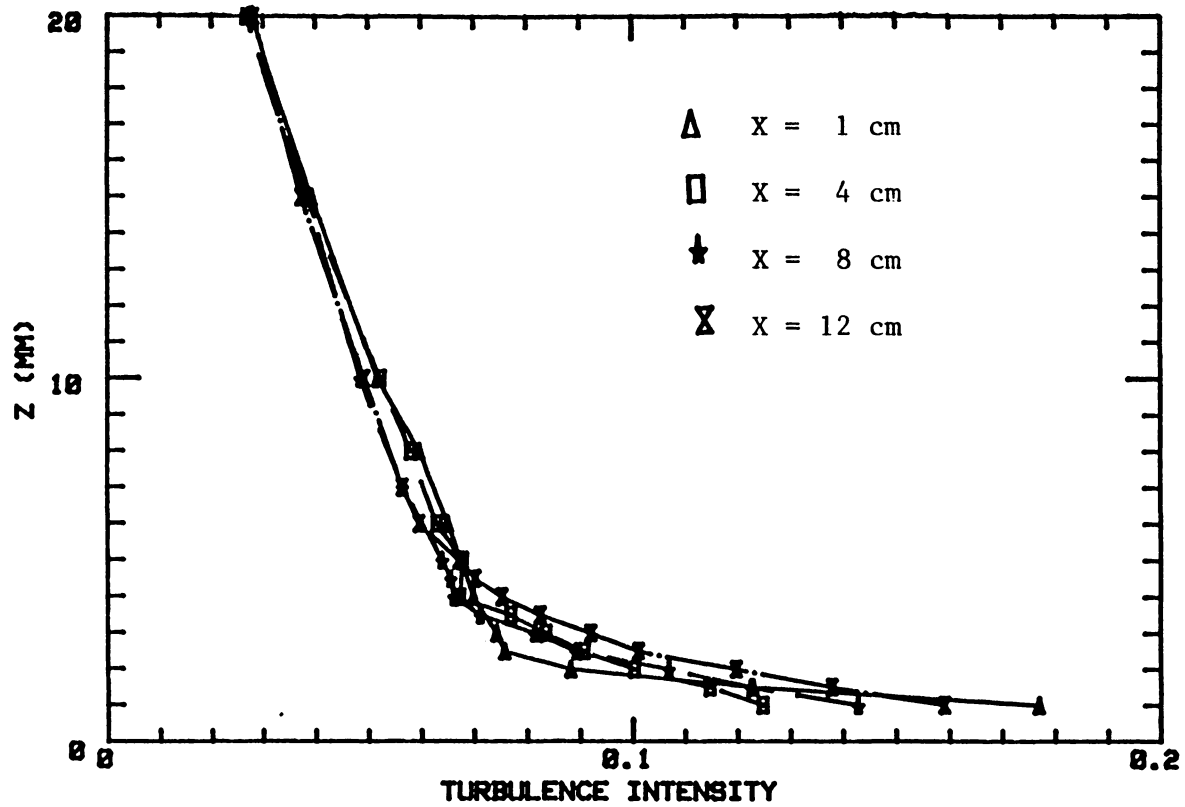


Figure VIII-19. Turbulence Intensity Profiles at 1, 4, 8, and 12 Centimeters From the Leading Edge.

the boundary. The turbulence also tended to decrease as  $x$  increased and Reynolds number increased. The mainstream turbulence was not approached until approximately 70 mm above the boundary; the mainstream mean velocity was approached within  $z = 3$  to 5 mm of the boundary. As a result of the large turbulence at  $z = 1$  mm, one would expect the boundary layer to be well mixed near the surface.

Wigley (1974) found that the turbulence intensity approached a maximum value within  $z = 1$  mm of the boundary surface. He found that the maximum value tended to increase and also move further away from the surface (still within 1 mm of the boundary) as the Reynolds number increased. Thus, the maximum turbulence intensity values were probably not measured in this experiment.

Grace and Wilson (1976) reported the boundary layer at  $z = 0.9$  mm above a model leaf remained laminar until a Reynolds number of 3600. The critical Reynolds number was experimentally determined as having a much lower value (2670) at  $z = 1$  mm in a laminar flow experiment. The boundary layer was turbulent everywhere; a laminar portion was not observed in these experiments due to the high velocity and the turbulence generated at the leading edge.

It appears that there may be three different regions on the experimental plate with respect to particle deposition. As the turbulence was greatest near the leading edge, the particle deposition rate would likely be greatest there. Particle deposition would likely decrease as the turbulent bursts dissipate, so particle deposition would decrease as the distance from the

leading edge increased. The velocity boundary layer became well-developed from  $x = 16$  to  $24$  cm and the turbulence intensity profiles were also quite similar. One would expect particle deposition to be uniform with a lower deposition rate in this region. The acceleration of airflow over the end of the plate prevented the boundary layer from developing normally over the trailing section of the plate ( $x = 26.5$  to  $27$  cm). One would expect the particle deposition rate to increase slightly in this region.

The intent of the next test was to characterize the velocity boundary layer over the experimental plate for a turbulent mainstream airflow (turbulence intensity of 0.11 and velocity of 2.5 m/s). Turbulence was induced by placing a grid in the wind tunnel approximately 40 cm upstream of the flat plate.

Vertical velocity profiles were made from  $z = 1$  mm to 20 mm ( $\pm 0.25$  mm) at distances from  $x = 1$  cm to 24 cm ( $\pm 0.1$  cm) from the leading edge. The profile at  $x = 1$  cm had the greatest velocity gradient, as shown in Figure VIII-20. The shapes of the other velocity profiles were quite similar to those for the laminar mainstream airflow (Figures VIII-15 and 16) except that the velocities were smaller near the boundary, as shown in Figures VIII-20 and 21. The velocity profiles at  $x = 12$ , 16, 20, and 24 cm were approximately the same, as shown in Figure VIII-21. The mainstream velocity increased slightly from 2.37 to 2.5 m/s over the seven hour sampling period. The velocity boundary layer was two to three times thicker

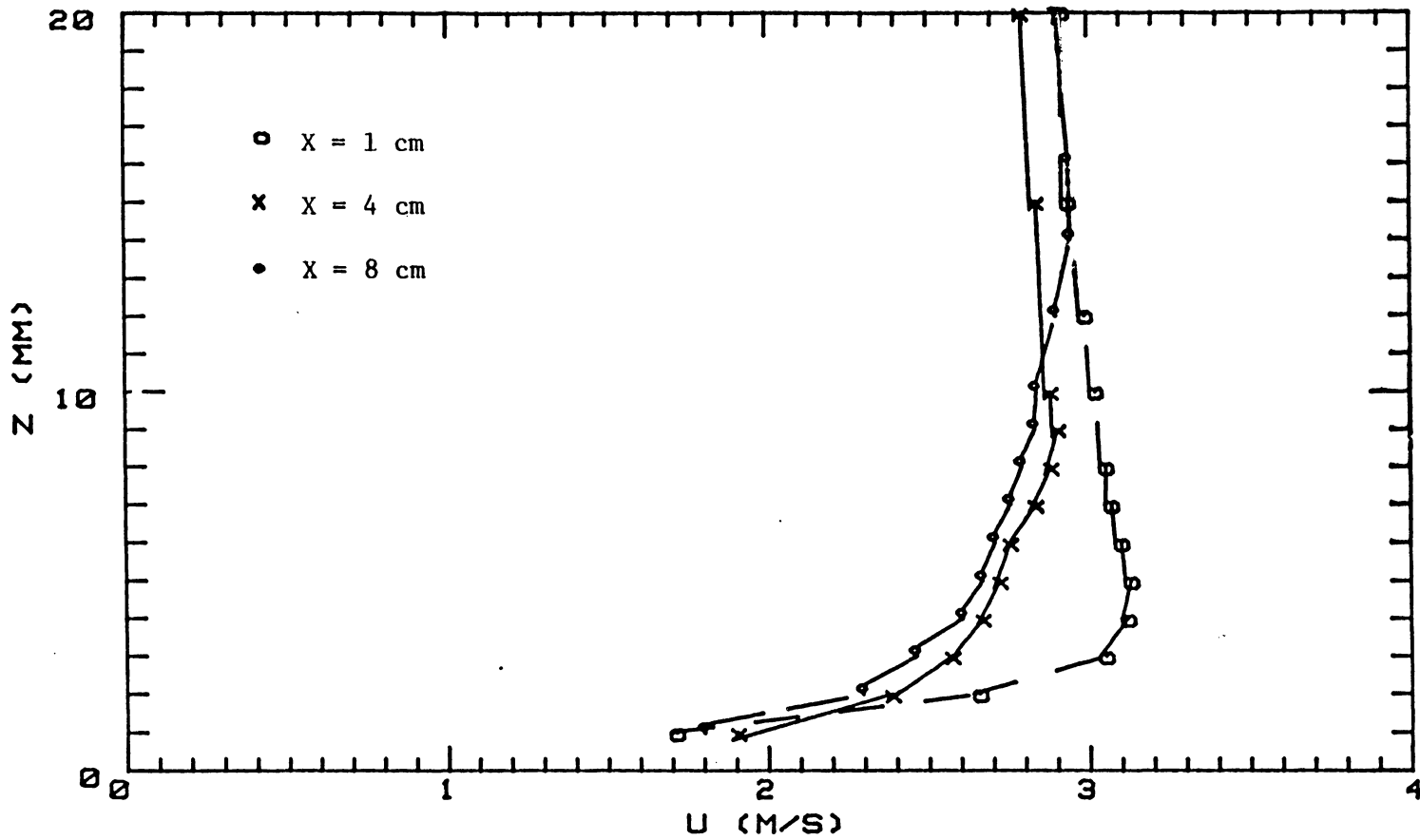


Figure VIII-20. Velocity Profiles at X = 1, 4, and 8 Centimeters from the Leading Edge.

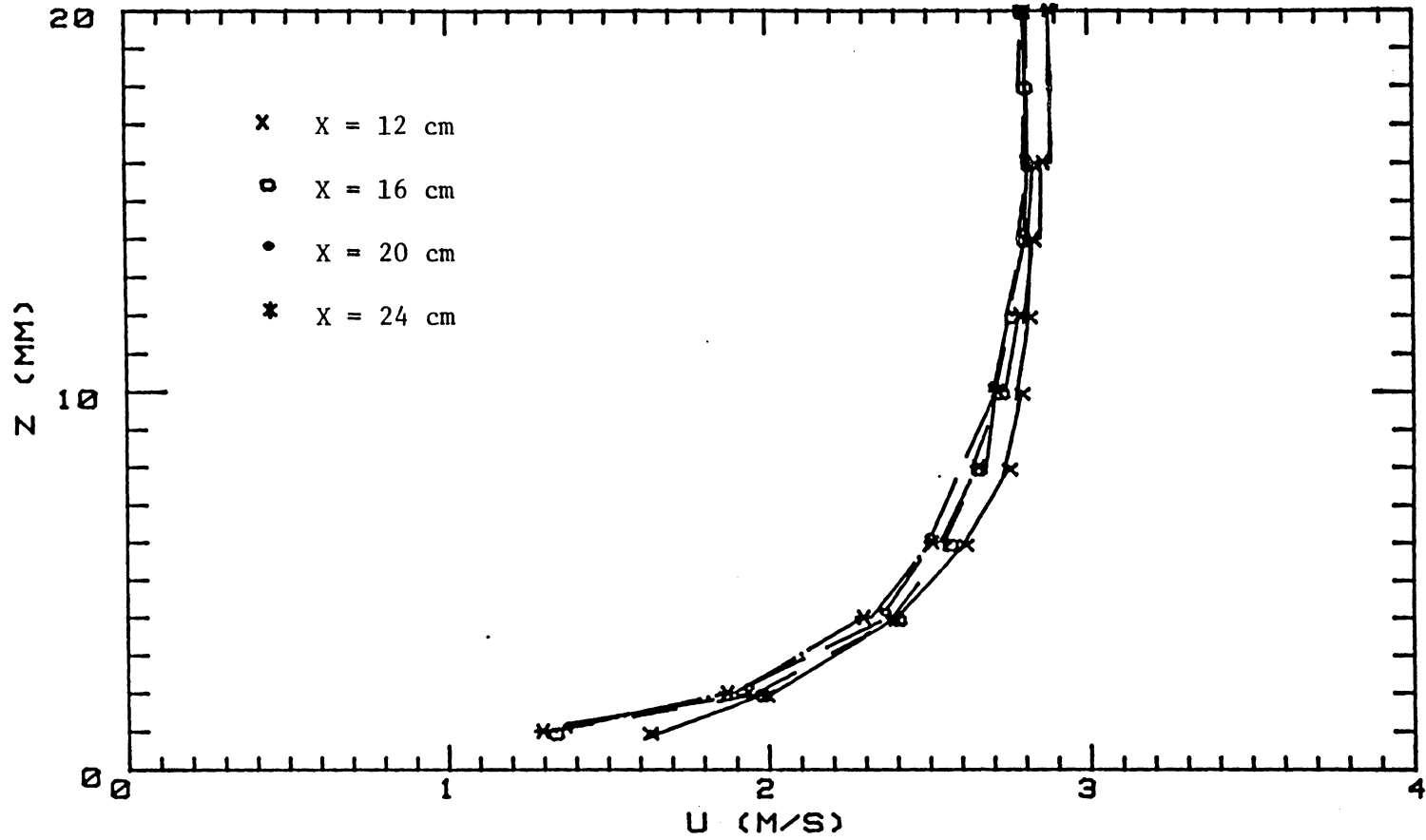


Figure VIII-21. Velocity Profiles at X = 12, 16, 20, and 24 Centimeters from the Leading Edge.



for the turbulent mainstream than for the laminar mainstream.

Figures VIII-22 and 23 show the shapes of the turbulence intensity profiles were also similar to those for the laminar mainstream airflow (Figures VIII-18 and 19), but the turbulence intensity values were somewhat greater. The turbulence intensity profiles at  $x = 12, 16, 20,$  and  $24$  cm were the same, as shown in Figure VIII-23. The turbulence intensity was as great as 0.36 near the leading edge (at  $x = 1$  cm). The increased turbulence served to trip the boundary layer airflow at the leading edge and increased the frequency of the vortex shedding. The perturbation of the airflow was exaggerated by the increase in the mainstream turbulence (Wigley, 1974).

It also appears that the same three previously discussed regions on the experimental plate occur with respect to particle deposition from the turbulent free stream. Although one would expect particle deposition to be greater for the turbulent mainstream than for the laminar mainstream. Acoustical noise, as well as vibration of the plate, may effect on the development of the turbulent boundary layer, but these effects could not be quantified (Hughes, 1984). During deposition experiments, suspended microspheres could act as dissipators of turbulence as well as turbulent wake generators (Hughes, 1984). These effects are thought to be minimal due to the low microsphere concentration.

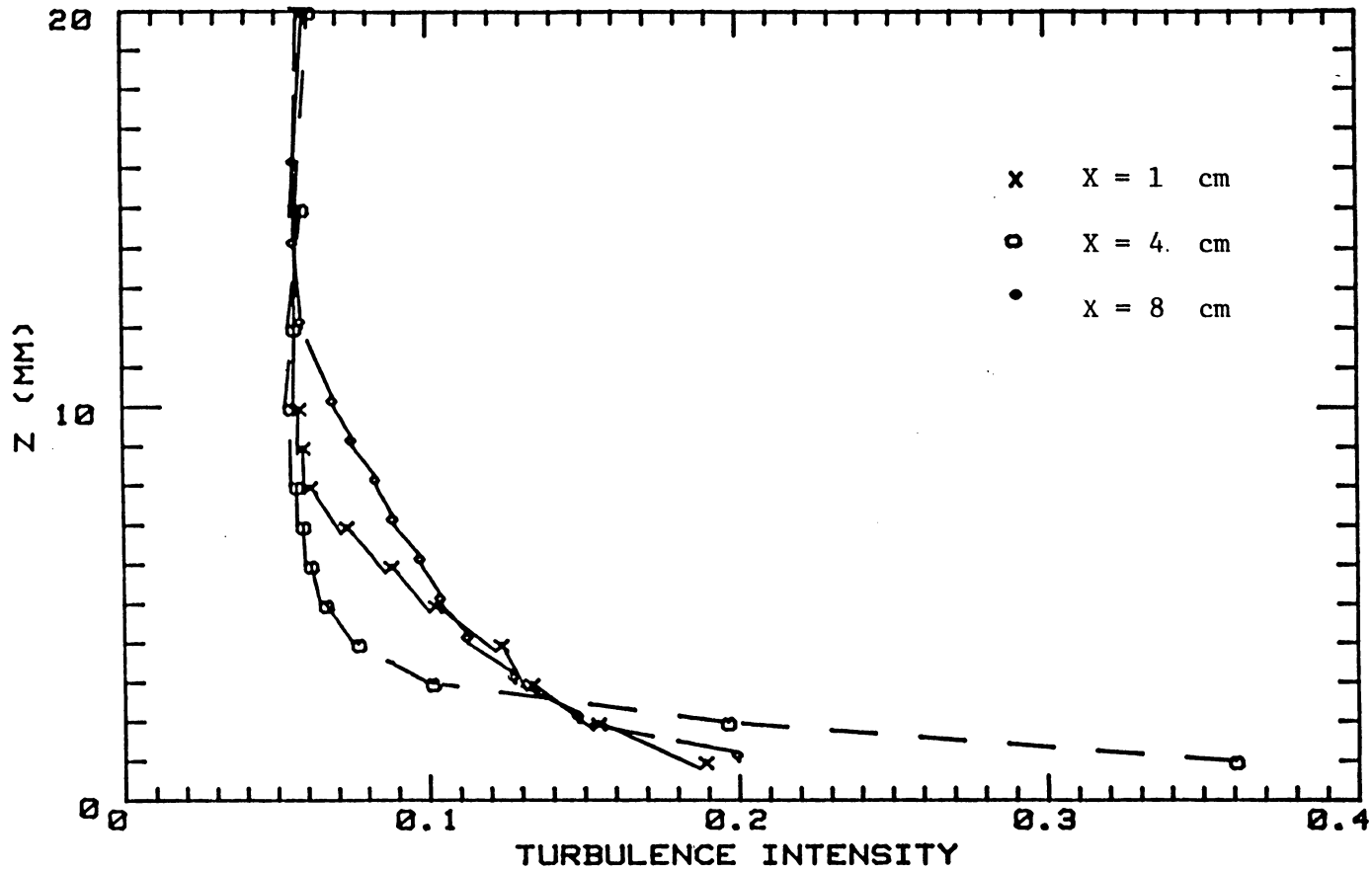


Figure VIII-22. Turbulence Intensity Profiles at X = 1, 4, and 8 Centimeters from the Leading Edge.

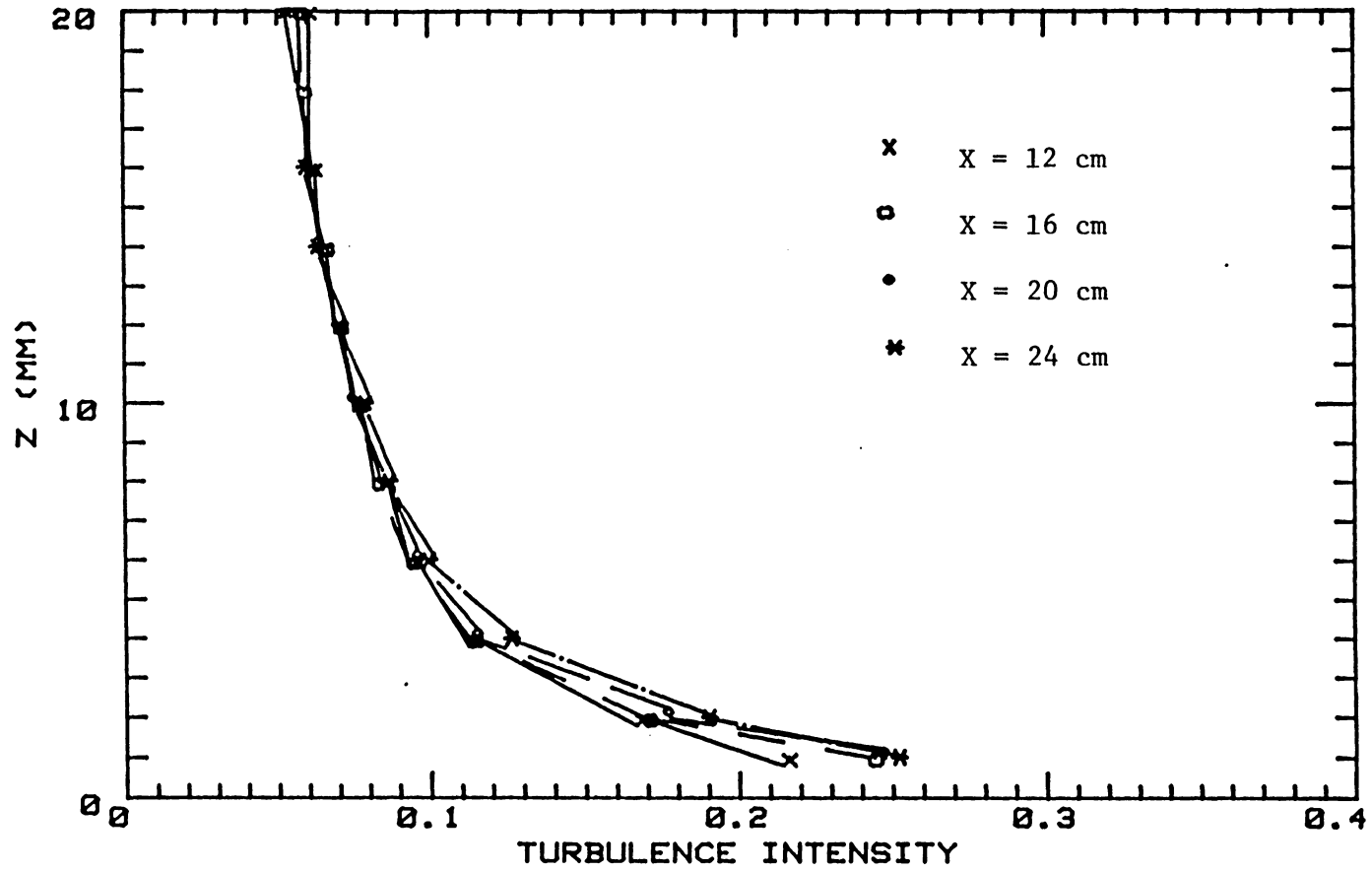


Figure VIII-23. Turbulence Intensity Profiles at X = 12, 16, 20, and 24 Centimeters from the Leading Edge.

### Particle Concentration Over The Experimental Plate

The intent of this test was to characterize particle concentration with location over the experimental plate. The laminar mainstream airflow was 2.1 m/s. The microspheres used in this experiment were 0.8 microns in diameter. The background concentration of 0.8 micron particles was approximately 30 particles/liter. Particle concentration profiles were made from  $z = 1$  to 20 mm  $\pm$  0.25 mm above the horizontal plate at distances from the leading edge of  $x = 0, 8, 16, 20,$  and 24 cm  $\pm$  0.1 cm. The data points on each profile represent the mean value of a 30 second average particle count from a strip chart record. The 30 second average was obtained from the electronic integration of the Climet output pulses by the ORTEC pulse height analyzer. The particle concentration data are listed in Appendix C.

Figure VIII-24 shows a semi-log plot of typical concentration profiles over the experimental plate. The particle concentrations were greatest at the leading edge and decreased as the distance from the leading edge increased due to plume dispersion in the  $y$  and  $z$  directions and plume transport in the  $x$  direction. Particle concentrations decreased only slightly from  $x = 16$  to 24 cm. The particle concentrations (for the same profile) at  $z = 2$  mm are approximately the same as those at  $z = 1$  mm as the boundary layer was well-mixed (indicated by the turbulence intensities in Figure VIII-19). Some of the concentration variation might have been due to the change in the sampling rate resulting from the lower velocity near the plate or the particle sampling probe might have disturbed

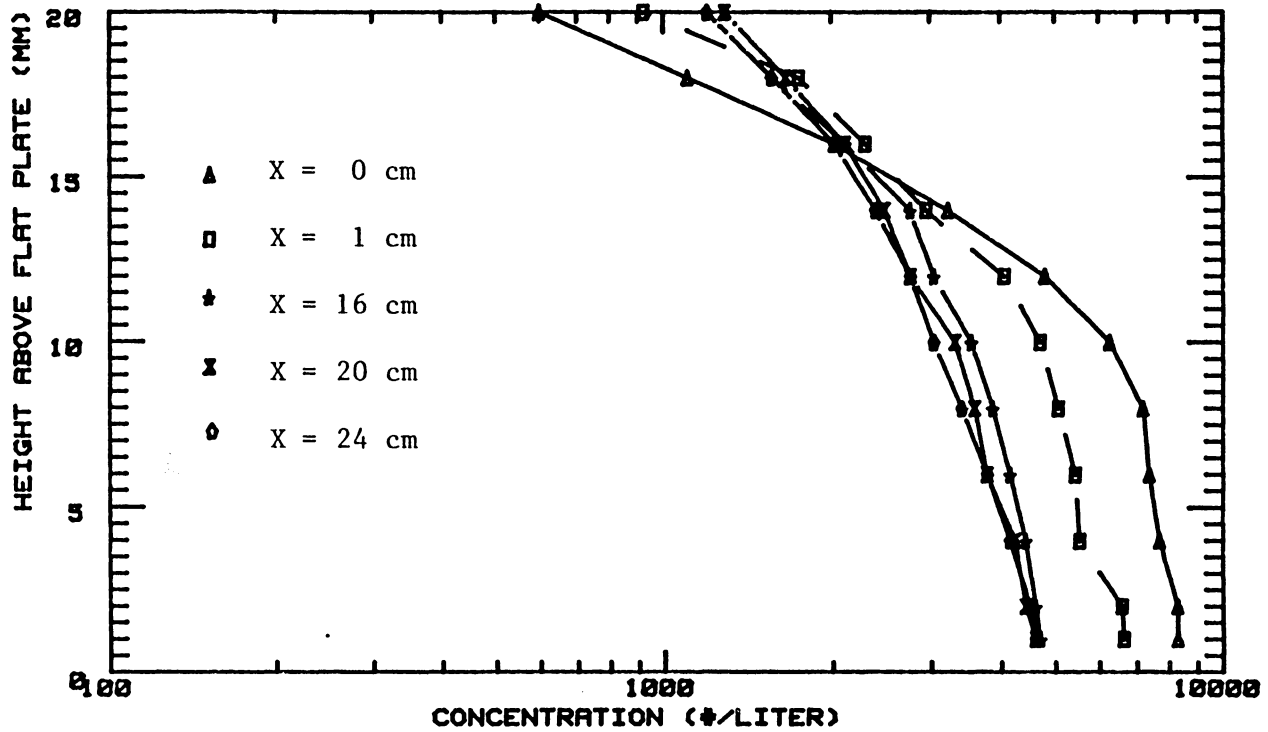


Figure VIII-24. Typical Particle Concentration Profiles Above the Experimental Plate at Distances of 0, 1, 16, 20, and 24 Centimeters From the Leading Edge.

the airflow near the experimental plate. The particle concentration profile shapes were quite similar at  $x = 16, 20,$  and  $24$  cm, the region of well-developed airflow.

Particle concentration traverses were then performed from  $x = 1$  to  $24$  cm  $\pm 0.1$  cm from the leading edge at  $z = 2$  mm  $\pm 0.25$  mm above the experimental plate. The traverse was repeated ten times in order to determine mean concentration values and standard deviations.

Figure VIII-25 shows a semi-log plot of the mean particle concentration with the standard deviation versus distance from the leading edge for the entire experimental plate. These data appear to fit an exponential curve. However, the mean particle concentration in the region of well-developed airflow is of more interest; these data were fairly linear.

The particle concentrations were normalized by dividing each by the particle concentration at  $x = 1$  cm and are shown plotted in Figure VIII-26. The slope of the curve for the particle concentration versus distance from the leading edge will remain the same even if the aerosol output changes (Pendergrass, 1983). The particle sampling probe may remain in a stationary position at  $z = 2$  mm and  $x = 24$  cm and not disturb the airflow or particle deposition in the upstream region. Thus, the particle concentration upstream may be predicted from Figure VIII-26 and the average particle concentration at  $x = 24$  cm.

Other deposition experiments have had a uniform particle concentration across the wind tunnel, rather than an expanding

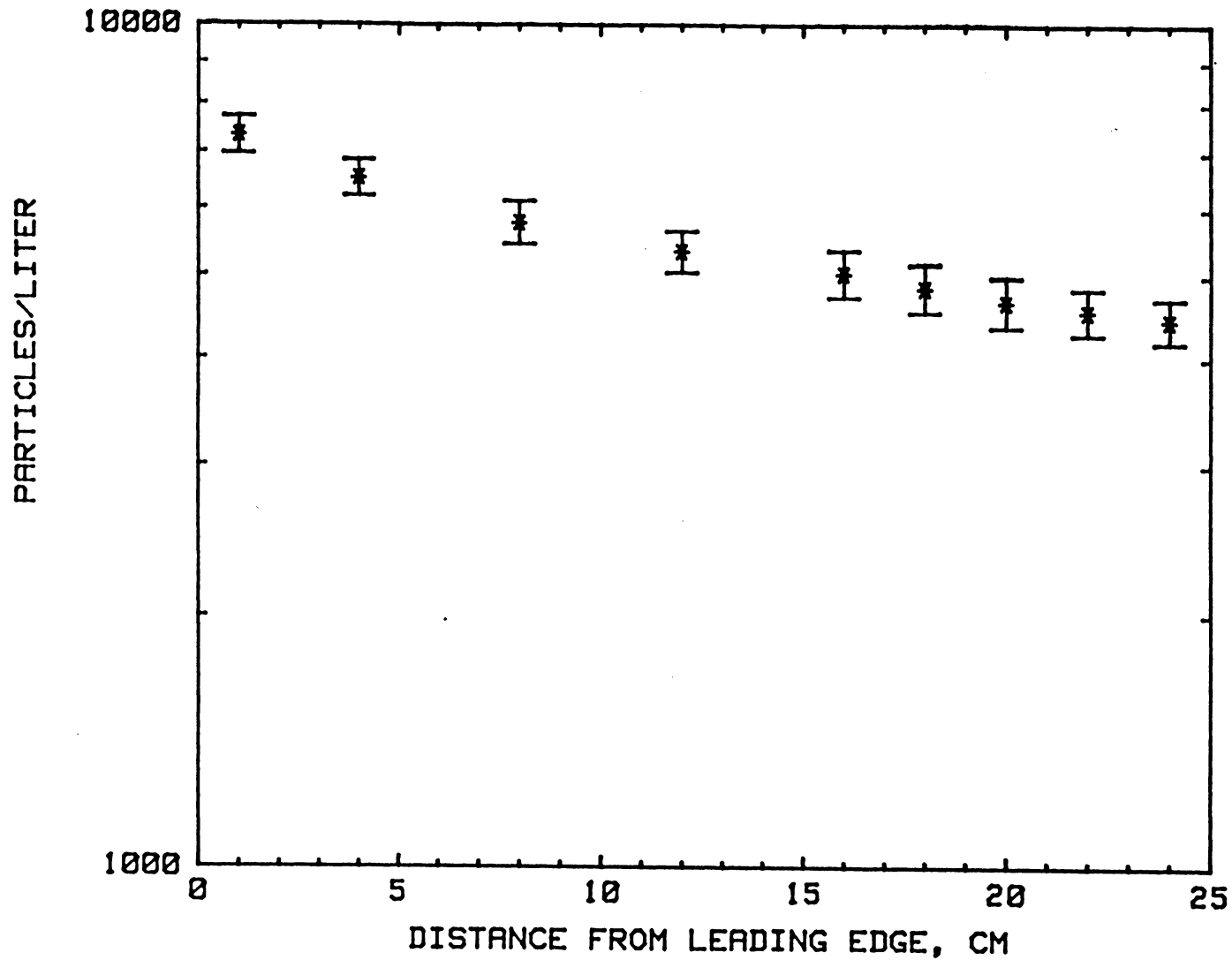


Figure VIII-25. A Plot of Particle Concentration at  $Z = 2$  mm Versus Distance from the Leading Edge.

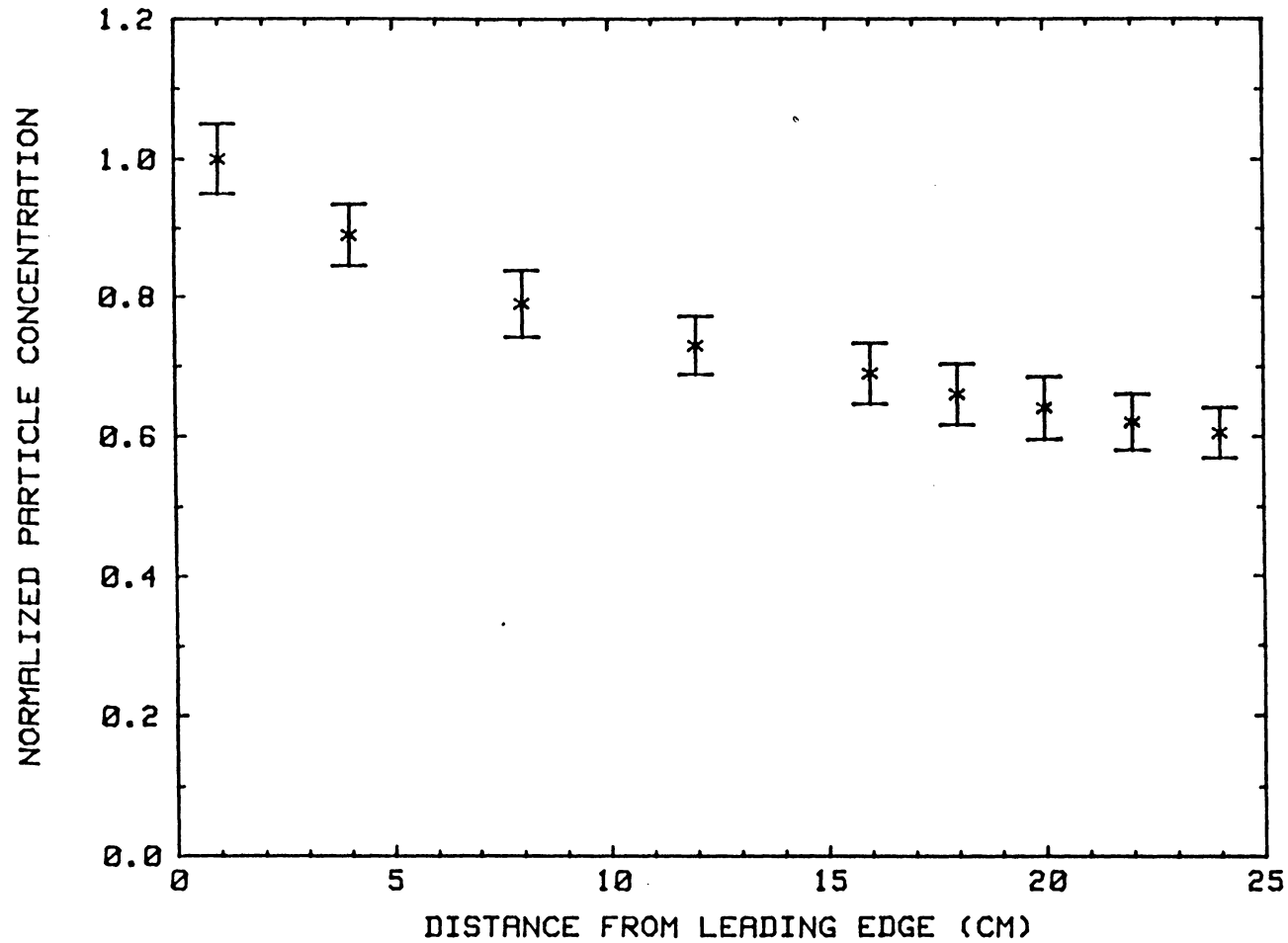


Figure VIII-26. Normalized Particle Concentration at  $Z = 2$  MM Versus Distance from the Leading Edge.



particle plume as in this study. Although Hicks (1984) contends that as a result of the expanding particle plume, the particle concentrations should be determined a small distance upwind of where the deposition occurs, this would not significantly effect the results.

CHAPTER IX  
EXPERIMENTAL DEPOSITION RESULTS

The intent of these experiments was to quantify the deposition velocity of microspheres being transported across the boundary layer that developed over the experimental plate. The resuspension of microspheres deposited on the experimental plate was also investigated. The experimental results are listed in Appendix D.

Table IX-1 presents a brief description of each experiment. All the experiments were performed with a mainstream mean velocity of 2 m/s, unless otherwise noted. The same flat plate was used in all the experiments. The ambient laboratory temperature was fairly constant at  $19 \pm 2$  degrees Celsius during the experiments. The relative humidity in the laboratory was 50 to 70 percent for Experiments 4 through 9, but the relative humidity was 20 to 30 percent for later experiments during which the heating system was in operation. The acrylic experimental plate was nonconductive and could not be electrically grounded. The particle flux was calculated by dividing the mean microsphere count per unit area on the experimental plate by the aerosol generation time. The experimental deposition velocity was calculated by dividing the particle flux by the aerosol concentration over the experimental plate measured at  $z = 2$  mm. Experiments 1 through 3 were preliminary in nature during which the methodology for depositing and counting the microspheres was developed.

TABLE IX-1. A SUMMARY OF THE EXPERIMENTS

---

Experiment Number	Microsphere Diameter, ( $\mu\text{m}$ )	Brief Experiment Description
1, 2, 3	0.9	Preparatory experiments
4	0.9	Deposition to an ideal surface
5	2.0	Electrostatic charge effect
6, 7, 9	0.8	Deposition to an ideal surface
8, 16	42.3	Resuspension from non-ideal surface
10, 11	1.1	Deposition to an ideal surface
12, 13, 14	1.1	Deposition to a non-ideal surface
15, 19, 20	1.1	Gravitational settling effect
17	1.1	Electrostatic charge effect
18	42.3 & 1.1	Effect of previously deposited large microspheres on deposition

---

### Ideal Surface

Microspheres 0.8, 0.9, 1.1, and 2.0 microns in diameter were deposited on an ideal (i.e., oil-coated) surface in Experiments 7, 4, 11, and 5, respectively. The deposition velocities are shown plotted versus the distance from the leading edge in Figure IX-1. For the 0.8, 0.9, and 1.1 micron diameter microspheres, the deposition velocities were greatest at the leading edge, decreasing slightly with distance from the leading edge until the deposition velocity became relatively constant. These results support the theory that the deposition is greatest at the leading edge where the turbulence is greatest. The deposition of the 2.0 micron microspheres showed an opposite effect; the deposition velocity increased as the distance from the leading edge increased. The only variation from the standard operating procedure was that the electrostatic charge neutralizer was not used in Experiment 5. It is possible that electrostatic charging of the aerosols may have affected the 2.0 micron diameter microsphere deposition.

The experimental deposition velocities increased as the microsphere diameters (i.e., mass) increased. The greatest deposition velocities occurred for the 2.0 micron diameter microspheres (possibly because of electrostatic effects); likewise, the smallest deposition velocities occurred for the 0.8 micron diameter microspheres. The experimental deposition velocities were approximately 3, 3.5, 100, and 170 times greater than the terminal gravitational settling velocities of 0.0023, 0.0029, 0.0038, and 0.013 cm/s (after BGI, 1980) for the 0.8, 0.9, 1.1, and 2.0 micron

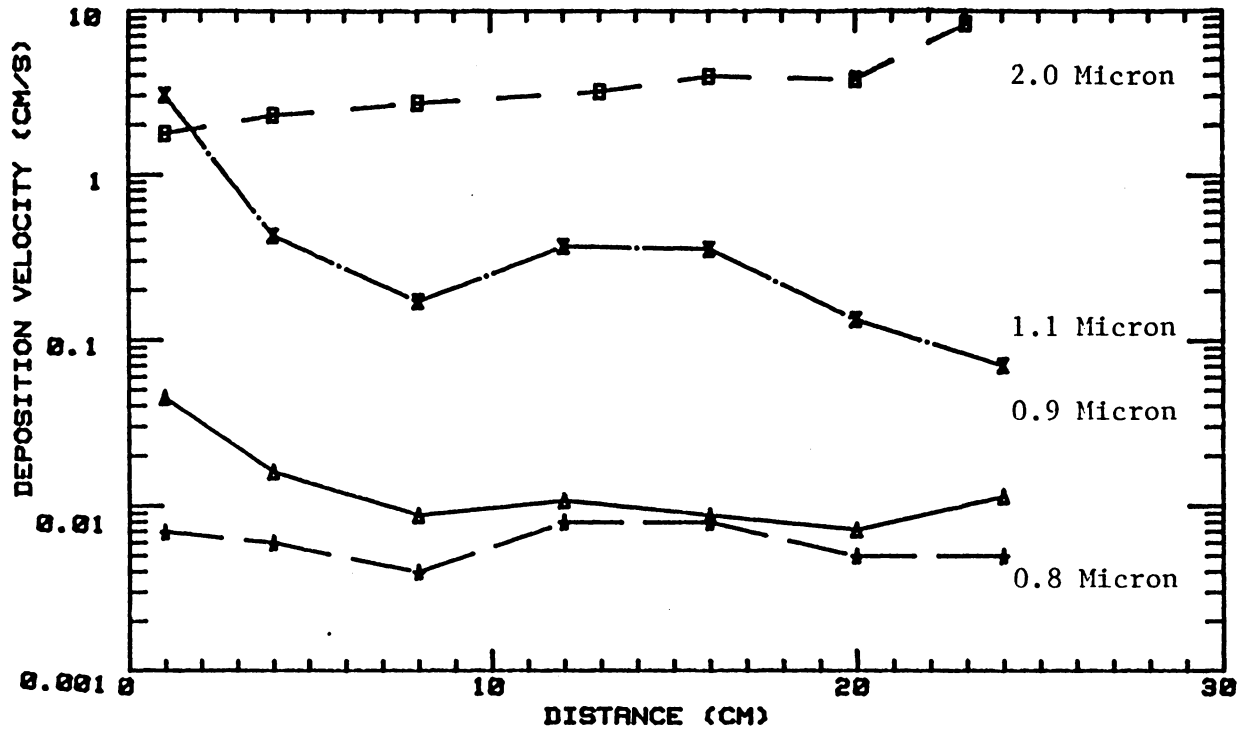


Figure IX-1. Deposition Velocities Plotted Versus Distance From the Leading Edge for the Deposition of 0.8, 0.9, 1.1, and 2.0 Micron Diameter Microspheres to an Ideal Surface in Experiments 7, 4, 11, and 5, Respectively.

diameter microspheres, respectively. This leads one to suspect that mechanisms other than gravitational settling increased the microsphere deposition.

#### Ideal Surface - 0.8 Micron Diameter

In the next set of experiments the run-to-run variation of the deposition velocity was investigated. The results of Experiments 6, 7, and 9 are presented in Figure IX-2 for the deposition of 0.8 micron diameter microspheres to an ideal (i.e., oil-coated) surface. The deposition velocity values ranged from 0.003 to 0.1 cm/s. The deposition velocities in Experiments 7 and 9 generally followed the same trend, but the deposition velocities in Experiment 9 were approximately 10 times greater than those in Experiment 7. Although the deposition velocity values in Experiment 6 varied considerably from the trend in Experiments 7 and 9, they did fall within the same range of values for Experiments 7 and 9.

The probable error for the deposition velocity is functionally dependent on both the particle flux and the aerosol concentration. The deposition velocity probable error was calculated by multiplying the calculated deposition velocity by the sum of the relative errors, on a percentage basis, for the flux and concentration measurements. The probable error bars are shown in Figure IX-3 for the deposition velocity results for Experiments 7 and 9; the probable error was as great as 100 percent for one of the deposition velocities in Experiment 7. The high probable error was primarily due to the

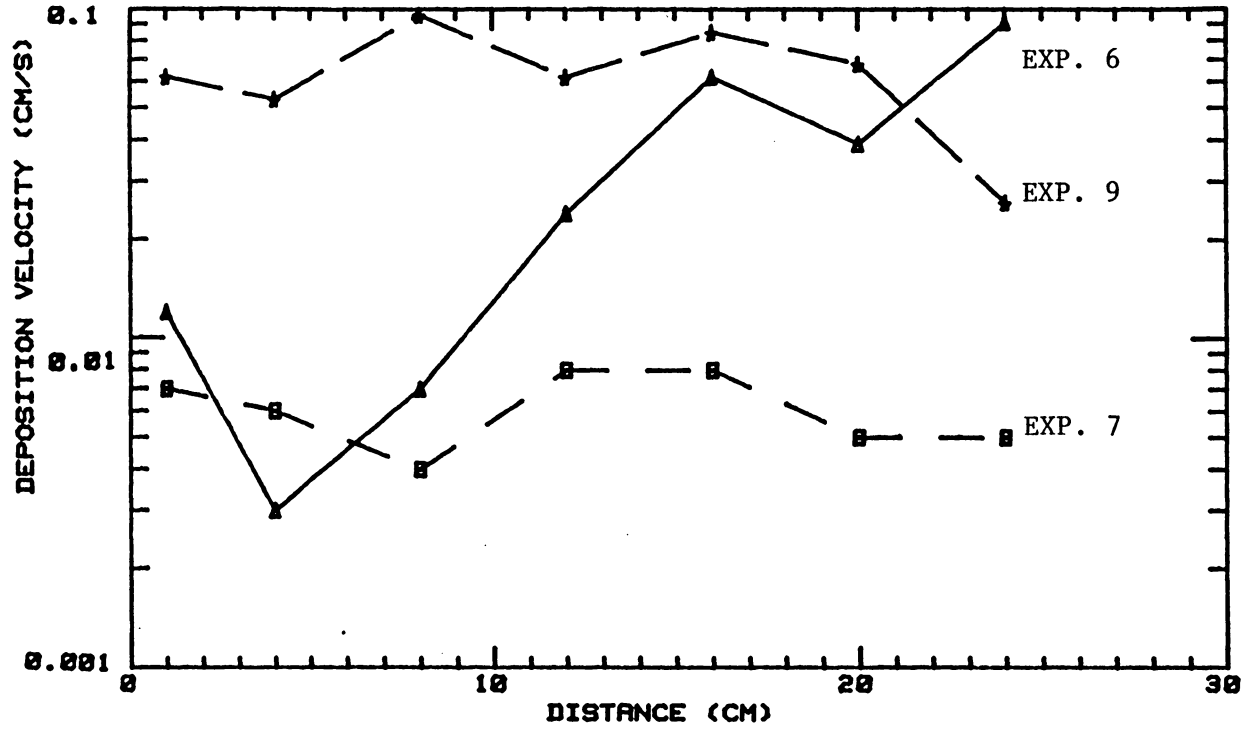


Figure IX-2. Deposition Velocities Plotted Versus Distance From the Leading Edge for the Deposition of 0.8 Micron Diameter Microspheres to an Ideal Surface in Experiments 6, 7, and 9.

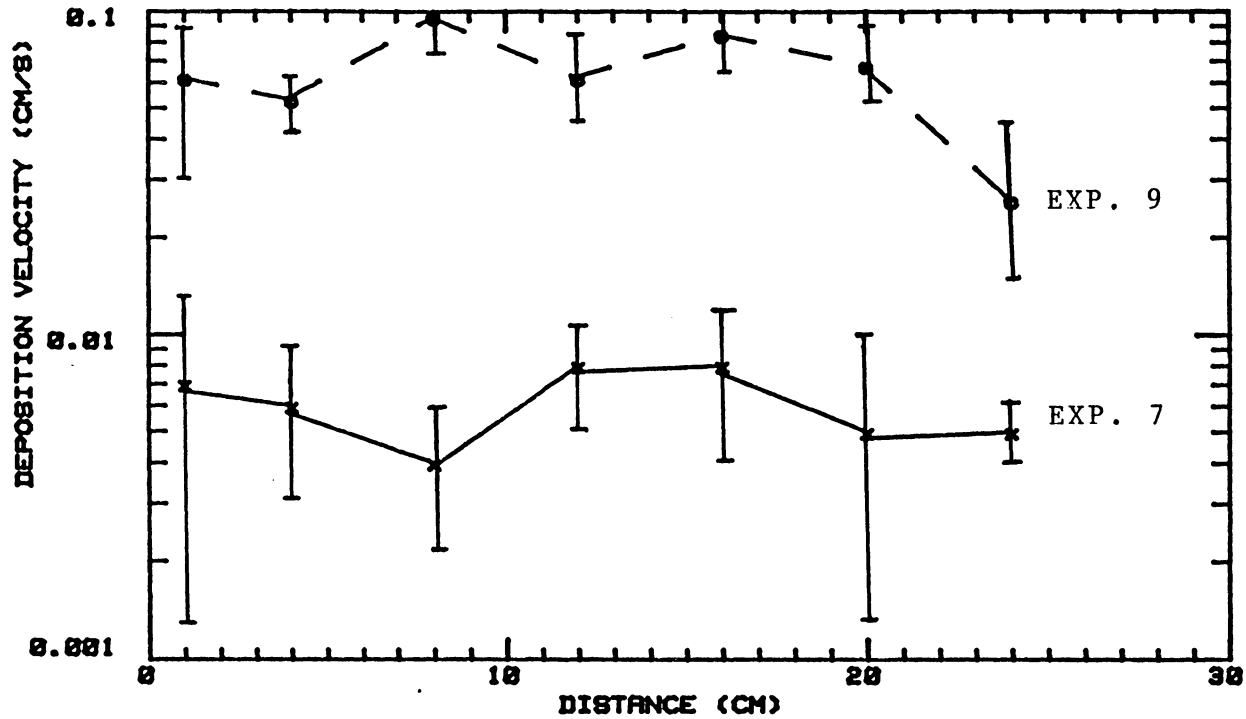


Figure IX-3. Deposition Velocities with Relative Error Bars Plotted Versus Distance From the Leading Edge for the Deposition of 0.8 Micron Diameter Microspheres in Experiments 7 and 9.



non-uniformity of the microsphere deposition on the experimental plate (i.e., some sites with a number of microspheres and other sites with few or no microspheres). Aerosols were generated for approximately two hours in each experiment; the deposition results represent a two-hour average. The high probable error was due to a lesser extent to the inaccuracy in evaluating the aerosol concentrations over the experimental plate.

#### Ideal Surface - 1.1 Micron Diameter

The run-to-run variation of the deposition velocity of 1.1 micron diameter microspheres to an ideal (oil-coated) surface was investigated in Experiments 10 and 11. The deposition velocities are shown plotted versus the distance from the leading edge in Figure IX-4. The deposition velocity values varied considerably from approximately 0.1 to 3 cm/s. The values followed the same general trend; they were greatest at the leading edge and generally decreased with distance from the leading edge.

#### Non-Ideal Surface - 1.1 Micron Diameter

The run-to-run variation of the deposition velocity of 1.1 micron diameter microspheres onto a non-ideal surface was then investigated. The experimental plate was not coated with oil in Experiments 12, 13, and 14. Any initial electrostatic charge was neutralized by passing a Polonium 210 source over the surface for two minutes. Experiments 12, 13, and 14 were performed while the relative humidities in the lab were approximately 40, 25,

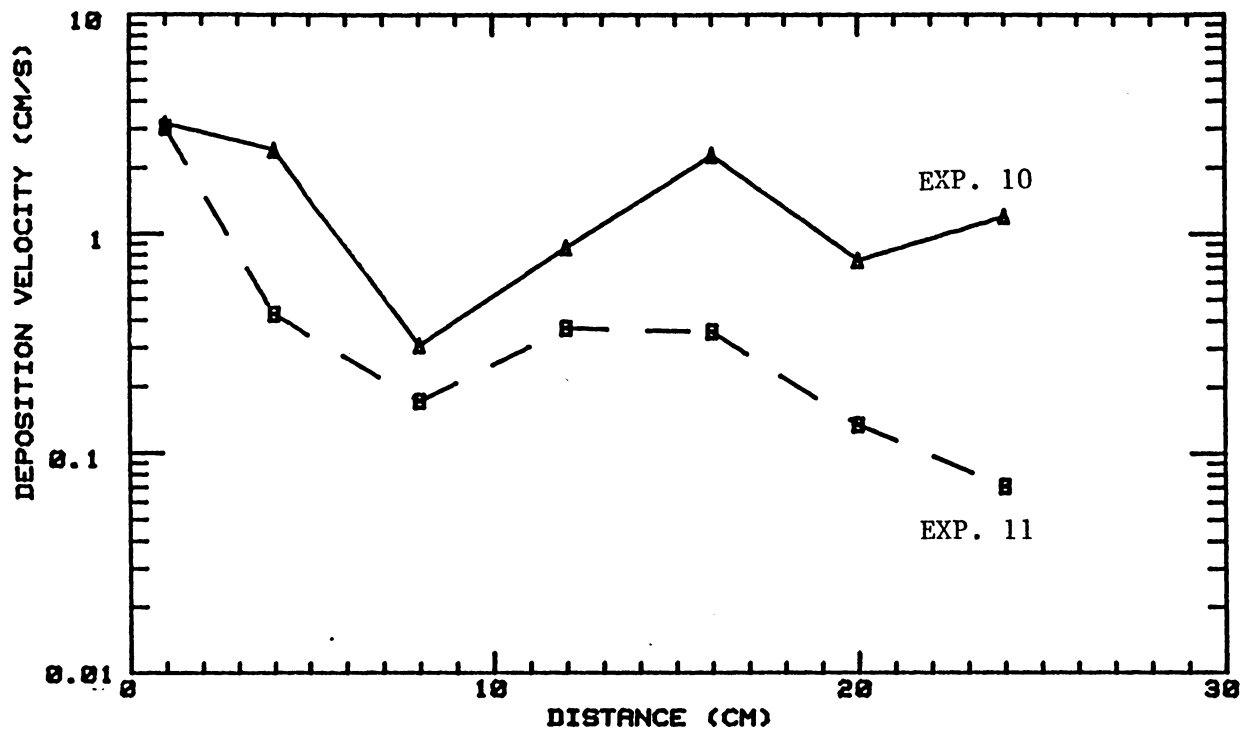


Figure IX-4. Deposition Velocities Plotted Versus Distance From the Leading Edge for the Deposition of 1.1 Micron Diameter Microspheres to an Ideal Surface in Experiments 10 and 11.

and 22 percent, respectively. The low relative humidities would tend to enhance any electrostatic charging effects. The deposition velocities are shown plotted versus distance from the leading edge in Figure IX-5. The deposition velocity values ranged from 0.02 to 0.4 cm/s. Although the deposition velocities followed the same trend at the leading edge, they varied considerably at distances greater than 8 cm from the leading edge. The average deposition velocity for the ideal surface in Experiment 11 was greater than that for the non-ideal surface. It appears that significant particle resuspension or bounce-off did occur on the non-ideal surface and that the oil-coated surface did enhance particle retention.

The deposition velocity results in these experiments were approximately 25 times greater than Sehmel's (1973) results for a smooth, electrically grounded surface. The results of Sehmel may be extrapolated to yield a deposition velocity of 0.008 cm/s for one micron diameter particles. The wind tunnel conditions were similar. The mean velocity was 2.2 m/s and the friction velocity was 11.4 cm/s.

#### Gravitational Settling Effect - 1.1 Micron Diameter

In Experiments 15, 19, and 20, 1.1 micron diameter microspheres were deposited without the aid of the gravitational settling mechanism. In order to eliminate the gravitational settling effect, the experimental plate was inverted. The standard experimental procedure was followed, but the deposited microspheres were counted

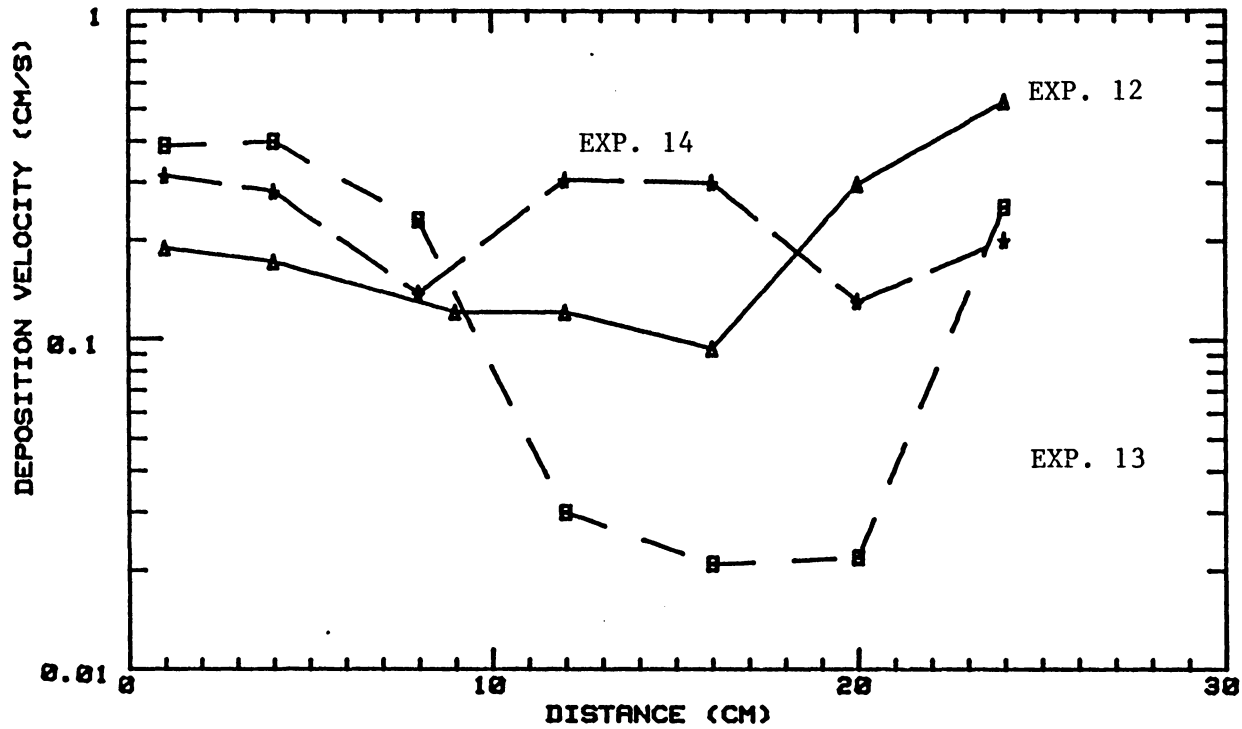


Figure IX-5. Deposition Velocities Plotted Versus Distance From the Leading Edge for the Deposition of 1.1 Micron Diameter Microspheres to an Uncoated Surface in Experiments 12, 13, and 14.

on the underside of the plate. The relative humidities in the laboratory were approximately 22, 25, and 30 percent during Experiments 15, 19, and 20, respectively. The deposition velocities are shown plotted versus distance from the leading edge in Figure IX-6. The underside deposition velocity values ranged from 0.005 to 0.03 cm/s, approximately 50 times less than the deposition velocities to the upper surface in Experiment 11. The deposition velocities to the underside were of the same order of magnitude as the terminal gravitational settling velocity, 0.0038 cm/s. One might initially attribute the difference in the deposition velocity results between Experiments 11 and 15 to the gravitational settling effect, as this was the intended control parameter. However, the difference in deposition velocities is approximately 0.2 cm/s, or 50 times greater than the theoretical settling velocity. It appears that another deposition mechanism, possibly electrostatic attraction, must have increased the microsphere deposition.

The deposition velocity results in these experiments were approximately 10 times greater than those of Wells and Chamberlain (1967) for 1.1 micron diameter droplets depositing to smooth vertical surfaces. In their pipe flow experiments, the deposition velocity values ranged from 0.0004 to 0.0007 cm/s for friction velocity ( $u_{*}$ ) values of 10 to 20 cm/s over an electrically grounded, smooth, brass surface. The electric space charge distribution would be different for pipe flow and wind tunnel studies (Hughes, 1984).

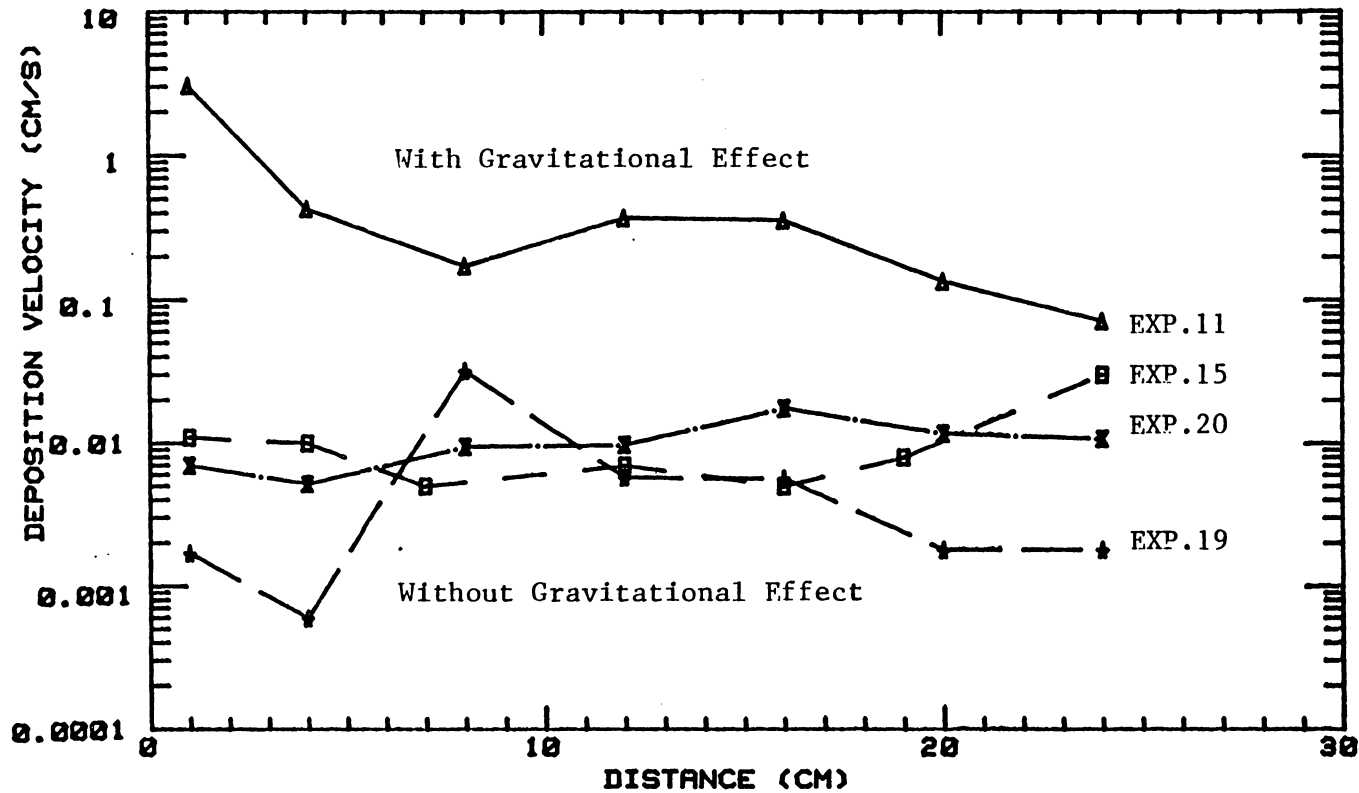


Figure IX-6. Deposition Velocities Plotted Versus Distance From the Leading Edge for the Deposition of 1.1 Micron Diameter Microspheres to an Ideal Surface With and Without the Gravitational Effect for Experiments 11, 15, 19, and 20, Respectively.

### Electrostatic Charging Effect - 1.1 Micron Diameter

The effect of electrostatic charge on the deposition of 1.1 micron diameter microspheres onto an ideal surface was investigated in Experiment 17. The only change from the standard experimental procedure was that the electrostatic charge neutralizer was removed from the aerosol generation system, so that the microspheres were electrostatically charged. The low relative humidity, approximately 22 percent, in the laboratory during the experiment would have enhanced the electrostatic charging effect. Figure IX-7 shows the deposition velocities plotted versus distance from the leading edge for Experiment 11 (with the electrostatic charge neutralizer in place) and for Experiment 17 (without the electrostatic charge neutralizer). The deposition velocities were much less in Experiment 17 within 12 cm of the leading edge of the experimental plate. The deposition velocity could not be accurately assessed at distances greater than 12 cm from the leading edge, because numerous microsphere agglomerates ranging from two to approximately 100 microspheres occurred at these distances. The microsphere agglomerates were not observed on the plate at distances less than 12 cm from the leading edge. The agglomerates appear to have been formed on the plate rather than above the plate. Agglomerates were not observed in Experiment 5 during the deposition of 2.0 micron particles. It also appears that the charge neutralizer did function properly in Experiment 11 and reduce the electrostatic charge on the aerosol. It did not appear that the oil on the experimental plate surface distributed the

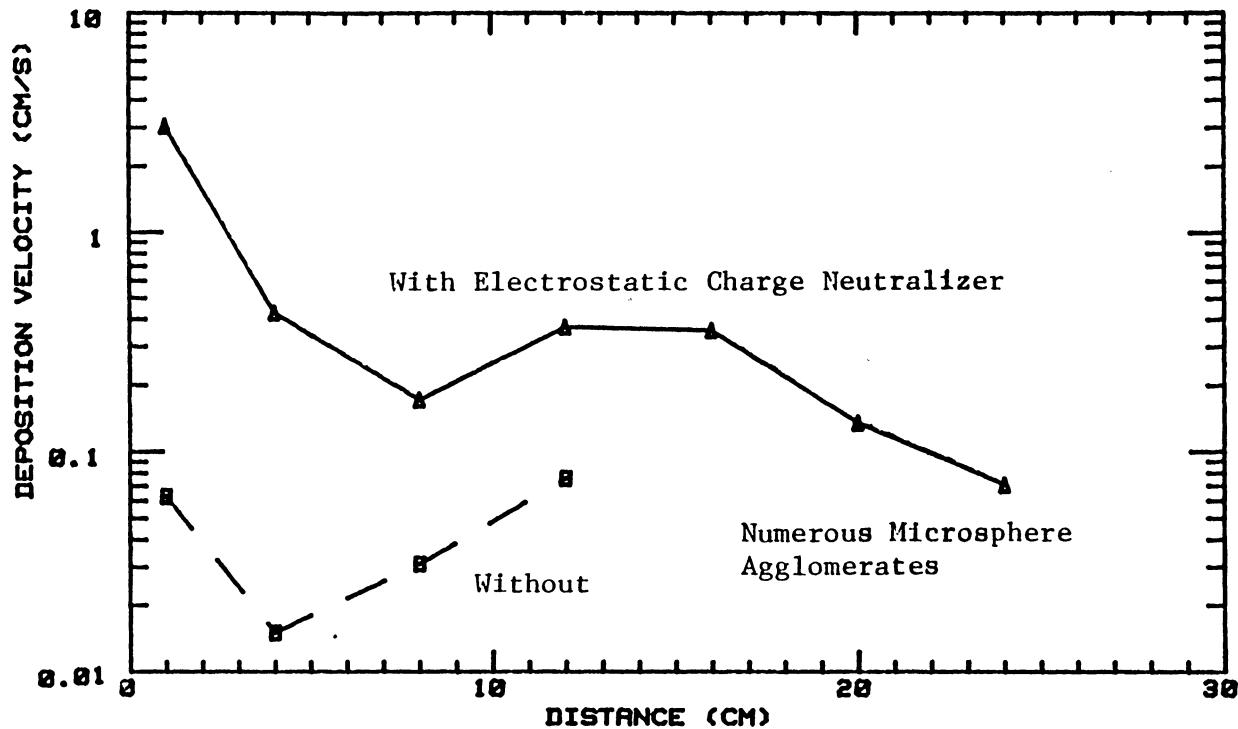


Figure IX-7. Deposition Velocities Plotted Versus Distance From the Leading Edge for the Deposition of 1.1 Micron Diameter Microspheres to an Ideal Surface With and Without the Electrostatic Charge Neutralizer for Experiments 11 and 17, Respectively.



electrostatic charge as anticipated. One might hypothesize that the trailing edge of the experimental plate developed "patches" of high electrostatic charge which attracted the charged microspheres and resulted in the agglomerate formation.

#### Effect of Protuberances

The deposition of 1.1 micron diameter microspheres onto previously deposited 42 micron microspheres was investigated in Experiment 18. The intent was to determine if the previously deposited large microspheres served as preferred sites of deposition for smaller microspheres. The results of this experiment were inconclusive.

#### Resuspension - 42 Micron Diameter

The dry deposition of the chemical species of concern also includes particles that are quite large. Therefore, it was considered necessary to investigate the resuspension of these large particles in Experiments 8 and 16. A deposited 42 micron diameter microsphere should extend well above the viscous sublayer into the region of turbulent flow above the experimental plate.

In Experiment 8, a dilute microsphere suspension was sprayed onto the untreated experimental plate. The plate was thoroughly wetted. It was allowed to dry for 18 hours. The plate was then placed in the wind tunnel for 1, 11, 60 and 360 minutes at an airspeed of 2 m/s and then for 60 minutes at 4 m/s. A particle count was made prior to testing and then after each of the wind

tunnel tests. The particle count remained approximately the same. Although it is possible that the microspheres may have rolled a few microns, they were not significantly redistributed on the experimental plate. Many small particles were observed surrounding the large particles. It appears that as the water evaporated the small particles were drawn toward the large particles due to surface tension.

In Experiment 16, a dilute suspension of 42 micron diameter microspheres was sprayed at a height of approximately 60 cm and allowed to gravitationally deposit on the experimental plate. The plate remained relatively dry after the microsphere deposition, although there were a few tiny droplets on the surface. The plate was then tested in the wind tunnel for 5 and 70 minutes at an airspeed of 2 m/s. A particle count was made prior to testing and after each of the wind tunnel tests. The particle count was again relatively constant.

It appears that microspheres deposited in this manner develop such a great force of adhesion to the experimental plate that they are not significantly resuspended.

CHAPTER X  
DEPOSITION MODEL PREDICTIONS

Particle deposition to the experimental plate was predicted using the theoretical transport models previously presented in Chapter IV. In order to predict the deposition velocities, it first was necessary to obtain values of the friction velocity,  $u_*$ , and the dimensionless particle relaxation time,  $\tau_+$ . The experimental results were then compared to the theoretically predicted deposition velocities.

Friction Velocity

The turbulence in the viscous sublayer ( $Z_+ < 5$ ), the region of maximum resistance to particle transfer, may be characterized by the friction velocity. The friction velocity was not directly measured in these experiments but was calculated using two different methods. The simplest method used the theory of Schlichting (1968), as presented by Wood (1981). The following experimentally derived equation may be used for a hydraulically smooth flow regime (i.e., roughness element height much less than the sublayer thickness) over a flat plate:

$$u_* = 0.707 U [(2 \log_{10} (Ux/\nu) - 0.65)]^{-1.15} \quad (X-1)$$

The theoretical friction velocities for the experimental plate ranged from 19.5 to 12.1 cm/s, as listed in Table X-1. However,

TABLE X-1. THEORETICAL FRICTION VELOCITIES AND DIMENSIONLESS  
PARTICLE RELAXATION TIMES ALONG THE EXPERIMENTAL PLATE

Distance x (cm)	Friction Velocities, $u_*$ (cm/s)			Dimensionless Particle Relaxation Time, $\tau^+$
	A	Laminar B	Turbulent B	
1	19.5	10.7	3.8	0.0091
4	15.6	10.2	8.6	0.0058
8	14.1	10.4	8.7	0.0047
12	13.4	9.0	7.3	0.0043
16	12.9	13.1	9.9	0.0040
20	12.5	9.7	9.1	0.0037
24	12.3	10.3	9.3	0.0036
26.5	12.1	9.7	-	0.0035

- (A) Friction velocities were calculated using the theory of Schlichting (1968) after Wood (1981).
- (B) Friction velocities were calculated using the "law of the wall" theory of Hinze (1975) and the velocity profiles measured for both the laminar and turbulent mainstream.
- (C) For 1.1 micron diameter particles

the friction velocity decreased only slightly from 12.9 to 12.3 cm/s in the region of well-developed flow ( $x = 16$  to  $24$  cm).

The second method used to calculate the friction velocity is based on the "law of the wall" theory of Hinze (1975):

$$\Delta U / \Delta Z = u_*^2 / \nu \quad (X-2)$$

where  $\Delta U/\Delta Z$  is the slope of the velocity profile in the sublayer region ( $Z_+ < 5$ ). Although the friction velocity values varied widely, as shown in Table X-1, they were of the same order of magnitude as those calculated by the first method. The values calculated for the laminar mainstream were greater than those calculated for the turbulent mainstream. The sparsity of data probably accounts for some the variation of the friction velocity values with distance along the experimental plate. More velocity measurements below  $z = 1$  mm are needed; some of the velocity measurements used to determine the slope were actually in the boundary layer transition region. The boundary layer friction velocities calculated from the theory of Schlichting (1968) were used to predict the microsphere deposition velocities. This theory does not differentiate between the different levels of turbulence intensity generated in the wind tunnel.

#### Dimensionless Particle Relation Time

The dimensionless particle relaxation time,  $\tau_+$ , was calculated using Equation (IV-9); the value is a function of the friction

velocity and the particle relaxation time (a constant of  $3.57 \times 10^{-6}$  seconds for a 1.1 micron diameter particle). Values of  $\tau_+$  are also listed in Table X-1.

#### Theoretically Predicted Deposition Velocities

The deposition of 1.1 micron diameter particles was predicted using the turbulent boundary layer theory of Sehmel (1971) as presented in Equations (IV-15, 16, and 17). The lower limit of deposition predicted by this model is the particle terminal gravitational settling velocity.

The deposition velocities for Experiment 7 and the model for 0.8 micron diameter microspheres to an oil-coated surface are shown in Figure X-1. The model predicted the deposition velocity to be a constant 0.0023 cm/s along the experimental plate. Although the deposition velocities for Experiment 7 are approximately 2 to 3 times greater than the model predictions, the predictions did fall within the range of the probable error for the experimental results at distances of 1, 8, and 20 cm from the leading edge.

The deposition velocities for Experiment 4 and the model for 0.9 micron diameter microspheres to an oil-coated surface are shown in Figure X-2. The model predicted the deposition velocity to be a constant 0.0029 cm/s along the plate. The experimental results are 3 to 16 times greater than the model predictions. The model predictions fall within the range of the probable error for the experimental results at distances of 16,

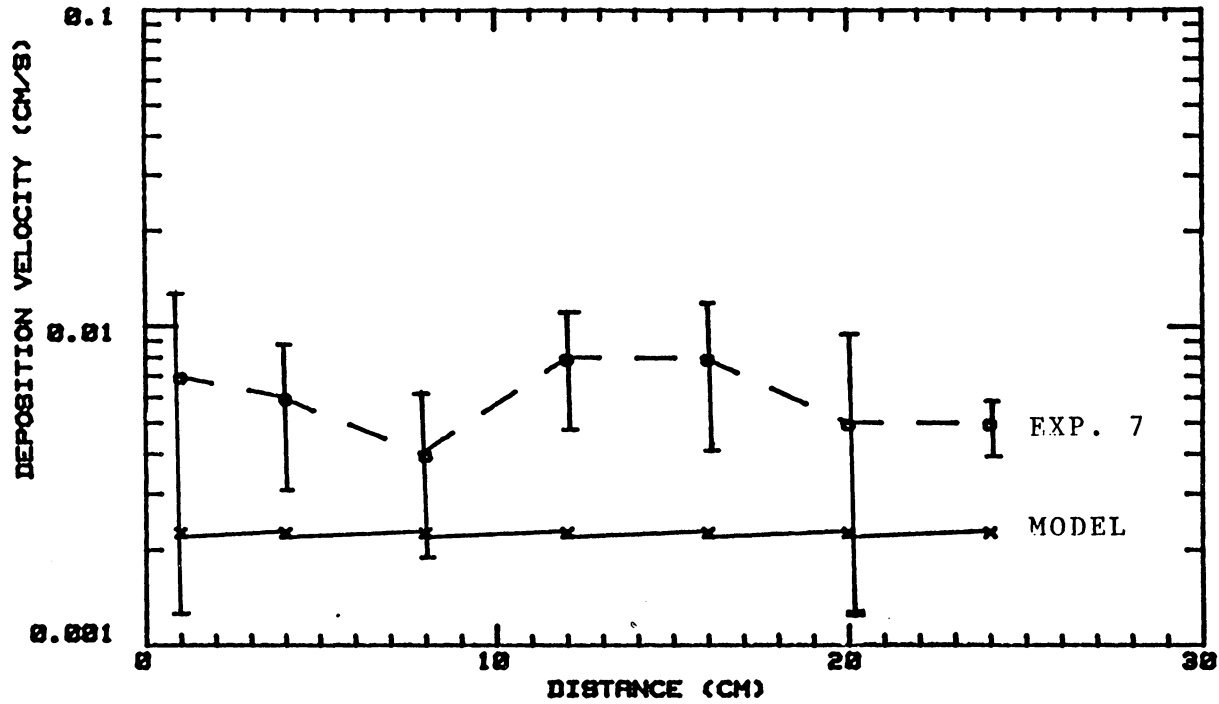


Figure X-1. Deposition Velocities Plotted Versus Distance From the Leading Edge for 0.8 Micron Diameter Microspheres for Experiment 7 and for the Deposition Model.

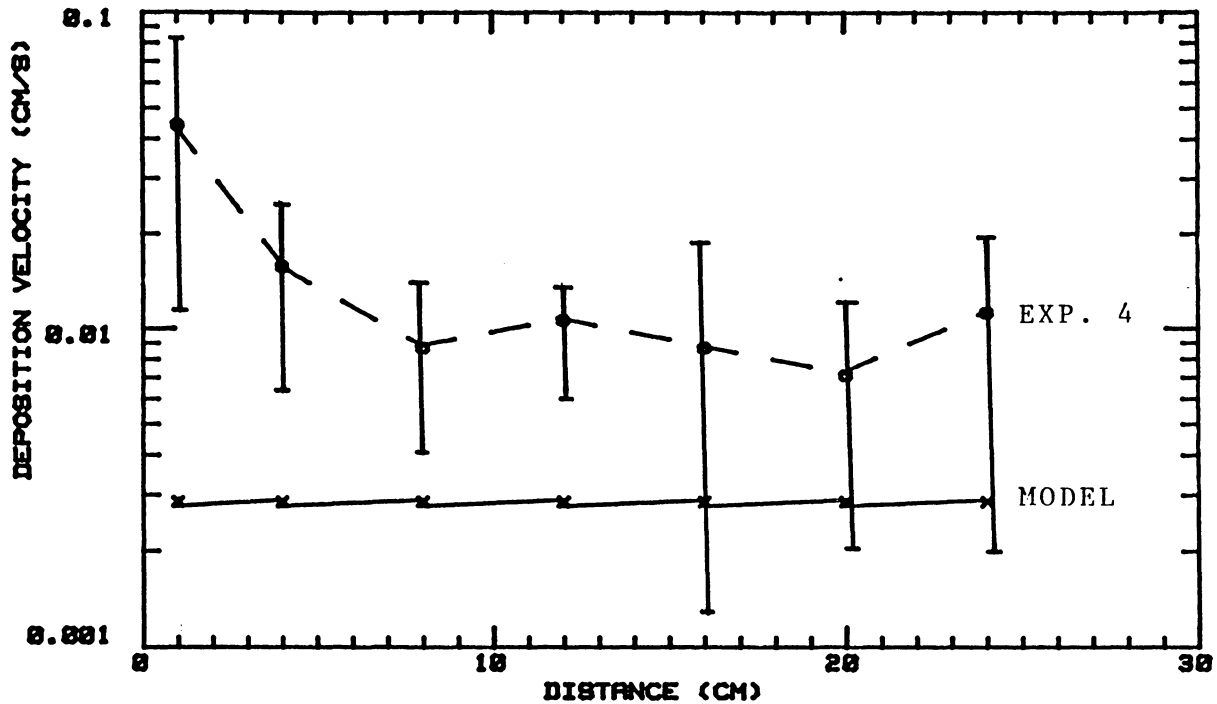


Figure X-2. Deposition Velocities Plotted Versus Distance from the Leading Edge for 0.9 Micron Diameter Microspheres for Experiment 4 and the Deposition Model.



20, and 24 cm from the leading edge.

The deposition velocities for Experiment 11 and the model for 1.1 micron diameter microspheres to an oil-coated surface are shown in Figure X-3. The model predicted the deposition velocity to be a constant 0.0038 cm/s along the plate. The experimental results are from 23 to 850 times greater than the model predictions.

The deposition velocities for Experiment 14 and the model for 1.1 micron diameter microspheres to a non-ideal (i.e., uncoated) surface are shown in Figure X-4. The model predicted the deposition velocity to be a constant 0.0038 cm/s along the plate. The experimental results are 37 to 90 times greater than the model predictions.

If one eliminates the high deposition velocities at  $x = 1$  cm due to the increased turbulence at the leading edge, the model underestimates the experimental results by approximately four times for the 0.8 and 0.9 micron diameter microspheres to an oil-coated surface. The probable error associated with the model is not shown, although there are uncertainties associated with the gravitational settling velocity, friction velocity, and aerosol concentration values. The model integral equation is solved by an approximation method, Simpson's One-third Rule. Although more data are needed to perform a rigorous error analysis, it is significant that the model predictions and experimental results correlate so well. A better correlation might occur if the effects of flow separation at the leading edge, or electrostatic

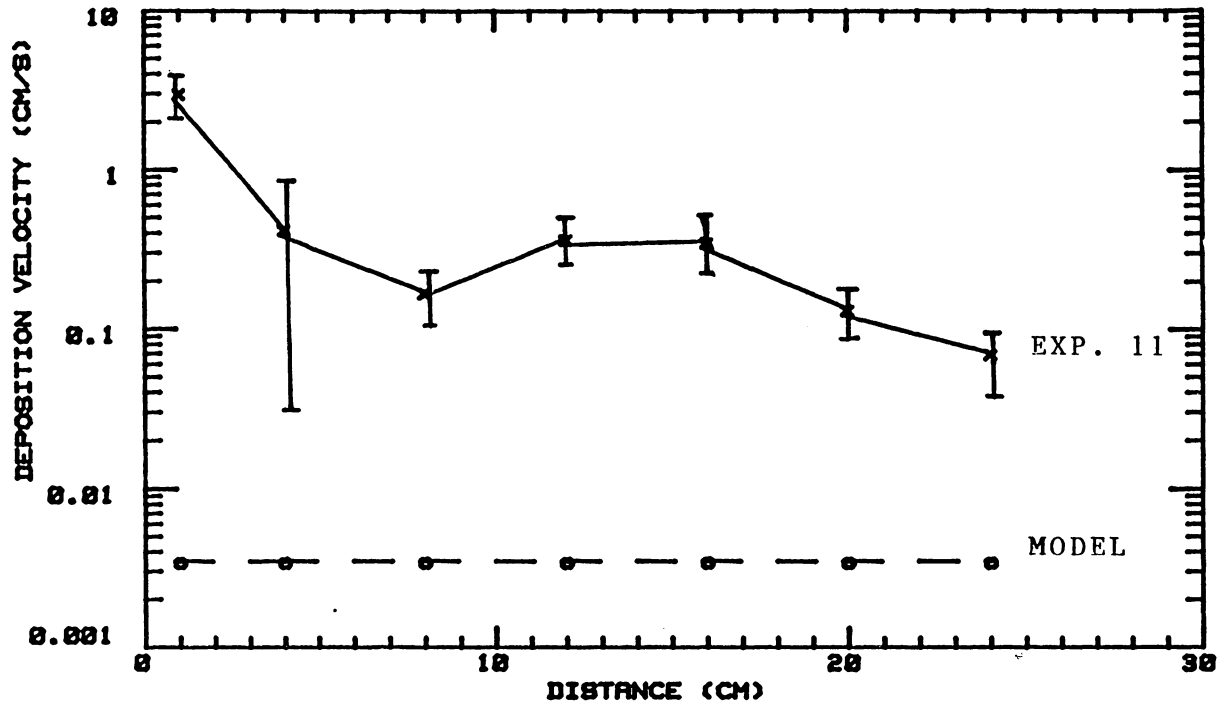


Figure X-3. Deposition Velocities Plotted Versus Distance from the Leading Edge for 1.1 Micron Diameter Microspheres for Experiment 11 and for the Deposition Model.

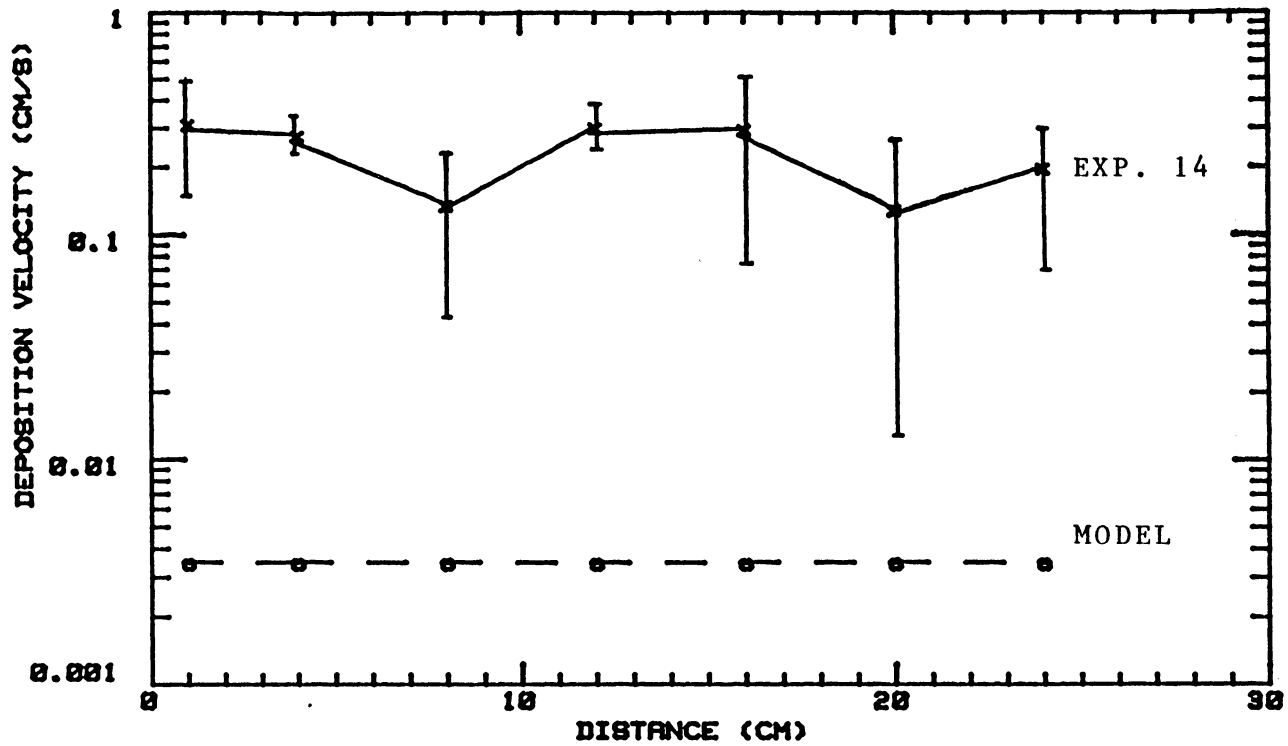


Figure X-4. Deposition Velocities Plotted Versus Distance From the Leading Edge for 1.1 Micron Diameter Microspheres to an Uncoated Surface for Experiment 14 and for the Deposition Model.

attraction were included in the development of the model.

The theory of Sehmel (1971) was modified with respect to the gravitational settling mechanism in order to predict particle deposition to the underside of the experimental plate. The terminal settling velocity was considered positive in Equation (IV-5), so the numerators in Equations (IV-15, 16, and 17) became positive. The theoretically predicted deposition velocities to the underside ranged from  $5.16 \times 10^{-10}$  to  $8.7 \times 10^{-16}$  cm/s, as shown in Figure X-5. The average experimental deposition velocity in Experiments 15, 19 and 20 was approximately  $10^{-2}$  cm/s, many orders of magnitude greater than the theoretical predictions.

The experimental deposition velocities for Experiments 4, 7, and 11 for 0.9, 0.8, and 1.1 micron diameter particles, respectively, were correlated to the intermittent turbulence theory of Hicks and Slinn (1982) as presented in Equation (IV-18). The normalized experimental deposition velocity,  $V_d Re^{0.25}/U$ , is shown plotted versus Schmidt number,  $\nu/D$ , in Figure X-5, following Figure 4 of Hicks and Slinn (1982). Values of  $n$  equal to 0.5, 0.67, and 1.0 are shown as lines in Figure X-6. The results of Experiments 4, 7, and 11 do not correlate well to this model, Brownian diffusion is the most important deposition mechanism in this model. The experimental results indicate that eddy diffusion and gravitational settling are more important than Brownian diffusion for particles in this size range. However,

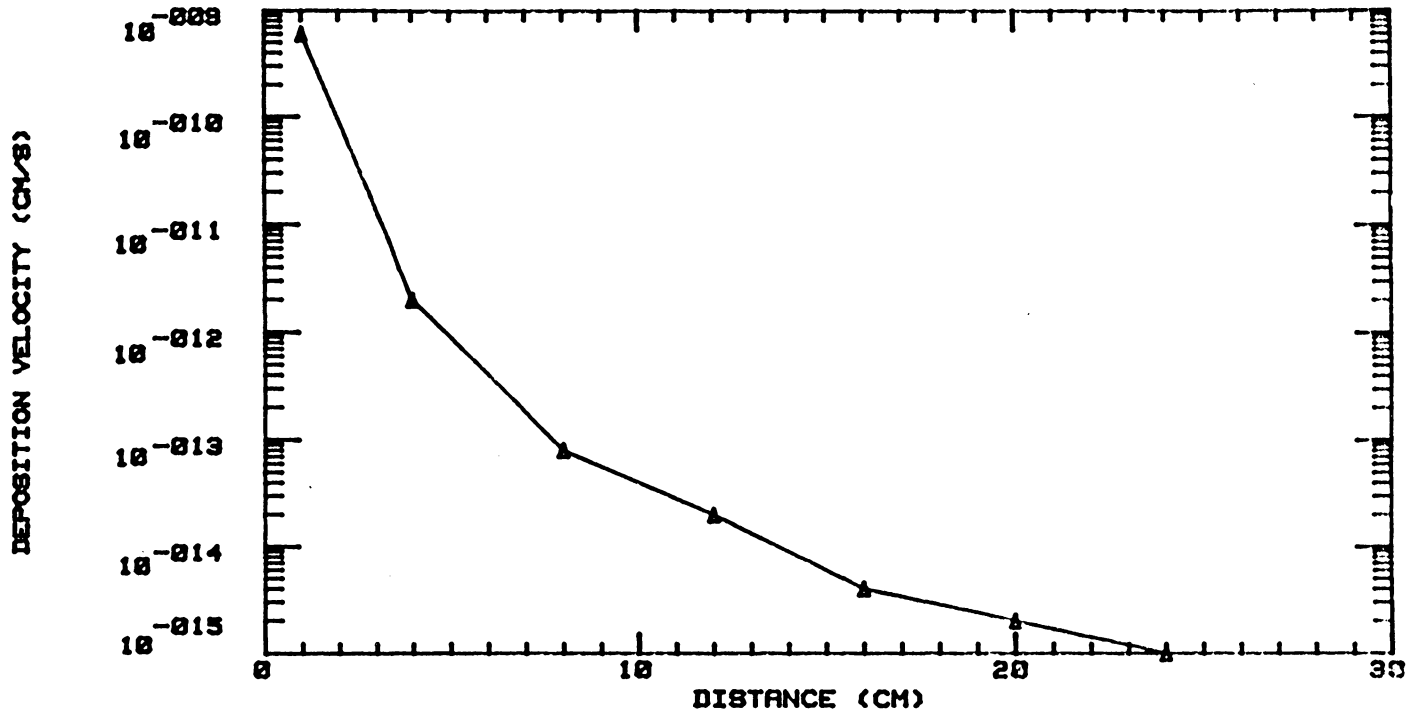


Figure X-5. Predicted Deposition Velocities Plotted Versus Distance from the Leading Edge for 1.1 Micron Diameter Microspheres for the Deposition to the Experimental Plate Underside.

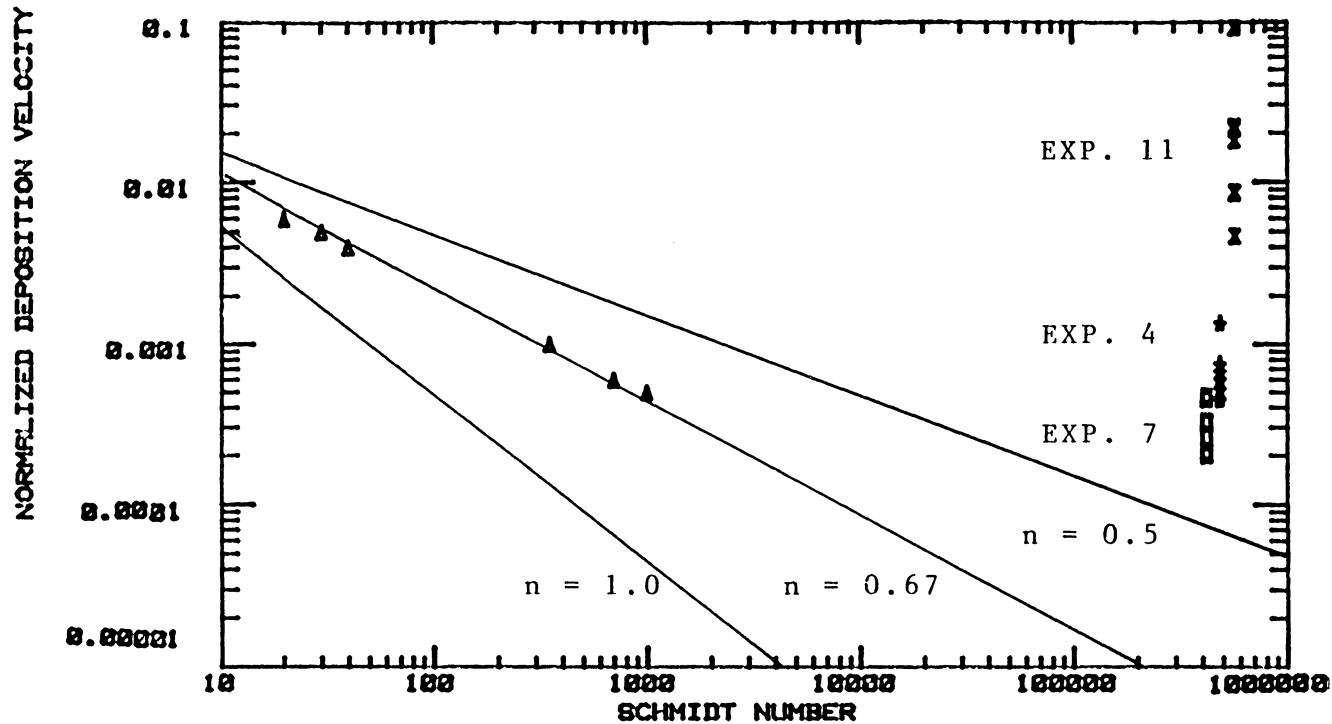


Figure X-6. Normalized Deposition Velocities Plotted Versus Schmidt Number for 0.8, 0.9, and 1.1 Micron Diameter Microspheres in Experiments 7, 4, and 11, Respectively.

the results presented by Hicks and Slinn (1982) after Wells and Chamberlain (1967) for particles less than 0.001 micrometer in diameter (Schmidt number less than 650) did correlate well with this model for  $n = 0.667$ .

## CHAPTER XI

### CONCLUSIONS AND RECOMMENDATIONS

The objective of this study was to investigate small particle (i.e., one micron diameter range) transport across the aerodynamic boundary layer that developed over a flat plate. Specific conclusions are :

- 1) The experimental procedure for determining the particle flux had inadequacies. Counting the microspheres was quite time consuming and caused eye strain. It was difficult to identify microspheres smaller than one micron on the experimental plate. The deposition surface was limited to a material that transmits light so that the deposited microspheres could be counted with a compound microscope. The experimental plate was nonconductive and could not be electrically grounded.
  
- 2) The experimental deposition velocities to oil-coated surfaces were approximately 3, 3.5, 100, and 170 times greater than the terminal gravitational settling velocities for 0.8, 0.9, 1.1, and 2.0 micron diameter microspheres, respectively. It appears that in these experiments another deposition mechanism, possibly electrostatic attraction, was more important than gravitational settling .
  
- 3) There was run-to-run variation in the experimental deposition velocities. The non-uniform nature of the microsphere deposition resulted in high probable errors in the deposition velocity values.



Longer experimental test periods might have resulted in a more uniform microsphere deposition and smaller probable errors.

4) Even for such a simple surface as a flat plate, aerodynamics affected microsphere deposition. Deposition velocity was a function of location on the experimental plate. There was a trend toward maximum microsphere deposition at the leading edge, where the turbulence was greatest; in some experiments the deposition velocity decreased with distance from the leading edge. Thus, a range of deposition velocities appears to be more representative than a single deposition velocity for microsphere deposition to the experimental plate. Deposition velocities for 1.1 micron diameter particles ranged from 0.02 to 3.0 cm/s.

5) The deposition velocities for 1.1 micron diameter microspheres to the non-ideal surface were approximately 25 times greater than those reported by Sehmel (1973). The low relative humidity in the laboratory and the fact that the experimental plate could not be electrically grounded would enhance the electrostatic charging effect. It appears that the experimental plate may have developed an electrostatic charge which served to increase the microsphere deposition. However, there is no quantitative evidence to support this theory.

6) The deposition velocities for 1.1 micron diameter microspheres to the underside of the experimental plate were on the same order

of magnitude as the terminal gravitational settling velocity and were 10 times greater than those reported by Wells and Chamberlain (1967). This also might be attributed to electrostatic charging of the experimental plate.

7) The deposition velocities were approximately 10 times greater for the ideal (i.e., oil-coated) surface than for the non-ideal surface. It appears that significant microsphere resuspension or bounce-off occurred on the non-ideal surface.

8) Particles deposited to a moist surface were retained after the surface dried. There was no significant resuspension of the 42 micron diameter microspheres after the experimental plate was tested in the wind tunnel at 2 m/s for 6 hours and at 4 m/s for one hour.

9) Although airflow and environmental conditions may be controlled in the wind tunnel, the wind tunnel does not exactly model atmospheric deposition. Caution must be exercised when comparing wind tunnel and atmospheric deposition results. The range of eddy size is much greater in the atmosphere, and thermal effects occur; the development of a simple boundary layer on common environmental surfaces may not occur. Surface motion (e.g., leaf flutter) may also affect deposition-related phenomena.

10) Although the turbulent pipe flow model underestimated the

deposition velocities, it is significant that the deposition model correlated so well with the experimental results for the deposition of 0.8 and 0.9 micron diameter microspheres to an oil-coated surface even though it fails to consider the effects of increased turbulence at the leading edge, or of electrostatic charging.

11) The experimental results did not correlate well with the intermittent turbulence theory. Brownian diffusion is the dominant deposition mechanism in this theory. However, the experiments indicate that, for this size range of particles, eddy diffusion, gravitational settling, and possibly electrostatic attraction are the important deposition mechanisms.

## RECOMMENDATIONS

Additional investigation should be directed toward evaluating factors that affect microsphere deposition. Specific areas for study are :

- 1) Investigating the effect of electrostatic charge on particle deposition. This appears to be an extremely important mechanism. The experimental plate should be electrically grounded. One way to do this would be to deposit a very thin film of conductive material on the acrylic plate (Hosker, 1984).
- 2) Repeating each of the experiments many times would produce results that are statistically more significant.
- 3) Investigating the effect of turbulence on particle deposition in more detail would be significant. More information is needed on turbulence within one millimeter of the surface. A probe system capable of measuring two-dimensional turbulence ( $u'$  and  $w'$ ) may be more successful in quantifying turbulence effects. Additional experiments at lower airspeeds (in-canopy airspeeds are lower) and varying degrees of turbulence would be significant.
- 4) Performing additional experiments at various angles of incidence of the experimental plate to the airflow, in order to determine the effect on microsphere deposition. The resulting improved

understanding of the process might enhance the understanding of the effects of leaf flutter or other surface motions.

5) One might develop a standard surrogate surface for routine atmospheric dry deposition monitoring. It would consist of a thin circular teflon disk with an aerodynamic edge (Hicks, 1983). It would be of interest to compare the wind tunnel results using this standard surrogate surface with, for example, the dry deposition plate used by Lindberg, Harriss, Turner, Shriner, and Huff (1979) for routine atmospheric dry deposition monitoring. Smoke visualization studies in the large ATDD wind tunnel suggest that the rim on the Lindberg plate affects particle deposition (Hosker, 1983; Pendergrass, 1983).

## REFERENCES

1. Agarwal, J.K. and G.J. Sem. "Generating Submicron Monodisperse Aerosols for Instrument Calibration." TSI Quarterly, 3, May/June (1978).
2. Belot, Y. and D. Gauthier. "Transport of Micronic Particles from the Atmosphere to Foliar Surfaces." (Chapter in Heat and Mass Transfer in the Biosphere, D.A. de Vries, Ed.) Scripta Publishing Co., Washington (1975).
3. Berglund, R.N. and B.Y.H. Liu. "Generation of Monodisperse Aerosol Standards." Env. Science and Tech., 7 (2) 147 (1973).
4. BGI, Incorporated. "Tables for Use in Aerosol Physics." Waltham, MA (1980).
5. Billard, F., G. Madelaine, and J. Delhaye. "Quelques Remarques Sur la Generation et la Mesure Des Spheres de Latex Polystyrene." Aerosol Science, 1, 357 (1970).
6. Bricard, J. and J. Pradell. "Electric Charge and Radioactivity of Naturally Occurring Aerosols." (Chapter IV in Aerosol Science, C.N. Davies, Editor), Academic Press, New York (1966).
7. Brock, J.R. and W.H. Marlow. "Charged Aerosol Particles and Air Pollution." Env. Letters, 10(1), 53, (1975).
8. Browne, L.W.B. "Deposition of Particles on Rough Surfaces during Turbulent Gas Flow in a Pipe." Atmos. Env., 8, 801 (1974).
9. Chamberlain, A.C. "Aspects of the Deposition of Radioactive and Other Gases and Particles." Int. J. Air Pollution, 3, 63 (1960).
10. Chamberlain, A.C. "Mass Transfer to Bean Leaves." Boundary-Layer Meteorology, 6, 477 (1974).
11. Chamberlain, A.C. and P. Little. "Transport and Capture of Particles by Vegetation." (Chapter in Plants and Their Atmospheric Environment, J. Grace, Ed.) Blackwell Scientific Publishers, Boston (1981).
12. Chamberlain, A.C. "Deposition and Resuspension." Proceedings of the 4th International Dry Deposition Conference, Santa Monica, CA (1982).
13. Climet Instruments Company. CI-226 Operator's Manual. Redlands, CA, June (1982).

14. Cooper, D.W., and P.C. Reist. "Neutralizing Charged Aerosols with Radioactive Sources." J. Colloid Interface Science, 45, 17 (1973).
15. Cooper, G., G. Langer, and J. Rosinski. "Submicron Aerosol Losses in Aluminized Mylar Bags." Amer. Meteorological Society, 18, 57 (1979).
16. Corn, M. "The Adhesion of Solid Particles to Solid Surfaces, Part I." JAPCA, 11(11), 523 (1961). ✓
17. Corn, M. and F. Stein. "Re-entrainment of Particles from a Plane Surface." J. Am. Industrial Hygiene Asc., 325 (1965). ✓
18. Corn, M. "Adhesion of Particles." (Chapter XI in Aerosol Science, C.N. Davies, Editor), Academic Press, New York (1966). ✓
19. Dahneke, B.J. "The Capture of Aerosol Particles by Surfaces." ✓ ✱  
Journal Colloid Interface Science, 37, 342 (1971).
20. Dahneke, B.J. "The Influence of the Flattening on the Adhesion of Particles." J. Colloid Int. Sci., 40, 1 (1972). ✓
21. Dahneke, B.J. "Measurements of Bouncing of Small Latex Spheres." J. Colloid Int. Sci., 45, 584 (1973).
22. Davidson, C.I. "Deposition of Trace Metals Aerosols." Ph.D. Dissertation, Cal Tech (1977).
23. Davidson, C.I. and S.R. Friedlander. "A Filtration Model for Aerosol Dry Deposition." J. Geophys. Res., 83, 2343 (1978).
24. Davidson, C.I., J.M. Miller, and M.A. Pleskow. "The Influence of Surface Structure on Predicted Particle Dry Deposition to Natural Grass Surfaces." Water, Air, and Soil Pollution, 18, 25 (1982).
25. Davies, C.N. "Deposition of Lycopodium Spores upon Glass Slides exposed in a Wind Tunnel." Brit. J. Applied Physics, 11, 535 (1960).
26. Davies, C.N. "Deposition from Moving Aerosols". (Chapter XII in Aerosol Science) Academic Press, New York (1966).
27. Dennis, Richard. Handbook of Aerosols. ERDA / NTIS No. 26608 (1976).
28. Duke Scientific Corporation. Analytical Reference Particles. Bulletin 81, Palo Alto, CA (1982).

29. Ellenbecker, M. and R.A. Gussman. May/Research Engineers Cascade Impactor, BGI, Inc., Waltham, MA (1982).
30. El-Shobokshy, M.S. and I.A. Ismail. "Deposition of Aerosol Particles from Turbulent Flow onto Rough Pipe Wall." Atmos. Env., 14, 297 (1980).
31. El-Shobokshy, M.S. "Experimental Measurements of Aerosol Deposition to Smooth and Rough Surfaces." Atmos. Env., 17, 639 (1983).
32. Esmen, N., P. Ziegler, and R. Whirfield. "The Adhesion of Particles upon Impaction." J. Aerosol Science, 9, 547 (1978).
33. Friedlander, S.K. and H.F. Johnstone. "Deposition of Suspended Particles from Turbulent Gas Streams." Ind. and Eng. Chem., 49, 1951 (1957).
34. Friedlander, S.K. "Particle Diffusion in Low-Speed Flows." J. Colloid Inter. Science, 23, 157 (1967).
35. Friedlander, S.K. Smoke, Dust, and Haze--Fundamentals of Aerosol Behavior. John Wiley and Sons, New York (1977).
36. Fuchs, N.A. The Mechanics of Aerosols. MacMillan Company, New York (1964).
37. Grace J. and J. Wilson. "The Boundary Layer over a Populus Leaf." J. Exp. Botany, 27, 231 (1976).
38. Grace J. "The Effects of Wind on Plants." Biometeorology, 7(2), 231 (1980).
39. Harper, W.R. Contact and Frictional Electrification. Clarendon Press, Oxford (1967).
40. Hewlett-Packard Company. "Integration by Simpson's Rule." Numerical Analysis Library For Model 9845B, Fort Collins, CO (1979).
41. Hicks, B.B., M.L. Wesely, and J.L. Durham. "Critique of Methods to Measure Dry Deposition-Workshop Summary." EPA 600/9-80-050 (1980).
42. Hicks, B.B. and W.G.N. Slinn. "Surface Fluxes of Small Particles." ATDL Contribution # 82/26 , Oak Ridge, TN (1982). ✓
43. Hicks, B.B., Personal Communication (1983).
44. Hinze, J.O., Turbulence. McGraw-Hill, New York (1975). ✓



45. Hosker, R.P. and S.E. Lindberg. "Review: Atmospheric Deposition and Plant Assimilation of Gases and Particles." Atmos. Env., 16(5), (1982).
46. Hosker, R.P., Personal Communication (1983).
47. Hughes, J.M., Personal Communication (1984).
48. John, W., G. Reischl, W. Devor, and J. Weslowski. "Investigation of Particulate Matter Monitoring Using Contact Electricity." EPA Report No. EPA-600/2-70-212, Research Triangle Park, NC (1978).
49. John, W. "Particle Charge Effects." (Chapter in Generation of Aerosols and Facilities for Exposure Experiments, K. Willeke, Ed.) Ann Arbor Science, Ann Arbor, MI (1980). ✓
50. Keithley Instruments, Inc. Instruction Manual for Model 427 Current Amplifier. Cleveland, OH (1975).
51. Kraemer, H.F. and H.F. Johnstone. "Collection of Aerosol Particles in the Presence of Electrostatic Fields." Ind. Eng. Chem., 47(12), 2426 (1955).
52. Langer, G. "Particle Deposition and Reentrainment from Coniferous Trees, Part II." Kolloid-Zeitschrift, 204, 119 (1965). ✓
53. Leong, K.H., H.C. Wang, J.J. Stukel, and P.K. Hopke. "An Improved Constant Output Atomizer." J. Am. Ind. Hygiene Assoc. 43, 135 (1982).
54. Lin, C.S., R.W. Moulton, and G.L. Putnam. "Mass Transfer between Solid Walls and Fluid Streams." Ind. Eng. Chem., 45, 636 (1953).
55. Lindberg, S.E., R.C. Harriss, R.R. Turner, D.S. Shriner, and D.D. Huff. Atmospheric Deposition to a Deciduous Forest Watershed. Oak Ridge National Lab Report TM-6674 (1979).
56. Little, P. and R.D. Wiffen. "Emissions and Deposition of Petrol Engine Exhaust." Atmos. Env., 11, 437 (1977).
57. Liu, B.Y.H. and J.K. Agarwal. "Experimental Observation of Aerosol Deposition in Turbulent Flow." Aerosol Science, 5, 145 (1974).
58. Liu, B.Y.H. and T.A. Ilori. "Aerosol Deposition in Turbulent Pipe Flow." Environ. Science Tech., 8, 351 (1984).
59. Liu, B.Y.H. and D.Y.H. Pui. "Electrical Neutralization of Aerosols." Aerosol Science, 5, 465 (1974).

60. Liu, B.Y.H. and K.W. Lee. "An Aerosol Generator of High Stability." Am. Industrial Hygiene Assoc. J., 861 (1975).
61. Maltby, R.L. and R.F. Keating. "The Surface Oil Flow Technique for Use in Low Speed Wind Tunnels." AGARDograph No. 70, 29, (1962).
62. McMahon, T.A. and P.J. Denison. "Empirical Atmospheric Deposition Parameters-A Survey." Atmos. Env., 13, 571 (1979). ✓
63. Merzkirch, Wolfgang. Flow Visualization. Academic Press, New York (1974).
64. Monteith, J.L. "Coupling of Plants to the Atmosphere." (Chapter in Plants and Their Atmospheric Environment, J. Grace, Ed.) Blackwell Scientific Publication, Boston (1981).
65. Moore, A.D., Editor. Electrostatics and Its Applications. Wiley-Interscience, New York (1976).
66. Owen, P.R. "Dust Deposition from a Turbulent Airstream." (Chapter in Aerodynamic Capture of Particles, E.G. Richardson, Ed.) Pergamon Press, New York (1960).
67. Pau U, K.T. and W.E. Reifsnyder, "The Relevance of Particle Rebound and Deposition in Plant Canopies." Proceedings of the Sixth Conference on Forest Meteorology, Seattle (1981).
68. Payatakes, A.C. "Model of Transient Aerosol Particle Deposition in Fibrous Media with Dendritic Patterns." J. AIChE., 23, 192 (1977).
69. Pendergrass, W.R. ATDL Applied Fluid Dynamics Laboratory Computer Users Guide. Oak Ridge, TN (1983).
70. Pendergrass, W.R. Personal Communication, (1983).
71. Penny, G.W. "Role of Adhesion in Electrostatic Precipitation." Archives Env. Health, 4, 91 (1962).
72. Ranz, W.E. and J.B. Wong. "Impaction of Dust and Smoke Particles on Surface and Body Collectors." Industrial Eng. Chem., 44, 1371 (1952).
73. Rosinski, J. "Efficiency of Scavenging Devices Used in Determining Fallout." Armour Research Foundation, Chicago (1957).
74. Rosinski, J. and C.T. Nagamoto. "Particle Deposition and Re-entrainment from Coniferous Trees, Part I." Kolloid-Zeitschrift, 204, 111 (1965). ✓

75. Rosinski, J. and G. Langer. "Deposition of Aerosol Particles on Flat Plates." Powder Technology, 1, 167 (1967).
76. Rouhiainen, P.O. and J.W. Stachiewicz. "On the Deposition of Small Particles from Turbulent Streams." J. of Heat Transfer, 92, 169 (1970).
77. Schlichting, H. Boundary Layer Theory. McGraw-Hill, New York (1968).
78. Sehmel, G.A. "Complexities of Particle Deposition and Re-entrainment in Turbulent Pipe Flow." J. Aerosol Science, 2, 63 (1971).
79. Sehmel, G.A. "Particle Eddy Diffusivities and Deposition Velocities for Isothermal Flow and Smooth Surfaces." J. Aerosol Science, 4, 125 (1973).
80. Sehmel, G.A. "Particle and Gas Dry Deposition: A Review." Atmos. Env., 14, 983 (1980). ✓
81. Slinn, W.G.N. "Dry Deposition and Resuspension of Aerosol Particles." (Chapter in Atmospheric-Surface Exchange of Particles and Gaseous Pollutants) ERDA Conference No. 740921 (1974). ✓
82. Slinn, W.G.N. "Formulation and Solution of the Diffusion-Deposition-Resuspension Problem." Atmos. Env., 10, 763 (1976). ✓ ☆
83. Slinn, W.G.N. "Predictions for Particle Deposition to Vegetative Canopies." Atmos. Env., 16, 1785 (1982).
84. Slinn, W.G.N. "A Potpourri of Deposition and Resuspension Questions." Proceedings of the 4th International Dry Deposition Conference, Santa Monica, CA (1982). ✓
85. Snyder, W.H. "Guideline for Fluid Modeling of Atmospheric Diffusion." USEPA 450/4-79-016, Research Triangle Park, NC (1979).
86. Thermal Systems Inc. TSI Quarterly, V, May/June (1979).
87. Thom, A.S. "Momentum, Mass, and Heat Exchange of Plant Communities." (Chapter in Vegetation and the Atmosphere, Vol. 1, J.L. Monteith, Ed.) Academic Press, London (1975).
88. Vennard, J.K. Fluid Dynamics. John Wiley and Sons, 4th Edition, New York (1965).
89. Wedding, J.B., R.W. Carlson, J.J. Stukel, and F.A. Bazzaz. "Aerosol Deposition on Plant Leaves." Env. Sci. Tech., 9(2), 151 (1975).

90. Wells, A.C. and A.C. Chamberlain. "Transport of Small Particles to Vertical Surfaces." Brit. J. Appl. Physics, 18, 1793 (1967).
91. Whitby, K.T. and B.Y.H. Liu. "The Electrical Behavior of Aerosols." (Chapter in Aerosol Science, C.N. Davies, Ed.) Academic Press, New York (1966).
92. Whitby, K.T. and B.Y.H. Liu. "Polystyrene Aerosols-Electrical Charge and Size Distribution." Atmos. Env., 2, 103 (1968).
93. Wigely, G. Transport in the Boundary Layers of Real and Model Leaves, Ph.D. Dissertation, Univ. of Nottingham, England (1974).
94. Wood, N.B. "A Simple Method for the Calculation of Turbulent Deposition to Smooth and Rough Surfaces." J. Aerosol Sci., 12, 275 (1981).

## APPENDIX A

## APPENDIX A

## LIST OF SYMBOLS

C	Concentration
$C_c$	Cunningham slip correction factor
d	Diameter
$d_d$	Diffusion boundary layer thickness
$d_u$	Velocity boundary layer thickness
D	Brownian diffusion coefficient
$D_p$	Particle diameter
e	Elementary unit of electrostatic charge
E	Electrostatic field intensity
f	Friction coefficient
F	Force of attraction
g	Acceleration of gravity
I	Stokes number
J	Dry deposition flux
k	Boltzmann's constant, also surface roughness
K	Eddy diffusion coefficient
$K_+$	Dimensionless eddy diffusion coefficient
$K_t$	Effective particle diffusivity
L	Characteristic length
N	Number of particles
Q	Magnitude of electrostatic charge

$r$	Distance separating electrostatic charges, also radius
$r_d$	Resistance to deposition
Re	Reynolds number = $U L/v$
S	Particle stopping distance
Sc	Schmidt number = $v/D$
$T_a$	Absolute temperature
$T_i$	Turbulence intensity
$u_*$	Friction velocity
$u, v, w$	Velocity vectors in the x, y, and z directions
$U_n$	Normal component of the turbulent velocity
$U_+$	Dimensionless velocity
$V_d$	Deposition velocity
$V_e$	Deposition velocity due to electrostatic field
$V_t$	Terminal settling velocity
$Z_+$	Dimensionless distance from boundary surface
$\mu$	Absolute viscosity
$\nu$	Kinematic viscosity
$\rho$	Density
$\tau$	Particle relaxation time
$\tau_o$	Tangential shearing stress
$\tau_+$	Dimensionless particle relaxation time

## APPENDIX B



## APPENDIX B

## CALCULATIONS FOR NEUTRALIZING CHARGED AEROSOLS

## USING THE METHOD OF COOPER AND REIST (1973)

Source of ionizing radiation = Polonium 210

Half-Life = 138.4 days

Alpha activity =  $3.7 \times 10^{10}$  disintegrations / sec curie

Energy of alpha particle =  $5.3 \times 10^6$  electron volts

A. Range of alpha particle, R

$$R = 1.24 E - 2.62$$

$$= 1.24 (5.3 \text{ Mev}) - 2.62 = 3.95 \text{ cm}$$

B. Specific Ionization Constant, k

$$k = \text{ion pairs produced} = \text{alpha energy} / \text{alpha range} \times 35.5 \text{ ev}$$

$$= 5.3 \times 10^6 \text{ ev} / 3.95 \text{ cm} \times 35.5 \text{ ev}$$

$$= 3.8 \times 10^4 \text{ ion pairs} / \text{cm}$$

C. Activity of Polonium 210 Source, S

$$S = (3.7 \times 10^{10} \text{ dis} / \text{s curie}) \times 2 \times 10^{-3} \text{ curie}$$

$$= 7.4 \times 10^7 \text{ disintegrations} / \text{s}$$

## D. Energy Flux, F, Inside a Cylindrical Neutralizing Chamber

Cylinder radius = 2.4 cm

Cylinder inside height = 34 cm

$$\begin{aligned}
 F &= S / 4 \pi r h \\
 &= (7.4 \times 10^7 \text{ dis/s}) / 4 \times 3.14 \times 2.4 \text{ cm} \times 34 \text{ cm} \\
 &= 7.2 \times 10^4 \text{ disintegrations / s cm}^2
 \end{aligned}$$

## E. Ion Production Rate, Q

$$\begin{aligned}
 Q &= k F \\
 &= (3.8 \times 10^4 \text{ ion pairs/cm}) \times 7.2 \times 10^4 \text{ dis/ s cm}^2 \\
 &= 2.7 \times 10^9 \text{ ion pairs / s cm}^3
 \end{aligned}$$

F. Time to Approach Equilibrium Concentration,  $t_e$ 

$$\begin{aligned}
 \alpha &= 3 \times 10^{-6} \text{ cm}^3/\text{s} \text{ from Cooper and Reist (1973)} \\
 t_e &= (\alpha Q)^{-0.5} \\
 &= (2.7 \times 10^9 \text{ ion pairs/s cm}^3 \times 3 \times 10^{-6} \text{ cm}^3/\text{s})^{-0.5} \\
 &= (8.1 \times 10^3)^{-0.5} = 0.011 \text{ seconds}
 \end{aligned}$$

G. Aerosol Residence Time in Neutralizing Chamber,  $t_r$ 

$$\begin{aligned}
 t_r &= V / Q \\
 &= (3.14 \times 2.4^2 \text{ cm}^2 \times 34 \text{ cm}) / (4600 \text{ cm}^3/\text{m} \times \text{m}/60 \text{ s}) \\
 &= 8.0 \text{ seconds}
 \end{aligned}$$

H. Equilibrium Ionic Concentration,  $n_\alpha$ 

$$\begin{aligned}
 n_\alpha &= 2 (Q / \alpha)^{0.5} \\
 &= 2 (2.7 \times 10^9 \text{ ion pairs/cm}^3 \text{ s} / 3 \times 10^{-6} \text{ cm}^3/\text{s})^{0.5} \\
 &= 2 (8.1 \times 10^{16})^{0.5} \\
 &= 5.6 \times 10^8 \text{ ions / cm}
 \end{aligned}$$

I. Time to Approach Boltmann's Equilibrium,  $t_n$ 

$$\begin{aligned}
 t_n &= 2.8 \times 10^5 \text{ cm}^{-3} / n_\alpha \\
 &= 2.8 \times 10^5 / 5.6 \times 10^8 \\
 &= 0.005 \text{ seconds}
 \end{aligned}$$

J. Completeness of Neutralization,  $t^*$ 

$$\begin{aligned}
 t^* &= t_{\text{res}} / t_n \\
 &= 8.1 \text{ s} / 0.005 \text{ s} \\
 &= 1620
 \end{aligned}$$

Cooper and Reist (1973) recommended that  $t^*$  be much greater than one to insure complete neutralization. They found  $t^*$  ranged from 36 to 110 for various electrostatic charge neutralizers in the literature. A large value of  $t^*$  results in a more complete aerosol charge neutralization which more closely approaches the Gaussian distribution predicted by Boltzmann's Law (Liu and Pui, 1974).

## APPENDIX C

TABLE C-1. WIND TUNNEL VELOCITY CALIBRATION - HORIZONTAL.

---

Distance From Wall	Mean Velocity	Turulence Intensity
Y (cm)	U (m/s)	T.I. (%)
11	2.26	2.87
12	2.23	3.04
13	2.22	3.30
14	2.21	3.38
15	2.21	3.44
16	2.20	3.43
17	2.20	3.52
18	2.20	3.46
19	2.16	3.72
20	2.14	4.16

---

X = 18 CM FROM AEROSOL OUTLET

Z = 7 CM ABOVE FLOOR

TABLE C-2. WIND TUNNEL VELOCITY CALIBRATION - VERTICAL.

---

Distance Above Floor	Mean Velocity	Turbulence Intensity
Z (cm)	U (m/s)	T.I. (%)
3	1.98	9.97
4	2.07	10.7
5	2.21	9.96
6	2.35	7.44
7	2.43	4.57
8	2.46	2.90
9	2.48	2.20
10	2.54	1.79

---

X = 18 CM FROM AEROSOL OUTLET

Y = 16 CM FROM REAR WALL

TABLE C-3. VELOCITY PROFILE OVER EXPERIMENTAL PLATE  
 LAMINAR MAINSTREAM AT X = 1 CM AND Y = 0.

---

Distance Above Plate	Mean Velocity	Turbulence Intensity
Z (mm)	U (m/s)	T.I. (%)
1	1.51	17.7
1.5	1.87	12.3
2	1.95	8.82
2.5	1.98	7.59
3	1.99	7.43
4	1.99	6.99
5	1.99	6.75
6	2.00	6.50
8	2.06	5.97
10	2.12	5.17
15	2.16	3.93
20	2.16	2.77
25	2.15	2.14
60	2.14	1.45

---

TABLE C-4. VELOCITY PROFILE FOR LAMINAR MAINSTREAM

AT  $X = 4$  CM AND  $Y = 0$ .

---

Distance Above Plate	Mean Velocity	Turbulence Intensity
Z (mm)	U (m/s)	T.I. (%)
1	1.37	12.5
1.5	1.72	11.5
2	1.91	10.0
2.5	1.96	9.08
3	1.98	8.36
4	2.03	6.73
5	2.06	6.78
6	2.07	6.29
8	2.07	5.80
10	2.08	5.23
15	2.12	3.83
20	2.12	2.66
25	2.16	2.03
60	2.15	1.48

---



TABLE C-5. VELOCITY PROFILE FOR LAMINAR MAINSTREAM

AT X = 8 CM AND Y = 0.

---

Distance Above Plate	Mean Velocity	Turbulence Intensity
Z (mm)	U (m/s)	T.I. (%)
1	1.24	14.3
1.5	1.60	12.2
2	1.78	10.7
2.5	1.92	8.92
3	2.01	8.15
3.5	2.06	7.12
4	2.09	6.62
4.5	2.08	6.56
5	2.07	5.65
7	2.08	5.65
10	2.09	4.85
15	2.12	3.85
20	2.17	2.65
25	2.19	2.10
60	2.20	1.40

---

TABLE C-6. VELOCITY PROFILE FOR LAMINAR MAINSTREAM

AT X = 12 CM AND Y = 0.

---

Distance Above Plate	Mean Velocity	Turbulence Intensity
Z (mm)	U (m/s)	T.I. (%)
1	1.08	15.9
1.5	1.43	13.8
2	1.62	12.0
2.5	1.84	10.1
3	1.96	9.21
3.5	2.02	8.25
4	2.06	7.53
4.5	2.05	7.02
5	2.06	6.71
6	2.07	5.96
7	2.07	5.65
10	2.11	4.93
15	2.16	3.72
20	2.19	2.81
25	2.22	1.99
60	2.18	1.44

---

TABLE C-7. VELOCITY PROFILE FOR LAMINAR MAINSTREAM

AT X = 16 CM AND Y = 0.

Distance Above Plate	Mean Velocity	Turbulence Intensity
Z (mm)	U (m/s)	T.I. (%)
1	0.76	17.7
1.5	1.34	15.7
2	1.58	13.6
2.5	1.71	12.3
3	1.83	10.9
3.5	1.92	9.47
4	1.96	8.50
4.5	2.04	7.29
5	2.10	6.36
5.5	2.13	6.09
6	2.14	5.79
6.5	2.12	5.67
8	2.12	4.83
10	2.14	4.48
15	2.16	3.56
20	2.21	2.62
25	2.24	2.20
60	2.18	1.48

TABLE C-8. VELOCITY PROFILE FOR LAMINAR MAINSTREAM

AT X = 20 CM AND Y = 0.

---

Distance Above Plate	Mean Velocity	Turbulence Intensity
Z (mm)	U (cm/s)	T.I. (%)
1	0.95	18.7
1.5	1.26	16.0
2	1.54	13.5
2.5	1.74	11.7
3	1.89	10.0
3.5	1.97	9.46
4	2.07	8.12
4.5	2.09	7.24
5	2.11	6.29
5.5	2.11	5.86
8	2.14	4.65
10	2.15	3.73
15	2.17	3.00
20	2.21	2.26
60	2.24	1.37

---

TABLE C-9. VELOCITY PROFILE FOR LAMINAR MAINSTREAM

AT X = 24 CM AND Y = 0.

---

Distance Above Plate	Mean Velocity	Turbulence Intensity
Z (mm)	U (m/s)	T.I. (%)
1	1.09	15.6
1.5	1.44	14.0
2	1.63	11.9
2.5	1.78	10.8
3	1.92	8.82
3.5	2.03	8.08
4	2.12	6.67
4.5	2.16	6.10
5	2.17	5.38
5.5	2.18	5.49
6	2.19	4.62
8	2.22	3.46
10	2.23	3.01
15	2.24	2.53
20	2.28	1.92
60	2.27	1.14

---

TABLE C-10. VELOCITY PROFILE FOR LAMINAR MAINSTREAM

AT X = 26.5 CM AND Y = 0.

---

Distance Above Plate	Mean Velocity	Turbulence Intensity
Z (mm)	U (cm/s)	T.I. (%)
1	1.16	11.9
1.5	1.54	10.4
2	1.79	9.12
2.5	1.97	7.78
3	2.05	7.34
3.5	2.16	6.66
4	2.26	5.11
4.5	2.31	4.81
5	2.30	4.51
5.5	2.30	4.09
7.5	2.31	3.15
10	2.31	2.85
15	2.30	2.45
20	2.29	1.93
60	2.23	1.42

---

TABLE C-11. VELOCITY PROFILE FOR LAMINAR MAINSTREAM, WITH  
AEROSOL GENERATOR OPERATING AT 50 PSI AT X= 1 CM AND Y = 0.

---

Distance Above Plate	Mean Velocity	Turbulence Intensity
Z (mm)	U (cm/s)	T.I. (%)
1	1.54	16.2
1.5	1.84	11.4
2	1.95	8.52
2.5	1.96	7.50
3	1.94	7.10
4	2.00	6.30
5	2.03	6.08
6	2.07	5.72
8	2.11	5.33
10	2.11	4.93
15	2.12	3.57
20	2.11	2.74
60	2.13	1.52

---

TABLE C-12. VELOCITY PROFILE OVER EXPERIMENTAL PLATE FOR  
TURBULENT MAINSTREAM AT X = 1 CM AND Y = 0.

---

Distance Above Plate	Mean Velocity	Turbulence Intensity
Z (mm)	U (m/s)	T.I. (%)
1	1.71	36.0 *
2	2.66	19.6
3	3.05	10.1
4	3.12	7.64
5	3.13	6.59
6	3.10	6.10
7	3.07	5.84
8	3.05	5.64
10	3.02	5.47
12	2.99	5.57
15	2.94	5.84
20	2.92	6.09
25	2.88	6.38
30	2.85	6.36
60	2.38	9.97

---

\* Hot-film anemometer is unreliable at this turbulence intensity.



TABLE C-13. VELOCITY PROFILE FOR TURBULENT MAINSTREAM

AT X = 4 CM AND Y = 0.

---

Distance Above Plate	Mean Velocity	Turbulence Intensity
Z (mm)	U (m/s)	T.I. (%)
1	1.90	18.9
2	2.39	15.4
3	2.57	13.3
4	2.57	1.23
5	2.72	10.2
6	2.76	8.76
7	2.83	7.26
8	2.88	6.08
9	2.90	5.85
10	2.88	5.73
15	2.84	5.66
20	2.79	5.91
25	2.75	5.96
60	2.45	9.26

---

TABLE C-14. VELOCITY PROFILE FOR TURBULENT MAINSTREAM

AT X = 8 CM AND Y = 0.

Distance Above Plate Z (mm)	Mean Velocity U (m/s)	Turbulence Intensity T.I. (%)
1	1.80	20.0
2	2.30	14.8
3	2.46	12.8
4	2.61	11.3
5	2.67	10.4
6	2.71	9.75
7	2.76	8.88
8	2.79	8.29
9	2.83	7.49
10	2.84	6.88
12	2.90	5.85
14	2.95	5.61
16	2.94	5.63
20	2.90	5.70
25	2.86	6.02
30	2.83	6.06
60	2.57	8.33

TABLE C-15. VELOCITY PROFILE FOR TURBULENT MAINSTREAM

AT X = 12 CM AND Y = 0.

---

Distance Above Plate	Mean Velocity	Turbulence Intensity
Z (mm)	U (m/s)	T.I. (%)
1	1.63	21.6
2	1.99	16.8
4	2.39	11.4
6	2.61	9.57
8	2.75	8.63
10	2.79	7.67
12	2.81	7.06
14	2.83	6.58
16	2.83	6.23
20	2.80	6.05
25	2.77	6.01
30	2.74	5.95
60	2.49	8.42

---

TABLE C-16. VELOCITY PROFILE FOR TURBULENT MAINSTREAM

AT X = 16 CM AND Y = 0.

---

Distance Above Plate	Mean Velocity	Turbulence Intensity
Z (mm)	U (m/s)	T.I. (%)
1	1.33	24.4
2	1.98	17.1
4	2.40	11.4
6	2.56	9.45
8	2.65	8.32
10	2.73	7.74
12	2.76	7.06
14	2.80	6.61
16	2.82	6.14
18	2.80	5.90
20	2.80	5.77
25	2.78	5.65
30	2.76	5.66
60	2.49	8.63

---

TABLE C-17. VELOCITY PROFILE FOR TURBULENT MAINSTREAM

AT X = 20 CM AND Y = 0.

---

Distance Above Plate	Mean Velocity	Turbulence Intensity
Z (mm)	U (m/s)	T.I. (%)
1	1.38	24.8 *
2	1.94	17.7
4	2.37	11.5
6	2.51	9.64
10	2.71	7.49
14	2.80	6.38
16	2.81	6.02
20	2.81	5.67
25	2.79	5.40
30	2.78	5.25
60	2.50	8.25

---

\* Hot-film anemometer is unreliable at this turbulence intensity.

TABLE C-18. VELOCITY PROFILE FOR TURBULENT MAINSTREAM

AT X = 24 CM AND Y = 0.

---

Distance Above Plate	Mean Velocity	Turbulence Intensity
Z (mm)	U (m/s)	T.I. (%)
1	1.29	25.1 *
2	1.87	19.0
4	2.29	12.5
6	2.50	9.90
8	2.65	8.64
10	2.71	7.81
12	2.78	6.99
14	2.82	6.24
16	2.86	5.86
20	2.88	5.23
25	2.85	5.07
30	2.82	4.97
60	2.50	8.38

---

\* Hot-film anemometer is unreliable at this turbulence intensity.

TABLE C-19. PARTICLE CONCENTRATIONS ALONG THE  
EXPERIMENTAL PLATE AT  $Z = 2$  MM AND  $Y = 0$ .

---

Distance From Leading Edge X (cm)	Mean Particle Concentration C (#/liter)	Standard Deviation (#/liter)	Normalized Particle Concentration
0	8077	295	1.000
1	7322	384	.906
4	6511	330	.806
8	5770	348	.714
12	5337	309	.661
16	5029	326	.623
18	4835	324	.599
20	4657	327	.576
22	4541	289	.562
24	4436	267	.549

---

#### Linear Regression Analyses

1) Mean Concentration; Slope = -136.5, Y Intercept = 7357

Correlation Coefficient = -0.957

2) Normalized Concentration; Slope = -0.0169, Y Intercept = 0.91

Correlation Coefficient = -0.957

The number of trials, N, for each concentration average is 10.

## APPENDIX D



TABLE D-1. DEPOSITION VELOCITY RESULTS FOR EXPERIMENTS 4, 5, AND 6.

Distance X (cm)	Experiment 4 $V_d$ (cm/s)	Experiment 5 $V_d$ (cm/s)	Experiment 6 $V_d$ (cm/s)
1	0.045±0.036	1.8±0.49	0.012±0.010
4	0.016±0.010	2.3±0.58	0.003±0.002
8	0.009±0.005	2.7±0.84	0.007±0.004
12	0.011±0.005	2.0±0.76	0.024±0.023
16	0.009±0.009	4.0±0.90	0.062±0.034
20	0.007±0.005	3.8±1.15	0.039±0.024
24	0.011±0.009	19.8±4.93	0.091±0.041
	N = 10	N = 10	N = 10

Where N is the number of trials used to calculate each deposition velocity.

TABLE D-2. DEPOSITION VELOCITY RESULTS FOR EXPERIMENTS 7, 9, and 10.

Distance X (cm)	Experiment 7 $V_d$ (cm/s)	Experiment 9 $V_d$ (cm/s)	Experiment 10 $V_d$ (cm/s)
1	0.007±0.006	0.06±0.03	3.16±0.68
4	0.006±0.003	0.05±0.01	2.41±0.60
8	0.004±0.002	0.10±0.03	0.31±0.12
12	0.008±0.003	0.06±0.02	0.87±0.34
16	0.008±0.004	0.09±0.03	2.29±0.52
20	0.005±0.005	0.07±0.02	0.76±0.26
24	0.005±0.001	0.03 -	1.21±0.45
	N = 10	N = 10	N = 10

Where N is the number of trials used to calculate each deposition velocity.

TABLE D-3. DEPOSITION VELOCITY RESULTS FOR EXPERIMENTS 11, 12, and 13.

Distance X (cm)	Experiment 11 $V_d$ (cm/s)	Experiment 12 $V_d$ (cm/s)	Experiment 13 $V_d$ (cm/s)
1	$3.0 \pm 0.30$	$0.19 \pm 0.11$	$0.39 \pm 0.12$
4	$0.43 \pm 0.40$	$0.17 \pm 0.10$	$0.40 \pm 0.28$
8	$0.17 \pm 0.06$	$0.12 \pm 0.05$	$0.23 \pm 0.21$
12	$0.37 \pm 0.08$	$0.12 \pm 0.05$	$0.03 \pm 0.03$
16	$0.36 \pm 0.16$	$0.09 \pm 0.14$	$0.02 \pm 0.02$
20	$0.14 \pm 0.04$	$0.30 \pm 0.11$	$0.02 \pm 0.02$
24	$0.07 \pm 0.03$	$0.53 \pm 0.16$	$0.25 \pm 0.21$
	N = 5	N = 5	N = 5

Where N is the number of trials used to calculate each deposition velocity.

TABLE D-4. DEPOSITION VELOCITY RESULTS FOR EXPERIMENTS 14, 15, AND 17.

Distance X (cm)	Experiment 14 $V_d$ (cm/s)	Experiment 15 $V_d$ (cm/s)	Experiment 17 $V_d$ (cm/s)
1	0.32±0.18	0.011±0.010	0.063±0.038
4	0.28±0.05	0.010±0.008	0.015±0.083
8	0.14±0.10	0.005±0.006	0.031±0.011
12	0.31±0.06	0.007±0.005	0.076±0.011
16	0.30±0.23	0.005±0.006	agglomerates
20	0.13±0.12	0.008±0.011	agglomerates
24	0.20±0.13	0.030±0.031	agglomerates
	N = 5	N = 5	N = 5

Where N is the number of trials used to calculate each deposition velocity.

TABLE D-5. DEPOSITION VELOCITY RESULTS FOR EXPERIMENTS 19 AND 20.

---

Distance X (cm)	Experiment 19 $V_d$ (cm/s)	Experiment 20 $V_d$ (cm/s)
1	0.0017±0.0037	0.0070±0.0060
4	0.0006±0.0014	0.0052±0.0075
8	0.0320±0.0160	0.0095±0.0057
12	0.0058±0.0095	0.0098±0.0114
16	0.0057±0.0047	0.0176±0.0183
20	0.0018±0.0026	0.0117±0.0129
24	0.0018±0.0026	0.0108±0.0046
	N = 5	N = 5

---

Where N is the number of trials used to calculate each deposition velocity.

**The two page vita has been  
removed from the scanned  
document. Page 1 of 2**

**The two page vita has been  
removed from the scanned  
document. Page 2 of 2**

# BOUNDARY LAYER TRANSPORT OF SMALL PARTICLES

by

David McCready

(ABSTRACT)

The transport of small particles across the aerodynamic boundary layer that developed over a smooth, flat, acrylic plate and their subsequent deposition was investigated. The velocity boundary layer over the flat plate was characterized for a wind tunnel mainstream velocity of 2 m/s. Particle deposition was quantified with respect to location on the experimental plate with a microscope.

The deposition of 0.8, 0.9, 1.1, and 2.0 micron diameter unit density, polystyrene latex microspheres on to oil-coated, uncoated, upper, and lower surfaces was investigated. Although experimental deposition velocities exhibited run-to-run variation, they were significantly greater than those reported in the literature.

A turbulent flow deposition model which included eddy diffusion, Brownian diffusion, inertial, and gravitational deposition mechanisms underestimated the experimental deposition velocities. The experimental plate was nonconductive and could not be electrically grounded. It appears the electrostatic attraction mechanism was responsible for the increased experimental deposition velocities; this mechanism was not included in the deposition model.

There was no significant resuspension of 42 micron diameter microspheres deposited to an initially moist experimental plate after 6 hours in the wind tunnel at a mean air velocity of 2 m/s.